UNIVERSIDADE DE SÃO PAULO
INSTITUTO DE FÍSICA DE SÃO CARLOS

Aissata Ousmane Kane

Lignocellulosic biomass valorization: study of plant biomass structure, composition, composition, and enzymatic digestibility after being submitted to different pretreatment steps

São Carlos

2022

Aissata Ousmane Kane

Lignocellulosic biomass valorization: study of plant biomass structure, composition, and enzymatic digestibility after being submitted to different pretreatment steps

Thesis presented to the Graduate Program in Physics at the Instituto de Física de São Carlos, Universidade de São Paulo to obtain the degree of Doctor of Science.

Concentration area: Biomolecular Physics

Advisor: Prof. Dr. Igor Polikarpov

Original version

São Carlos
2022

Kane, Aissata Ousmane
Lignocellulosic biomass valorization: study of plant biomass structure, composition, composition, and enzymatic digestibility after being submitted to different pretreatment steps / Aissata Ousmane Kane; advisor Igor Polikarpov -- São Carlos 2022.
179 p.

Thesis (Doctorate - Graduate Program in Biomolecular Physics) -- Instituto de Física de São Carlos, Universidade de São Paulo - Brasil , 2022.

1. Lignocellulosic biomass. 2. Pretreatment. 3. Enzymatic hydrolysis. 4. Cellulose nanofibers (CNF). I. Polikarpov, Igor, advisor. II. Title.

With my love,
to my family

Acknowledgments

Firstly, I thank the Good Lord for providing the health, strength, and courage to complete my Ph.D. program.

Seydou, my baby, I hope one day you will understand, mum. I apologize for this long absence. I love you!

I am thankful to my parents and Tierno for caring for my dear son, Seydou. I am very proud of you.

I am immensely grateful to my lovely family for their unrelenting support and prayers, especially my parents.

My profound gratitude goes to Prof. Dr. Igor Polikarpov for allowing me to work under his supervision and for his constructive remarks.

My deep appreciation goes to my colleagues in the Molecular Biotechnology group, who have spared no effort to facilitate my integration. Vanessa, Melissa, Regiane, Aline, Vinicius, Evandro, Lorenzo, Ane, Caio, Jorge, Paula, Raissa, Angelica, and Livia, I will be eternally grateful for the exceptional welcome I received from all of you and the helpful mentorship from Vanessa, Vinicius, Melissa, and Regiane. I wish to thank technicians Maria, João Possato, and Josimar for their availability.

I greatly appreciate Andre and Elisabeth's kindness, availability, and support in all my social and administrative procedures.

I want to thank the administration and staff of the Institute of Fisica de Sao Carlos and, more particularly, the post-graduation manager Silvio Cesar Athayde and Ricardo for their availability.

I am thankful to Prof. Dr. Balla Diop Ngom for his unconditional support. There will never be enough words to express my gratitude and pride.

I wish to thank my other family, the LPQEN group. I am proud to be part of this team.

I want to thank my friend Omar Faye for his support in every step of my journey in Brazil. You are a real brother.

Suleiman, Waqar, and Zeray, I appreciate your friendship. Thank you for always being there for me during my stay in BRAZIL. Suleiman, thank you for correcting the English for me.

Jorge, I thank God for allowing me to meet an exceptional and extraordinary person like you and Dona Leonilda. I appreciated every moment spent with you. Thank you for everything, my brother.

This study was financed in part by the Coordenação de Aperfeiçoamento de Pessoal de Nível Superior – Brasil (CAPES) – Finance Code 001

There's Plenty of Room at the Bottom

Richard Feynman

ABSTRACT

KANE, A. O. **Lignocellulosic biomass valorization**: a study of plant biomass structure, composition, composition, and enzymatic digestibility after being submitted to different pretreatment steps. 2022. 179p. Thesis (Doctor in Science) – Instituto de Física de São Carlos, Universidade de São Paulo, São Carlos, 2022.

Bioenergy has been proposed as one way to significantly meet global energy demand and prevent environmental problems using renewable energy resources. The valorization of lignocellulosic biomass as a renewable feedstock for producing bioethanol and biomaterial has attracted much attention. However, efficient lignocellulosic biomass conversions require the development of strategies and technologies safe and inexpensive. Sugarcane is an agricultural crop produced in several tropical countries, notably Brazil. This work has investigated sugarcane wastes as potential raw materials to produce second-generation biofuels and nanomaterials. Different configurations of two-stage pretreatments were applied to sugarcane wastes (SCC, SCB, SCL) to produce fermentable sugars after enzymatic hydrolysis as well as nanocellulose via enzymatic hydrolysis and mechanical disintegration of cellulose-enriched material. Enzymatic hydrolysis yields of raw and pretreated sugarcane wastes were determined and correlated with structural, morphological, and composition changes after pretreatments. Overall, after combined pretreatments, enzymatic convertibility was highly efficient for all studies, reaching over 97% for SCC after acid-alkaline pretreatment (NaOH2% / $H_2SO_4$2%), 91.2% for SCL acid-alkaline ($H_2SO_4$1% / NaOH1%), 99.57 % for sugarcane bagasse after liquid hot water - alkaline sulfonation (H_2O / Na_2SO_3 +NaOH). This efficiency was correlated to the removal of amorphous parts of lignocellulosic biomass, lignin, and/or hemicellulose, which also justify high crystallinity indices and crystallite sizes of pretreated biomass. An efficient carbohydrate extraction from sugarcane bagasse occurred during alkaline pretreatment using NaOH + H_2O_2, with a maximum delignification. Thermally and colloidally stable cellulose nanofibers were obtained. The enzymatic hydrolysis stage facilitated the defibrillation of blanched SCB, and the sulfonation introduced sulfonic groups in the CNF. The introduction of surface charges to CNF promotes their functionalization and widens their fields of application.

Keyworlds: Lignocellulosic biomass. Pretreatment. Enzymatic hydrolysis. Cellulose nanofibers (CNF)

RESUMO

KANE, A. O. Valorização da biomassa lignocelulósica: estudo da estrutura, composição e digestibilidade enzimática da biomassa vegetal após ser submetida a diferentes etapas de pré-tratamento. 2022. 179p. Tese (Doutorado em Ciências) – Instituto de Física de São Carlos, Universidade de São Paulo, São Carlos, 2022.

A bioenergia tem sido proposta como uma forma de atender significativamente a demanda energética global e prevenir problemas ambientais, utilizando recursos energéticos renováveis. A valorização da biomassa lignocelulósica como matéria-prima renovável para a produção de bioetanol e biomaterial tem despertado muita atenção. No entanto, a transformação eficiente da biomassa lignocelulósica em açúcares fermentescíveis requer o desenvolvimento de estratégias e tecnologias para rupturas da biomassa lignocelulósica. A cana-de-açúcar é uma importante cultura agrícola produzida em vários países tropicais, notadamente no Brasil. Este trabalho investigou resíduos de cana-de-açúcar como potenciais matérias-primas para a produção de biocombustíveis e nano materiais de segunda geração. Diferentes configurações de pré-tratamentos de duas etapas foram aplicadas aos resíduos de cana-de-açúcar (SC, SCB, SCL) para produzir açúcares fermentáveis após hidrólise enzimática, bem como nanocelulose via hidrólise enzimática e desintegração mecânica do material rico em celulose. Os rendimentos de hidrólise enzimática de resíduos de cana-de-açúcar não tratados e pré-tratados foram determinados e correlacionados com alterações estruturais, morfológicas e de composição após os pré-tratamentos. No geral, após pré-tratamentos combinados, a convertibilidade enzimática foi altamente eficiente para todos os estudos (capítulo 4-6, atingindo mais de 97% para SCC após pré-tratamento ácido-alcalino ($NaOH2\%/H_2SO_42\%$), 91,2% para SCL ácido-alcalino ($H_2SO_41\%$ / $NaOH1\%$), 99,57 % para bagaço de cana após LHW- sulfonação alcalina (H_2O/Na_2SO_3+NaOH). Essa eficiência foi correlacionada com a remoção de partes amorfas de biomassa lignocelulósica, lignina e/ou hemicelulose, que também justificam a alta cristalinidade índices e tamanhos de cristalitos da biomassa pré-tratada. Um eficiente fracionamento do bagaço de cana-de-açúcar ocorreu durante o pré-tratamento alcalino com $NaOH+H_2O_2$, com máxima deslignificação. A etapa de hidrólise enzimática facilitou a desfibrilação da biomassa branqueada, e a sulfonação da biomassa branqueada melhorou sua digestibilidade enzimática. A introdução de cargas superficiais no CNF promove suas funcionalizações e amplia seus campos de aplicação.

Palavras chaves: Biomassa lignocelulósica. Pré-tratamento. Hidrólise enzimática. Nanofibras de celulose.

LIST OF FIGURES

LISTE OF TABLE

LIST OF ABBREVIATION

AFM	***Atomic Force Microscopy***
BG	***β-glucosidase***
CAGR	***Compound Annual Growth Rate***
CBH	***Cellobiohydrolases***
CE	***Carbohydrate esterase***
CLSM	***Confocal Laser Scanning Microscopy***
CNC	***Cellulose Nanocrystals***
CO_2	***Carbon dioxide***
CBH	***Cellobiohydrolase***
CNF	***Cellulose Nanofiber***
DAP	***Diluted acid pretreatment***
DTG	***Differential Thermogravimetric***
EC	***Energy cane***
EU	***European Union***
GHG	***Green House Gas***
$GtCO_2$	***Gigatonne of CO_2***
HMF	***Hydroxymethyl Furfural***
HPLC	***High-Performance Liquid Chromatography***
H_2O_2	***Hydrogen Peroxide***
H2SO4	***Sulphuric acid***
LB	***Lignocellulosic biomass***
NaOH:	***Sodium Hydroxide***
NA_2SO_3	***Sodium sulfite***
LHW	***Liquid Hot Water***
NMR	***Nuclear Magnetic Mesonance***
NOx	***Nitrogen Oxides***
PMO	***Polysaccharide monooxygenases (PMO)***
SCB	***Sugarcane bagasse***
SC	***Sugarcane culm***
SCL	***Sugarcane leave***
SEM	***Scanning Electron Microscopy***
TEM	***Transmission electron microscopy***
TGA	***Thermogravimetric analysis***
USA	***United States of America***

XRD ***Xray Diffraction***

LISTE OF CONTENT

1 Chapter 1 - General Introduction

The primary global energy resource is mainly fossil fuels, such as petroleum, natural gas, and consumption (1); however, the supply of these fossils is non-renewable. Fossil depletion will happen because of its overexploitation due to industrialization, urbanization, and rapid population growth. (2) Meanwhile, when fossil fuels are burned, their carbon, sulfur, and nitrogen contents are converted into carbon oxides, sulfur oxides, and nitric oxides, resulting in greenhouse gas (GHG) emissions and environmental pollution. (3-4) Global fossil CO_2 emission was estimated to reach 36.4 $GtCO_2$ in 2021, with an enormous contribution from China, the USA, and EU countries. (5) To hope to decrease dependence on fossil fuels and limit global warming to a safe threshold, according to the key recommendations of the International Energy Agency (6), it is essential to immediately abandon any new project of exploration and exploitation of fossil fuels. The fixed threshold limits the increase of global temperatures to 1.5°C. (6) Thus, more efforts are being devoted to using renewable energy, such as solar, wind, and bioenergy, instead of fossil energy. (7) In this regard, alternative energy sources and sustainable technology capable of reducing dependence on these fossil fuels and protecting the environment are explored. (8) Thereby, fossil limitations cited above and oil price fluctuation motivated researchers and policymakers to pay attention to lignocellulosic biomass as a renewable resource to produce fuels, chemicals, and biomaterials that can replace petroleum-based polymers. (9)

Lignocellulosic biomass (LB), the most abundant renewable carbon resource on earth, remains a significant component of agricultural wastes (cereal straws), forest residues (wood), and dedicated crops (grasses). (10) LB is a primary feedstock for biofuel (bioethanol) production, which does not compete with soil usage for food and feed crops (11), and a driving force for developing bio-based products (food, feed, chemicals, and materials) that pollute less than petroleum-based fuels and chemicals. (12) Promising chemical compounds, such as n-butanol(13), isobutanol (14), 2,3-butanediol (15), and lactic acid (16), can be synthesized from lignocellulosic biomass. The chemical compounds may be employed as raw materials for producing a wide range of products, including biopolymers and solvents.(17) Equally, attractive materials and nanomaterials, including nanocelluloses (18), nanolignins (19), hemicellulose-based material (20), etc., have been developed. These lignocellulose-based materials showed outstanding proprieties that increased their applications in water treatments, drug delivery, bioenergy, etc. (21-22)

Lignocellulosic biomass refers to plant biomass composed of cellulose (38–50%), hemicellulose (23–32%), and lignin (15–25%). (23) These three components form a complex and resistant three-dimensional structure maintained by various intermolecular bonds and Van der Waals forces, making it resistant to enzymatic hydrolysis. (24) Cellulose is the most natural available polymer composed of glucose and provides structural support to plants, hemicellulose is responsible for binding between lignin and cellulose, and lignin ensures the robustness of the whole structure. (25) The production of bioethanol from lignocellulose involves the conversion of cellulose and hemicellulose into monomer sugars. This biological conversion by enzymes and microbes consists of four main steps: 1. pretreatments to make the cellulosic parts more suitable for the enzymatic reaction, 2. enzymatic saccharification to hydrolyze the cellulose/hemicellulose into monomeric sugars (fermentable sugars), 3. microbial fermentation to convert monomeric sugars into fuels and chemicals, and 4. product recovery and purification. (26) Pretreatment stages require special attention since the subsequent saccharification, and the fermentation process is highly related to the result of the pretreatment. Conversion of lignocellulosic biomass into fermentable sugars demands a disruption or fractionation of LB through pretreatments. However, this is one of the most expensive and least technologically mature stages in converting biomass to fermentable sugars, accounting for approximately 40% of the total production cost. (27) In addition, LB-derived compounds can be generated during pretreatment, which often has an inhibitory effect on enzymes and microorganisms, decreasing the sugar yield from hydrolysis and negatively affecting biocatalytic fermentation processes. (28) Thereby, the ideal pretreatment method is the one that provides good sugar yield with less inhibitor production in an inexpensive and eco-friendly way. (29)

On the other hand, LB must be characterized beforehand to surround its chemical characteristics and composition. A better understanding of LB characteristics may allow for gauging biomass recalcitrance. This preliminary step facilitates the development of efficient deconstruction strategies to minimize the loss of carbohydrates and maximize fermentable sugar yields during saccharification. (30) Several physicals, chemical, and biological pretreatment approaches are available. (31–34) Each pretreatment of LB has a specific effect on the feedstock chemical properties, especially on lignin, hemicellulose, and cellulose fractions. However, there are drawbacks to using most of these methods on a large scale because of high treatment costs and the generation of toxic inhibitors during the pretreatment stage. (28)

These limitations collectively restrict existing processes and justify the continual exploration of new ways to optimize pretreatment conditions and select LB as a potential feedstock for bioethanol and biomaterial production. In this present thesis, the performance of different configurations of combined or sequential pretreatments on various LB follows in this wake. The synergic action of two or more low-cost pretreat sequences can increase the pretreatment efficiency. We applied different configurations of two-stage pretreatments (acid-alkaline pretreatments, LHW-sulfonation pretreatment) upon biomass from sugarcane (sugarcane bagasse, sugarcane culm, sugarcane leaves) to test their potential utilization as feedstock for bioethanol production, through biophysical characterizations as well as enzymatic hydrolysis of untreated and pretreated biomass. On the other hand , cellulose nanofibers was extracted from obtained cellulose-enriched material after SCB delignification or blanchiment through the promising and safe enzyme assisted approach .

1.1 Objectives of the thesis

The present research aims to develop technologies based on renewable raw materials, mainly to improve the potential of using lignocellulosic biomass as feedstock for bioethanol and bio-based material production by developing efficient pretreatment processes optimizing the enzymatic digestibility of lignocellulosic biomass. The detailed objectives of this thesis were as follows:

- To investigate the enzymatic hydrolysis efficiency of different kinds of lignocellulosic biomasses subjected to combined pretreatments (acid-alkaline treatments, LHW, and neutral/alkaline sulfonation)
- To understand the relationships between biomass composition and pretreatment efficiency
- To evaluate the effects of pretreatments on lignocellulosic biomass's structural, morphological, and crystallinity.
- To compare the efficiency of different lignocellulosic biomasses for bioethanol production through enzymatic hydrolysis effects.
- To produce nanomaterial of cellulose extracted from lignocellulosic biomass through pretreatment stages and enzymatic hydrolysis.

1.2 Thesis outline

This thesis contains 8 chapters, which comprise a General Introduction (Chapter 1), a review of the literature (Chapter 2), characterization technics (Chapter 3), Methodology (Chapter 4), published journal papers (Chapters 5 and 6), Results and discussion of sulfonated SCB and cellulose nanofiber (Chapter 7), and general conclusions (chapter 8).

The context, main objectives, and outlines of this research are defined and summarized in Chapter 1 as a General Introduction.
Chapter 2 presents a literature review of lignocellulosic biomass, particularly sugarcane wastes, and its conversion into Bioethanol.
Chapter 3 summarize the principles of the different characterization technics used during this work.
Chapter 4 describes the materials and methods utilized for experiments and analysis

Chapter 5 is a published paper that report the potential utilization of culms from sugar and energy cane varieties grown in Argentina for second-generation ethanol production.

Chapter 6 is a published paper that discuss leaves from four sugarcane varieties as potential renewable feedstocks for second-generation ethanol production: pretreatments, chemical composition, physical structure, and enzymatic hydrolysis yields.

Chapter 7 presents and discuss the results from sequential LHW and sulfonation pretreatment of SCB for bioethanol production as well as cellulose nanofibers and sulfonated cellulose production via enzymatic hydrolysis and mechanical disintegration

Chapter 8 concludes the thesis with the main concluding remarks and suggestions for future research, which could be carried out as an extension of this work.

2 Chapter 2 Review of the literature: state of the art on lignocellulosic biomass

2.1 Lignocellulosic biomass derived from sugarcane

Lignocellulosic biomass (LB) consists of carbohydrate polymers (cellulose and hemicellulose), aromatic polymers (lignin), and small amounts of acids and minerals, which are turned into ash after combustion. (35) Figure 2-1 represents a lignocellulosic biomass structure from crop bioenergy. The commonly used lignocellulosic biomass is essentially agriculture residues (corn stover, wheat straw, sugarcane bagasse, rice straw, sugarcane straw, etc.), energy crops (poplar trees, miscanthus, switchgrass, big bluestem, etc.), and forestry residues (wood chips, fruit bunch, sawdust), etc. (36)

Sugarcane bagasse is sucrose-free culm in the form of the fibrous residue obtained after extracting juice from sugarcane**,** which is considered one of the most abundant agricultural residues and a promising renewable resource for biorefinery due to its fast growth, wide distribution, and low cost. (37) Sugarcane is one of the most broadly cultivated crops in the world, mainly produced in tropical countries such as Brazil, India, China, Thailand, Pakistan, and Mexico. (38) Worldwide sugarcane production is expected to exceed 2.2 billion tons by 2026. (39) It may be a source of ethanol, sugar, and biomass residue (bagasse) used to produce electrical energy**.** On one side, sugarcane is the most important source of sugar in the world. On another side, sugar industries are one of the most polluting in terms of the generated solid wastes, wastewater, and gaseous emissions of carbon monoxide, volatile organic compounds, and greenhouse gases during crop cultivation. (40) Population growth increased the need for sugar, enhancing sugarcane production. This sugar rise justifies the abundance of residues from sugarcane, such as bagasse, leaves, etc., and their total valorization contributes to reducing the inconveniences associated with sugar production. Brazil is a major sugarcane producer, an essential crop for its economic development. Every 1000 tons of processed sugarcane may generate around 270 tons of bagasse. (41) Brazilian Energy Plan scenarios estimated a mass sugarcane bagasse to be used only for second-generation ethanol, about 25.9×10^6 tons/year for 2030. (42)

The harvested part of the sugarcane is called a culm (Figure 2-2). The culm is structured as a long, solid, cylindrical internode interrupted at intervals by leaf-bearing nodes. During the growth of the

plant, the internode elongates, causing an increase in cellulose and lignin content and a decrease in hemicellulose. These elongation stages depend on the harvesting season and the cultivar. (43) Thus, sugarcane culm possesses different tissue organizations; this heterogeneity can influence the quality of the bagasse generated in the ethanol and sugar industry. (44) In the culm of modern commercial sugarcane varieties, soluble sugars represent around 35% of the photosynthetically fixed carbon and are present mainly in the form of sucrose. The other 65% of the fixed C in sugarcane plants is stored in plant cell walls under non-soluble complex carbohydrates, especially cellulose and hemicellulose. (45)

Another significant sugarcane waste, in the form of leaves (green and dry), is usually abandoned in the field after harvesting green cane. During harvest, removing the leaves by burning them before cutting the sugarcane is a common practice, as leaves are sharp, which causes severe air pollution. (46) The employment of these residues for producing electricity by cogeneration could guarantee the availability of sugarcane bagasse as raw feedstock for second-generation ethanol. (47) Moreover, leaves can also be employed to obtain second-generation ethanol, enhancing bioethanol production. However, in-depth studies on their characteristics as feedstock for biofuel production are still necessary. (47) Generally, the higher lignin and silica content allied with less cellulose percentage of sugarcane leaves makes it challenging to use for industrial applications. (46)

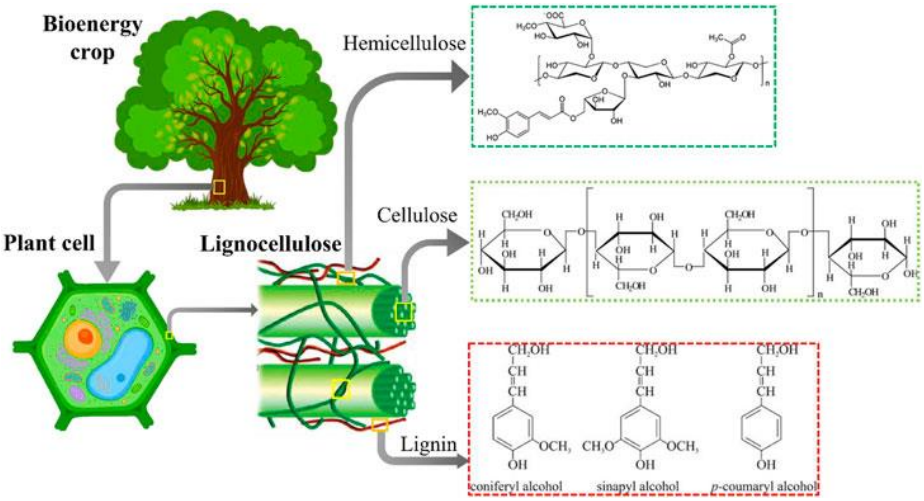

Figure 2-1 - Schematic illustration showing bioenergy crop (lignocellulosic biomass), where the plant cell wall is composed of lignocellulose consisting of carbohydrate polymers such as cellulose, hemicellulose, and the aromatic polymer which is known as lignin. The cellulose and hemicellulose accommodate 6 and 5 carbon sugars rigidly bound with the lignin.

Source: SANKARAN *et al.* (48)

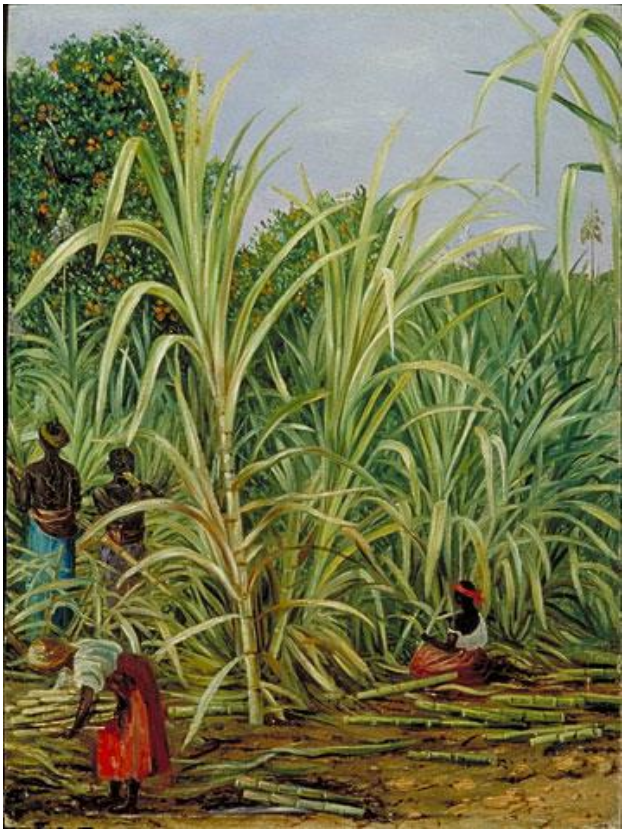

Figure 2-2 - Harvesting the Sugarcane in Minas Geraes, Brazil
Source: KEW. (49)

2.1.1 Cellulose

Cellulose, the most abundantly available natural polymer on earth, corresponds to the repeating unit of glucose homopolymer linked by the glycolic bond β-1,4. Cellulose is the primary substrate from lignocellulosic biomass used for fermentation in Bioethanol production. It is mainly produced by plants, bacteria, and some animals. (50) Cellulose is commonly present in lignocellulosic biomass as a chain packed into a complex structure. Figure 2-3 shows hydrogen bonds connect the cellulose inside (intramolecular) and outside the chains (intermolecular). (51) Individual cellulose chains are parallelly arranged and tightly bound to form crude fibers organized to establish larger fibrillar structures. (52) Six cellulosic polymorphs (I, II, III_1, III_{11}, IV_1, and IV_{11}) are identified. Cellulose I is found in nature. Others are cellulose polymorphs obtained after alteration, and all six polymorphs can be interconverted. (53-54) Cellulose fibers are divided into amorphous and crystalline domains, and their proportion depends strictly on the lignocellulosic

biomass source. The fibers are highly ordered in the crystalline area, whereas they are less organized in the amorphous regions. This structural repartition is an essential property since cellulose is quicker to react in the unstructured domain than in the crystalline area. (55-56) Cellulose possesses various properties, such as hydrophilicity, renewability, biodegradability, mechanical and thermal stability, etc. These proprieties justify its applications in multiple domains, including bioenergy, biomedical fields, pharmaceuticals, textiles, the papermaking industry, etc. (57)

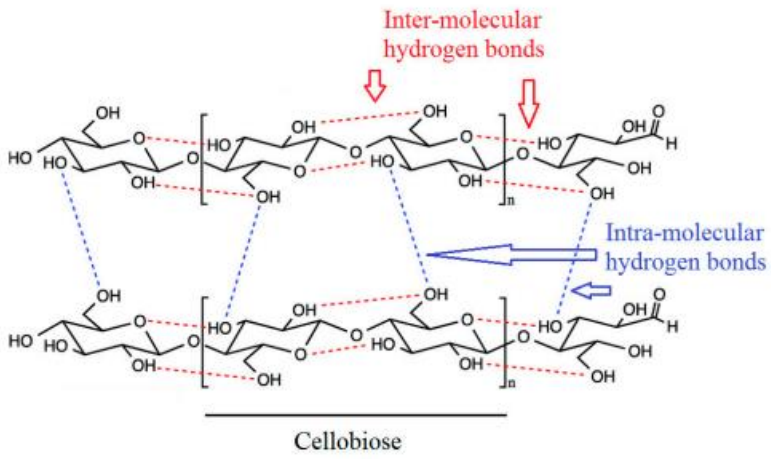

Figure 2-3 - Cellulose structure :
Source : BAGHAEI *et al.* (58)

2.1.2 Hemicellulose

Hemicelluloses widely exist in nature and represent a class of heteropolysaccharides in wood and annual plants. (59) Hemicelluloses consist of short and highly branched chains of various sugars, primarily pentoses (e.g., xylose and arabinose) and hexoses (e.g., mannose, glucose, galactose). (60) The hemicelluloses are located on the cellulose fibril surface and bind the cellulose together with lignin. These polymers are relatively easy to hydrolyze because of their high-branched and amorphous nature. In hardwood, hemicelluloses are composed of xylan, while softwood contains predominantly glucomannan. (52) Figure 2-4 shows an example of a hemicellulose structure (xylan). Due to its physical and chemical properties, such as high molecular weight, non-ionicity, and nontoxicity, hemicellulose is expected to be broadly applied in packaging, food, pharmaceutical, biomedicine, cosmetics, textile, and papermaking industries. (61)

v

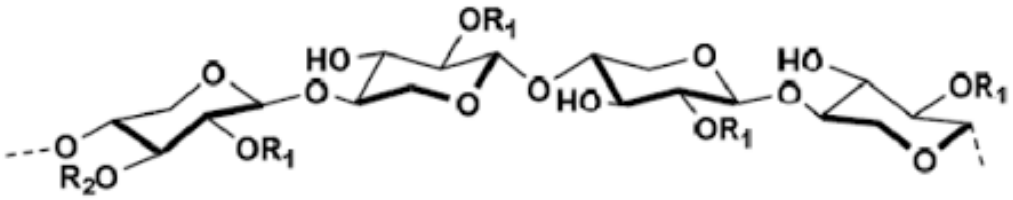

Figure 2-4 - Example of polymers in hemicellulose (xylan).
Source: NETICHA *et al.* (62)

Lignin is a heterogeneous, hydrophobic, and complex aromatic biopolymer formed by three different phenylpropanoid units. (30) The main precursors of lignin are trans-coniferyl alcohol, trans-sinapyl alcohol), and trans-p-coumaryl alcohol. These three phenylpropanoid units conduct the generation of lignin p-hydroxyphenyl (H), guaiacyl (G), and syringyl (S) units linked to each other by ether bonds (β-O-4, α-O-4, and 4-O-5), and carbon-carbon bonds (5-5, β-5, β-1, and β-β). This building block gave lignin an amorphous and complex irregular structure. (25) Depending on its source and the environment, lignin structure presents different concentrations of phenylpropanoid units. Hardwood contains G and S units in a relatively equal proportion. In contrast, softwood comprises G units. (63) The extraction method used for lignin isolation significantly affects lignin proprieties; the exact form of native lignin is still unknown. (64) The three main lignin components are represented in Figure 2-5.

Lignin and Hemicellulose form a protective covering surrounding cellulose and hinder the enzyme from accessing cellulose during enzymatic hydrolysis. Thereby, lignin is the primary responsibility of lignocellulosic recalcitrance to bioethanol production. Meanwhile, lignin is ideal for developing novel materials since its phenolic and aliphatic hydroxyl groups confer considerable potential for chemical modification. (65) Lignin is an excellent candidate for developing novel green materials, including polymer composite materials, thanks to its biodegradability, eco-friendliness, and wide ecological adaptability. (66) It can also be employed as adhesives, biosurfactants, antimicrobial agents in packaging and textiles, antioxidants, adhesives, anticorrosion, carbon fiber or carbon

black, cosmetics, reinforcing agents, hydrogel, phenolic resin, new biomedical materials, and others

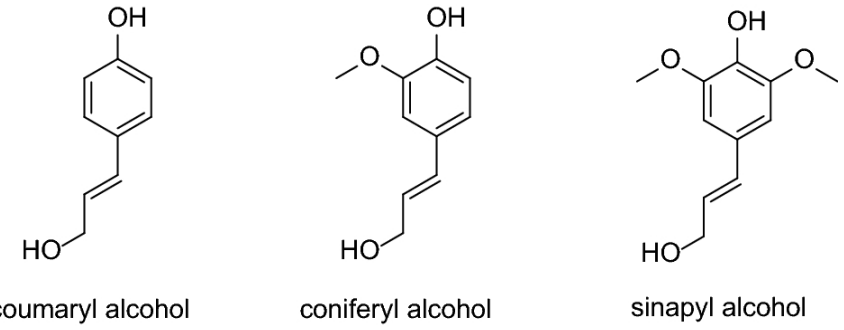

Figure 2-5 - Three main components of lignin.
Source: ERRANI *et al.* (67)

2.2 Bioethanol production from lignocellulosic Biomass

Bioethanol represents a type of alcohol (ethanol) produced through microbial fermentation of carbohydrates from plants or algae and various conversion technologies**.** (68) Although most research efforts focus on converting inexpensive cellulosic substrates to ethanol, cost-competitive methods for gasoline production are still lacking. However, since Bioethanol is appropriate to mix with gasoline in a standard gasoline engine (69), it can reduce fossil fuel dependency. Moreover, bioethanol can minimize particulate and NOx emissions in compression-ignition engines. Biofuel benefits are often linked to land use, adverse effects on gas (GHG) emission balances, ecosystem services, and food and water security. (70)

The first biofuels developed were bioethanol, initially obtained from starch, sugars, and crops (cereal grains, sugarcane, and sugar beets). However, the diffusion of these products, known as first-generation biofuels, found obstacles, including high market prices and competition between biofuels and food production. (71) In this regard, lignocellulosic biomass was investigated as an alternative feedstock to produce second-generation Bioethanol. (72) Meanwhile, two other generations of bioethanol are being developed. Marine biomass or algal biomass is exploited as feedstock for the third generation of bioethanol and has many benefits, such as no land use, a short growth cycle, and a reduction of greenhouse emissions into the environment (algae can rapidly absorb carbon dioxide). (73) Fourth-generation bioethanol production methods are being

developed, utilizing genetically engineered organisms (e.g., yeasts and algae) to improve the productivity of Bioethanol. (74)

Biofuel benefits are often linked to land use, adverse effects on gas (GHG) emission balances, ecosystem services, and food and water security. (70) To ensure food safety, energy accessibility, slow climate change, and sustainable agricultural development and activities, second-generation biofuels have been developed based on converting LB carbohydrates (Cellulose and Hemicellulose) into liquid fuels. Second-generation biofuels allow the use of whole plants, such as woody crops, agricultural residues or waste, and dedicated non-food energy crops grown on marginal lands, thus dramatically increasing productivity. (71) Bioethanol production from lignocellulosic biomass starts with preliminary feedstock preparation, which involves cleaning and reducing biomass size by milling, chopping, or grinding. Then, the bioethanol production process follows three main steps, as shown in Figure 2-6.

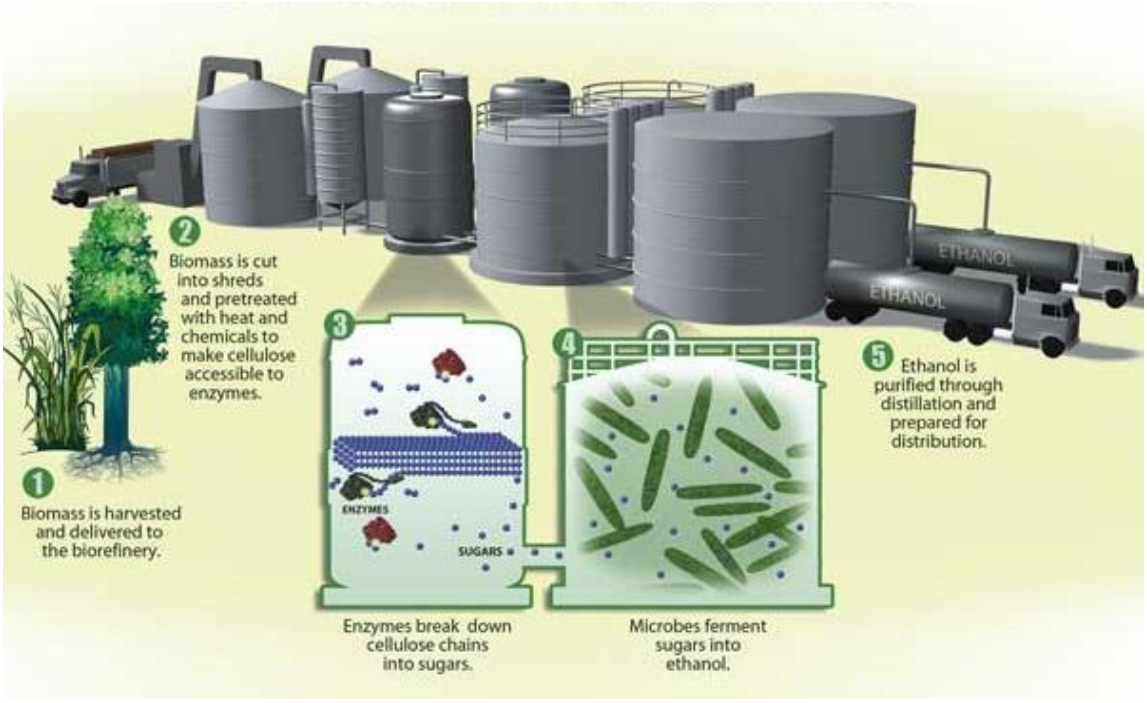

Figure 2-6 - Processes for bioethanol production.
Source: ZOGHLAMI *et al.* (75)

2.2.1 Pretreatments strategies

For liquid biofuel and biobased material productions from lignocellulosic biomass, pretreatment steps are essential. The main challenges faced during converting lignocellulosic biomass into biofuels are associated with the complex structure of biomasses. Indeed, the barrier formed by hemicelluloses and lignin restricts the action of the enzyme on cellulose. (76) Therefore, efficient pretreatments must be employed to disrupt the compact and complex structure under the following requirements: to improve the ability to form sugars by enzymatic hydrolysis, avoid the degradation or loss of carbohydrates, prevent the appearance of inhibitory products in the subsequent hydrolysis and fermentation processes, and be cost-effective. (77) For nanomaterial production, lignocellulose pretreatments aim efficiently fractionate the LB in its different components. (78) Many pretreatment techniques have been developed and generally categorized into physical such as ball milling, mechanical extrusion, etc. Chemical pretreatment involves chemicals such as acids, alkalis, ozone, sulfite, organic solvents, or ionic liquids, physicochemical such as a steam explosion, ammonia fiber explosion, CO_2 explosion, liquid hot water (LHW), wet oxidation, microwave, ultrasound, and biological approaches. The selection of the pretreatment method mainly depends on the composition and characteristics of the biomass. All the pretreatments have their advantages and disadvantages.

Physical pretreatment is considered a prerequisite before further applying the lignocellulosic biomass. Particle size reduction of biomass by milling, chopping, or grinding is the principal goal of physical treatment. (79) The particle size reduction improves the surface area, whereas crystallinity and degree of cellulose polymerization can decrease significantly. However, it requires high energy consumption, conducting to the escalation of electricity demand. (80)

Chemical pretreatments for the lignocellulosic materials involve mixing different chemical reagents with biomass. The primary objective of chemical pretreatment is to disrupt the biomass structure without the necessity of high energy. Chemical pretreatments can be operated efficiently at ambient or moderate temperatures. (81) However, this method may generate toxic substances., demands non-corrosive equipment, and involves different financial circumstances for chemical recovery to sustain the system. (82)

Biological pretreatment uses enzymes or microorganisms for lignin degradation. This process possesses advantages over the previous; it is environmentally friendly and does not generate inhibitors because of its mild reaction conditions. Moreover, biological pretreatment may conduct in higher product yields with less energy demand and less reactor resistance to pressure and corrosion. (83) In this process, microorganisms, such as bacteria and fungi, secrete different lignocellulolytic enzymes to efficiently reduce feedstock recalcitrance and enhance the digestibility with biomass hydrolyzing enzymes. However, there are a few limits to using this strategy for the large-scale process. Challenges of biological pretreatment include longer incubation time compared to conventional pretreatment strategies. (84)

2.2.1.1 Alkaline pretreatment

Alkaline pretreatment is a primary chemical method that utilizes bases such as sodium hydroxide, calcium hydroxide, potassium hydroxide, ammonia, etc., of which sodium hydroxides are more effective in breaking the ester and glycosidic side chain. (85) This method is usually carried out at ambient temperature and pressure, favoring its low capital costs with less special equipment than the acidic alternative. A high pH environment also helps maintain sterile conditions during pretreatment, avoiding the consumption of carbohydrates. Alkaline pretreatment is generally a process of delignification through cleavage of lignin-carbohydrate linkage, which improves the reactivity of the remaining polysaccharides. (86) Alkali reagents promote the decomposition of lignin into low-molecular-weight compounds through the breakup of the α- and β-aryl ethers and glycosidic bonds. In addition, this process can cause partial solubilization of hemicellulose by saponifying the intermolecular ester bonds (e.g., acetyl and ironic acid substitutions, etc.). The main drawback is the incorporation of non-recoverable salts into the biomass during pre-treatment. (87)

2.2.1.2 Dilute Acidic pretreatment (DAP)

Diluted acid pretreatment (DAP) is the most widely used commercial pretreatment, which can break covalent bonds in composite bonds, disrupting the lignocellulosic structure and effectively removing most hemicelluloses. (88) DAP has been applied to diverse plant species on an industrial scale for bioethanol production. (89–91) The most utilized acids are dilute sulfuric acid, nitric acid, and hydrochloric acid. Among these, dilute sulfuric acid is broadly employed due to its low cost

and high efficiency in delignification. (92) DAP is generally carried out over a temperature range of 120°C to 210°C with an acid concentration of less than 5% w/v and an incubation time varying from minutes to hours. DAP primarily leads to hemicellulose hydrolysis, which releases the monomeric sugars and soluble oligomers from the solid LB into hydrolysate, improving the enzymatic digestibility. Partial lignin removal can also occur; however, DAP suffers from some constraints. The main disadvantage during DAP is the formation of several inhibitory by-products such as hydroxymethyl furfural (HMF), furfural, and other derivatives such as phenyl compounds and aliphatic carboxylic acids. (28) Equally, a biomass size reduction is necessary, which consumes large amounts of energy and pH neutralization for the downstream processes. (93) Besides, although the accessibility of cellulose increases during DAP, lignin can form droplets on the surface of cellulose. Under severe conditions, lignin redeposition may occur. These droplets of lignin act as a physical barrier and binds to cellulases unproductively. (94) In addition, acids are highly corrosive to the equipment.(88)

2.2.1.3 LHW pretreatment

Liquid hot water pretreatment utilizes hot water instead of steam at temperatures of 170–240°C. Liquid hot water pretreatment uses higher pressure to maintain the water in its liquid state at elevated temperatures. (95) Then, flow-through processes pass this water through lignocellulosic biomass. This process reduces the downstream pressure by making cellulose more accessible to the enzymes and minimizes the formation of inhibitors that impede the growth of fermentative microorganisms. (96) LHW pretreatments are cost-effective due to the reduced cost of reactor material, with no catalyst requirement and low corrosion potential. Higher pentose sugar recovery and lower inhibitor formation is the most crucial benefit compared to DAP. (97) One of the limitations of liquid hot water pretreatment is the enormous water consumption during the process, which may be a barrier to making it practical for being promoted commercially. Moreover, since the water content is much higher than in steam pretreatment, the resulting sugar solution is more diluted and thus causes the downstream processes to be more energy demanding. (98)

2.2.1.4 Combined pretreatment

Combined or hybrid pretreatment involves combining two or more pretreatment techniques for treating the LB. These combinations show significant advantages, such as enhancing the sugar

production efficiency, limiting the production of inhibitors, and reducing the cost involved in recovery steps after pretreatment. Besides, maximum lignin and hemicellulose removal can occur by adding individual features of the different pretreatments. Currently, other configurations of combined pretreatments such as acid/alkaline (99,100), ozonolysis / liquid hot water (101), alkaline/enzyme (102), etc., have been implemented, and excellent yields of fermentable sugar were obtained after enzymatic hydrolysis.

2.2.2 Hydrolysis

The fuel production from lignocellulosic biomass goes through the conversion of carbohydrates into monomeric sugars by hydrolysis. Also known as saccharification, hydrolysis can be achieved either biologically (enzymatic hydrolysis) or chemically (acidic hydrolysis).

2.2.2.1 Acidic hydrolysis

Acid hydrolysis generally involves using sulfuric or hydrochloric acids to break down cellulose and hemicelluloses. Concentrated acid hydrolysis may be performed at a low temperature, and a high sugar yield is obtained (90% of the theoretical glucose yield). (103) However, it requires high acid concentrations, typically 30-70%, which results in equipment corrosion. Therefore, concentrated acid hydrolysis leads to economic and environmental problems. (104) Moreover, dilute acid hydrolysis requires a much lower amount of acid, 2–5%, which is more commonly applied in the industry. However, it requires a temperature of around 200°C, which can form different inhibitory compounds, such as acetic acid, furfural, HMF, and phenols. These compounds negatively affect the next fermentation step and decrease the sugar yield. (105)

2.2.2.2 Enzymatic hydrolysis

Hydrolysis can be catalyzed by enzymes that convert complex carbohydrates from LB into monomeric sugars. In the longer term, enzymatic hydrolysis processes offer the possibility of achieving competitive prices. Indeed, enzymatic hydrolysis requires mild temperature and pH conditions (50–60 °C and pH 4.5–5.5).(106) These conditions lead to low energy consumption, preventing equipment corrosion and inhibitory formation. In addition, an excellent enzymatic hydrolysis yield of sugars (80–99%) has been attained in eco-friendly conditions. (100,107)

Cellulose conversion into monosaccharides can be performed using a particular group of enzymes named cellulases and hemicellulases. Cellulases are enzymes that catalyze the cellulose polymer breakdown into smaller polymer branches or even into cellobiose and glucose. Complete hydrolysis of cellulose into glucose demands the synergetic actions of three specific enzymes: endo-β-1,4-glucanases (EC 3.2.1.4), cellobiohydrolases (EC 3.2.1.91), and β-glucosidase (EC 3.2.1.21). (108) Endoglucanases (EG) attack the more amorphous parts of the cellulose chains and break them in the middle, releasing more free ends. Cellobiohydrolases (CBH) depolymerize and hydrolyze the highly crystalline regions in cellulose from the ends of the chain, releasing soluble cello oligosaccharides with cellobiose as the primary product. Finally, β-glucosidases (BG) hydrolyze cello oligosaccharides into monomer glucose. (109) Due to the complexity of hemicellulose structure, enzymatic breakdown of hemicellulose requires a diverse set of enzymes such as non-arabinose- and arabinose-liberating endo-xylanases, endo-xylanases (GH families 10, 11, 30, 43, and 51), β-xylosidases (GH families 30, 39, 43, and 51), xyloglucanases (GH families 12 and 74), acetyl xylan esterases (CE families 1–6) and ferulic esterases (CE family 1), β-mannanases (GH families 5, 26, and 134), α-galactosidases (GH families 27 and 36), α-arabinofuranosidases (GH families 2, 3, 43, 51, 5,4 and 62) and α-glucuronidases (GH families 67 and 115), etc., acting on both backbone and the side groups of the hemicelluloses. Many hemicellulases can hydrolyze the spine and the side groups of the hemicelluloses. (84)

Besides cellulases and hemicellulases, non-hydrolytic accessory proteins are essential for disrupting the LB structure, such as polysaccharide monooxygenases, carbohydrate-binding modules, and expansion or expansion-like proteins. (110) Polysaccharide monooxygenases (PMO), a new class of enzymes previously called GH61, increase the efficiency of common cellulases, resulting in increased hydrolysis yields while reducing the required protein loading. They act on the crystalline part of cellulose by generating oxidized, non-oxidized chain ends. An external electron donor is needed to stimulate PMO activity. Several factors can negatively affect the enzymatic hydrolysis of LB polysaccharides. The estimated enzyme cost corresponding to 20% of ethanol production costs is one of the primarily enzymatic hydrolysis limitations. Other limitations of using enzymes are the slowness of reactions, which results in long hydrolysis times. (111) Several factors negatively affect the enzymatic hydrolysis of LB polysaccharides. Lignin bound to hemicelluloses constitutes a structural barrier to enzymes, decreasing its accessibility to cellulose. The higher crystallinity of the cellulose, the lower the enzymatic attack surface. Enzymes can also

bind unproductively to lignin. All these factors underline the importance of LB pretreatments. In addition, the inhibitor products during the pretreatments inhibit cellulases and hemicellulases. (112)

2.2.3 Fermentation

Alcoholic fermentation is a complex biochemical route through which yeasts, some other fungi, and bacteria transform monomeric sugars into ethanol, carbon dioxide, and other metabolic byproducts. (113) Indeed, fermentable monosaccharide and disaccharide sugars are released during enzymatic hydrolysis of cellulosic substrate. Then, yeast converts these sugars (e.g., glucose, galactose, xylose, and fructose) into ethanol, carbon dioxide, and other by-products under aerobic or anaerobic conditions. This process starts with the breakdown of glucose molecules into two pyruvate molecules through a glycolysis reaction. Two molecules of pyruvic acid are obtained during the glycolysis stage and then reduced to ethanol and carbon dioxide. (114) Three main fermentation strategies are employed for the commercial production of bioethanol: liquid/submerged state fermentation, the solid-state fermentation, and very high gravity fermentation. Each method may accomplish any feedstock fermentation; however, one way can be more suitable for a particular feedstock depending on its proprieties. Submerged fermentation is often utilized for first-generation bioethanol production and is based on the fermentable substrate liquefaction, a medium in which microbes. (115) Solid-state fermentation is usually used for second-generation bioethanol production. It is a process in which organisms grow on non-soluble material or solid substrates in the absence or near absence of free water. (116) In addition to bioethanol production, currently, solid-state fermentation is involved in a wide range of applications such as enzyme production, antibiotics, bioactive compounds, organic acids, and biodiesel. (76) A very high gravity fermentation is a possible way to improve ethanol production and reduce the production cost, using musts with high sugar concentrations. (117) In general, sugar concentrations for ethanol production can be divided into normal gravity (<180 g/L of total sugars), high gravity (180–240 g/L of total sugars), and very high gravity (≥250 g/L of total sugars). (109,113-114) Very high gravity fermentation can achieve more than 15% (*v*/*v*) of ethanol, compared to the average of 10–12% (*v*/*v*) generally obtained in most distilleries. (118)

2.3 Nanocelluloses

Nanocellulose is generally isolated from native cellulose found in plant cells. Nanocellulose is a cellulosic material with at least one of its dimensions in the nanometric scale (1 nm = 10^{-9} m). (119) Nanocellulose possesses attractive properties associated with its nanometric scale and intrinsic characteristics of cellulose. These remarkable properties, including high surface area, crystallinity, renewability, biodegradability, non-toxicity, high aspect ratio, low density, excellent mechanical properties, etc., justify the potential applications of nanocellulose in areas such as polymer composites and energy storage devices, rheology modifiers. (21)

The growth of nanocellulose studies portends its potential to replace most synthetic materials in various fields soon. Based on the study reported by Express Wire (2019), which focused mainly on North America, Europe, Asia–Pacific, South America, the Middle East, and Africa, a nanocellulose market is expected to grow at a compound annual growth rate (CAGR) of approximately growing at a CAGR of 22.7% from 2021 to 2026, reaching USD 963 million by 2026, USD 346 million in 2021. (120)

Three categories of nanocellulose morphology can be obtained: Cellulose Nanofiber (CNF), Cellulose Nanocrystal (CNC), and bacterial nanocellulose (BC). The latter is synthesized exclusively by a family of Gluconoacetobacter xylinius. (121) From plant-derived cellulose, cellulose nanocrystals (CNC) and cellulose nanofibrils (CNF) have been extracted following various routes.

Physico-chemical pretreatments have generally been employed to disrupt biomass structure and isolate cellulose from other LB components (Hemicellulose and lignin). (122) The obtained cellulose-rich material must be subjected to a top-down controlled deconstruction strategy to isolate the nanocelluloses defibrillation stage of cellulose fibers to obtain cellulose nanofibers (CNF). Mechanical defibrillation using equipment such as homogenizers, micro-fluidizers, sonicators, and grinders is the standard method to make nanocellulose. This method can provide good CNF yields but necessitate high energy consumption. (123) Thenceforth, to ensure fluidity in defibrillation and minimize energy requirement, chemical or biological pretreatments were generally applied to cellulose fibers prior mechanical disintegration stage. (124)

Chemical techniques take advantage of adding active chemical agents that degrade the cellulose, including acid hydrolysis (using HCl, H_2SO_4, HBr), ionic liquids, metal salts, and TEMPO-mediated oxidation. Several chemical treatment approaches, such as carboxymethylation, including TEMPO (2,2,6,6-tetramethylpiperidine-1-oxyl)-mediated oxidation or and periodate–chlorite oxidation, cationization, and acidic or basic pretreatments were reported in the literature to isolate CNFs. (122,125–127) These processes add charged groups (e.g., carboxyl or carboxymethyl) to the cellulosic fiber surface, enhancing the delamination of the nanofibrils by charge repulsion during mechanical disintegration. (128) Although very efficient, there are significant environmental problems related to using these chemicals for CNF production, particularly for TEMPO-mediated oxidation. (129-130) Concentrated mineral acid hydrolysis (mainly HCl or H_2SO_4) associated with a short mechanical disintegration is the most common method for cellulose nanocrystals (CNC) production. However, these chemical methods present potential environmental risks which limit their further exploitation on an industrial scale. (131)

Biological extraction methods or enzyme-mediated methods are the most eco-friendly, with lower expected capital and operating expenses than physicochemical techniques. Currently, it does not exist enzymes are specifically available for nanocellulose production. However, various enzymes, such as enzymatic cocktails, endoglucanases (EG), xylanases, and lytic polysaccharide monooxygenase, have been demonstrated to facilitate the defibrillation of cellulose fibers into CNF. (132-133) The enzymatic cocktail has the function of breaking the polymer of the cellulose into smaller polymers. The endoglucanases have a relatively moderate activity, which is suitable for the hydrolysis of amorphous cellulose regions without complete hydrolysis for glucose but preserving the crystalline cellulose domain accordingly. Combining enzymes/proteins such as xylanases and polysaccharide lytic monooxygenases (LPMO) can increase the hydrolytic performance of cellulase cocktails mainly by improving the accessibility of enzymes to the cellulosic component. (130) Synergistic actions of LPMO, cellulases, and/or xylanases for the cellulose fiber deconstruction and the production of CNF have been reported in the literature. (134) LPMO act on cellulosic chains by oxidative cleavage of glycosidic bonds, generating oxidized chain ends in different positions, enhancing the substrate sensitivity to cellulase action. (135) The main disadvantage of biological extraction is the high cost of enzymes.

3 Chapter 3 Technics of characterization

3.1 UV visible spectroscopy

UV-Visible spectroscopy is a non-destructive and fast method that provides qualitative access to information about the nature of the bonds present within the sample. Meanwhile, it quantitatively measures solution, specifically for determining concentrations of known solutes. This spectroscopy is widely used in practical chemistry work and chemical or biochemical analysis. (136,137) Spectrophotometers direct a light source through a sample, and a detector on the opposite side records transmitted light, as shown in Figure 3-2.

Light incident (known wavelength and intensity) focuses on the sample cuvette. A detector measures the transmittance light through the cuvette (sample). Considering the incident radiation (I_0) and the transmitted radiation (I), the amount of light absorbed by the sample at that wavelength can be easily calculated. Using the Beer-Lambert law, this absorption can be used to measure concentrations of known solutes:(138)

$$A = \log(I_0/I) = \varepsilon \, l \, C. \qquad (1)$$

where A is the measured absorbance, I_0 is the intensity of the incident light at a given wavelength, I is the transmitted intensity, l is the path length through the sample, c is the concentration of absorbing species, and ε is a constant known as the molar absorptivity or extinction coefficient for each species and wavelength.

However, when measuring in quartz cuvettes (UV-VIS region) or cuvettes made of special optical glass (VIS region), part of the light is lost through reflection at the cuvette surfaces. In order to eliminate this source of error, a reference measurement is made in a cuvette with the same path length but not containing the substance to be measured (Figure 3-1).

After passing through the analyzed substance, the radiation study makes it possible to obtain information on its nature. UV and UV-VIS spectra are recorded at high and low pH, and the results of both for the sample under question are compared with known standards.

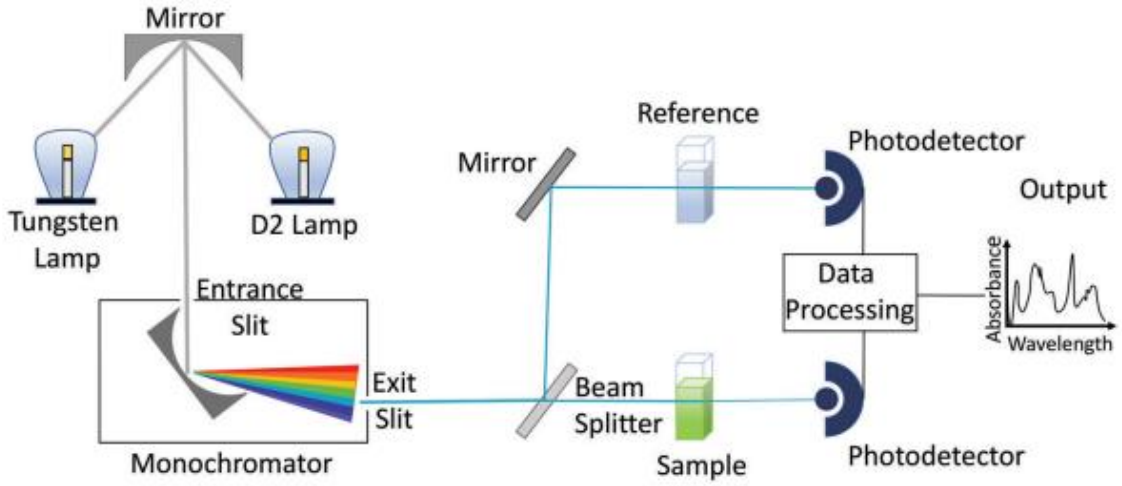

Figure 3-1 - UV-vis spectrophotometer schematic for a double beam instrument. The tungsten lamp emits visible light, while the D2 lamp generates ultraviolet light. The electromagnetic radiation is directed to a monochromator that chooses the wavelengths for the sample.
Source: MAYERHÖFER *et al.* (139)

3.2 High-Performance Liquid Chromatography (HPLC)

High-performance liquid chromatography (HPLC) is the most powerful separation method. It must easily separate mixtures with many similar analytes. (138) The separation process of HPLC is based on the distribution of the analyte (sample) between a mobile phase (eluent) and a stationary phase (column packing material). (140) The stationary phase can be either a solid, porous, surfactant material in small particles or a thin film of liquid deposited on a solid support or a column wall. The mobile phase is always liquid in all types of liquid chromatography. (141)

An HPLC system includes a solvent reservoir, a pump, an injection valve, a column, a detection unit, and a data processing unit (Figure 3-2). The mobile phase of solvent contents is retained in a solvent reservoir. A pump will aspirate the mobile phase from the solvent reservoir and will force it to pass through the column and detector system. Based on the chemical structure of the analyte, the molecules are delayed when they give to the stationary phase. The specific intermolecular

interactions between the sample molecules and the packing material define them “on column” time. Therefore, different constituents of a sample are eluted at other times. Thus, the separation of the ingredients from the sample is achieved. After leaving the column, a detection unit recognizes the analytes. (142) The commonly used detectors are UV-spectroscopy, fluorescence, mass-spectrometric and electrochemical detectors. The separated analytes are recorded as signal peaks by the detection unit. The signals are converted and recorded by a data management system (computer software) and displayed as a chromatogram (total amount of all peaks). Each peak provides qualitative and quantitative information about the analyte. The peak gives qualitative data (e.g., shape, signal intensity, and time of appearance in the chromatogram). Furthermore, the peak area is proportional to the concentration of the substance. Therefore, the chromatography data management software can calculate the sample concentration by integration. This provides quantitative information. (140)

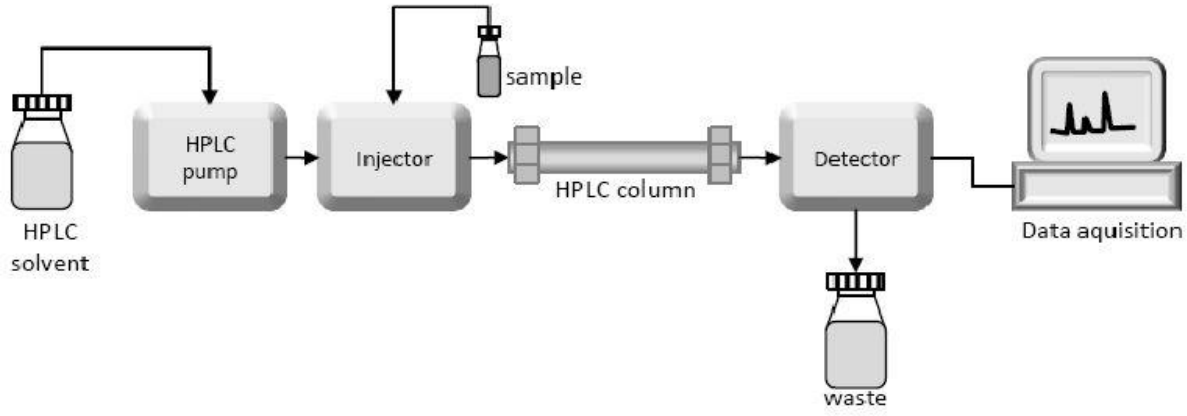

Figure 3-2 - Schematic diagram of the High-Performance Liquid Chromatography (HPLC) system.
Source: VERONIKA *et al.* (143)

3.3 Scanning Electron Microscopy (SEM)

SEM technique is utilized for materials characterization to obtain information about the topography, morphology, surface structure, and composition of materials at the micro-or nanoscale.

A beam of electrons is focused on the sample surface; the interactions (elastic and nonelastic) between electrons and material atoms provoke the emission of secondary and backscattered electrons. (144) Generally, the collected secondary electrons signal is primarily the signal used to

construct an image. The velocity and angle of these secondary electrons are related to the surface structure of the material. A detector catches the secondary electrons and forms an electronic signal that is amplified and transformed into a video scan-image monitored as a digital image. The material should be supported and coated with a conductive coating metal such as gold or platinum unless conductive. (145) The principle of SEM I described in Figures 3- 3.

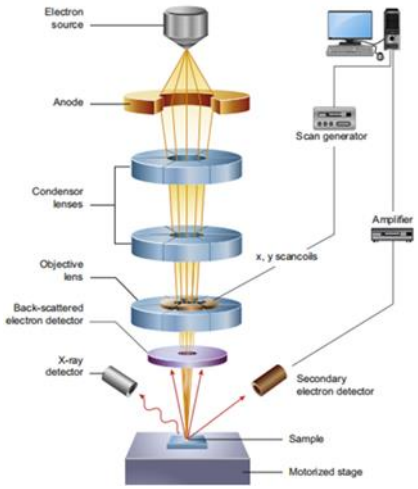

Figure 3-3 - Schematic diagram of the core components of an SEM microscope.
Source: CZAPLICKI. *et al*. (134)

3.4 Atomic force microscopy (AFM)

Atomic force microscopy (AFM), also called scanning probe microscope, is a powerful tool for material characterization on the nanoscale. (146) The AFM allowed the investigation of surface properties and the structure of nanomaterials. Furthermore, AFM measurement can provide quantitative data regarding the surface, including magnetic forces, surface potential, capacitance, friction, and viscoelasticity, as well as information on surface roughness and mechanical and physical properties. (147) AFM was used to analyze surfaces such as polymers, ceramics, and other non-conductive materials. The AFM devices have been used on conductive or insulating, soft or hard, bulk or powder, and organic or inorganic materials. (148)

The AFM devices typically possess a scanner, a cantilever with a pointed probe, a light source, an electronic feedback controller to maintain a given set-point, and a position-sensitive photodetector. Figure 3-4 displays an AFM setup's classic example. (149) The basic principle of AFM

measurement is scanning an excellent probe tip (often made of silicon with a radius of a few nm) across the surface sample. The deflection of the probe is then measured using a laser beam fired and reflected on the back of the cantilever. The reflected laser is detected by a position detector and sent to the signal analyzer. Alternatively, a piezoelectric cantilever is employed, and changes in amplitude or frequency can be electrically measured. (150) Usually, the material is mounted on a piezoelectric holder in the three space directions (x and y for scanning the material, z for maintaining a constant force). The obtained map represents the topography of the material. The primary modes of operation of an AFM are contact mode, non-contact mode, and dynamic contact mode. (150)

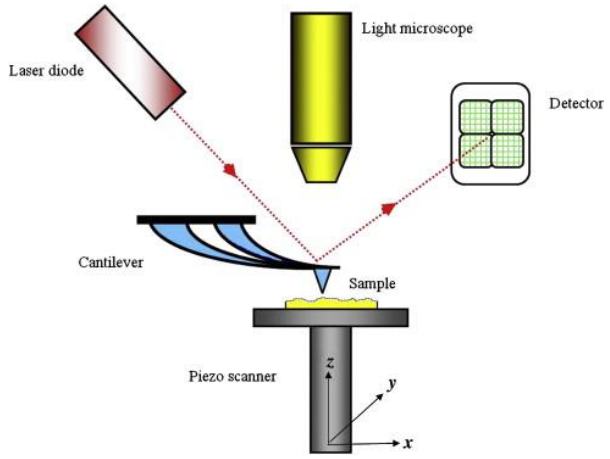

Figure 3-4 - Schematic atomic force microscope (AFM) equipment.
Source: FERRI *et al.* (151)

3.5 Transmission electron microscopy (TEM)

Transmission electron microscopy (TEM) represents one of the most powerful techniques to characterize materials with nanometer-scale features. This microscopy technique employs a beam of high-energy electrons to transmit through a specimen of nanometer thickness. (152) TEM can map samples at resolutions up to the atomic level because of the small de Broglie wavelength of electrons. This technique possesses multiple imaging modes that enable the examination of specimens from various aspects. Information can be collected during the electron beam interaction with the specimen, including size, shape, crystallinity, crystal defects, composition, and elemental mapping. (144)

As presented in Figure 3-5, in TEM operation, a tungsten filament (electron source), heated to incandescence, emits electrons accelerated by high voltage. A series of condenser lenses are then utilized to focus the electron beam to a small zone on the sample (3–5 µm). The lenses used in electron microscopy are electromagnetic, not glass or quartz lenses employed in light or UV microscopy. After penetrating the specimen, the beam passes through the intermediate and projective lens, and finally, the image is viewed on a fluorescent screen or photographic plate. (143)

- .

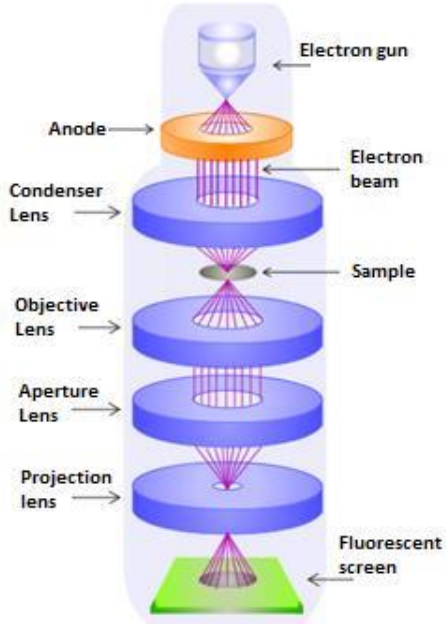

Figure 3-5 - Transmission electron microscope illustration.
Source : ZABEL *et al*. (153)

3.6 X-ray diffraction (XRD)

X-ray Diffraction (XRD) is a powerful and non-destructive technique used in research and industry, which has been performed to examine various materials such as minerals, polymers, plastics, metals, semiconductors, ceramics, solar cells, etc. (154-155) It provides detailed information about the crystallographic structure, chemical composition, and physical properties of materials. The method primarily identifies and characterizes compounds based on their diffraction pattern.

X-ray diffraction base is the interaction of a monochromatic beam of X-rays with a crystallized solid material. When an incident monochromatic x-ray beam interacts with the target material, the x-rays become scattered by the electrons moving around the nucleus of atoms within the target material. These interferences can be constructive or destructive depending on the directions and types of scattered wave interactions. (156) The constructive interference is named diffraction, and these phenomena occur if the target material is arranged under the crystal and polycrystalline forms. Crystalline materials are arranged in a regular pattern, which exhibits changes in properties with direction, and several crystals of different sizes and shapes are combined to form polycrystalline materials. Therefore, apparent to interpret the XRD graphs of crystalline substances. Bragg law described (Equation 1) diffraction conditions.

$$n\lambda = 2d\sin\theta \quad (2)$$

The wavelength of the incident rays is given by λ, d_{hkl} is the interplane spacing, θ is the angle subtending the surface and incident X-rays, and n is a multiplying integer representing the order of diffraction.

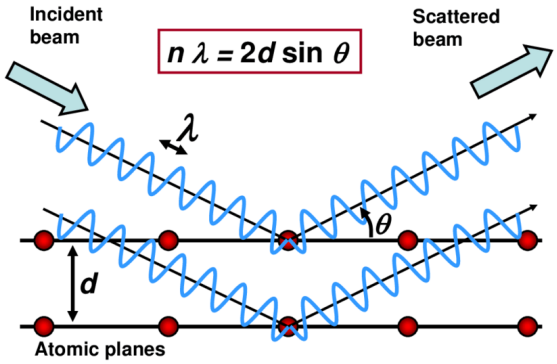

Figure 3-6 - Principle of X-ray diffraction.
Source: FULTZ *et al.* (157)

The obtained diffractograms can furnish qualitative and quantitative information on the material. Qualitative X-ray diffraction analysis compares the experimentally obtained peak positions and intensities to database values. The standard database (JCPDS) for the XRD pattern identifies the phase and determines a large variety of crystalline phases in the concrete specimens. Quantitative analysis involves fitting the pattern. Lattice parameters can be selected from the peak positions.

The FWHM of peaks gives information on crystallinity, non-uniform lattice strain, crystallite size. The XRD analysis can easily detect defects in a particular crystal, its resistance level to stress, its texture, size, degree of crystallinity, and virtually any other variable relating to the sample basic structure. (158)

3.7 Confocal Laser Scanning Microscopy (CSLM)

Confocal microscopy is a practical, wholly integrated electronic system. This advanced light microscopy method utilizes a ‘pinhole’ to eliminate out-of-focus light and is suitable for living and fixing cells and tissues. (159) Indeed, the advantage of a confocal microscope over conventional widefield microscopes is that discrete optical sections can be collected while eliminating out-of-focus light above and below the current plane of focus. For this reason, high-power lasers illuminate the sample to collect enough light only from the desired focal plane. This technique investigates molecules, cells, and living tissues that were impossible just a few years ago. (160)

CLSM configuration consists of one or more electronic detectors, a computer for displaying, processing, output, and storage images, several laser systems combined with wavelength selection devices, and a beam scanning assembly. (161) are presented in Figure 3-8. In a CSLM system, an excitation source (laser) emits coherent light scanned across the sample surface as described below: Coherent light emitted by the laser system (excitation source) passes through a pinhole aperture that is situated in a conjugate plane (confocal) with a scanning point on the specimen and a second pinhole aperture positioned in front of the detector (a photomultiplier tube). When the laser is reflected by a dichromatic mirror and scanned across the specimen in a defined focal plane, secondary fluorescence emitted from points on the specimen (in the same focal plane) passes back through the dichromatic mirror and is focused as a confocal point at the detector pinhole aperture. (162)

Significant fluorescence emission at points above and below the objective focal plane is not confocal with the pinhole (named out-of-focus light rays in Figure 3-). Since only a tiny fraction of the out-of-focus fluorescence emission is delivered through the pinhole aperture, most of this extraneous light is not detected by the photomultiplier. Consequently, it does not contribute to the resulting image. Refocusing the objective in a confocal microscope moves a sample's excitation

and emission points to a new plane that becomes confocal with the pinhole apertures of the light source and detector.

The image is collected by point scanning the area and assembled using a photomultiplier tube, so the image is easily quantifiable. By altering plane focus stepwise, a series of images, all in direction, can be collected over the full depth of the tissue.(162) Collecting optical sections at the correct intervals (see later) makes it possible to create a 3D reconstruction of the entire image series

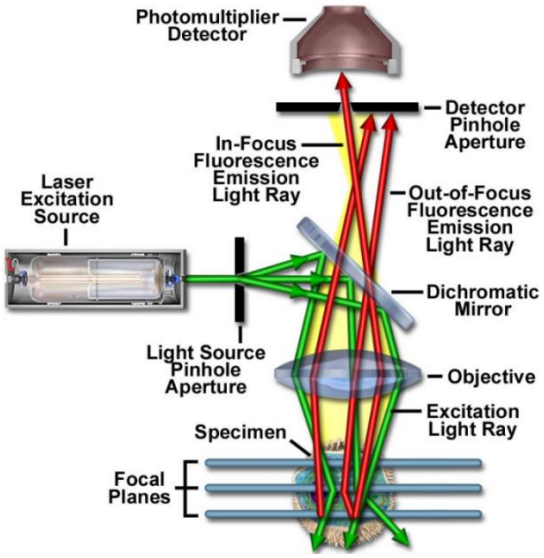

Figure 3-7 - Schematic diagram of the optical pathway and principal components in a laser scanning confocal microscope.
Source: CLAXTON *et al.* (162)

3.8 Nuclear magnetic resonance (NMR)

Nuclear Magnetic Resonance NMR spectroscopy is a valuable method for identifying single-molecular organic compounds. At the same time, NMR spectroscopy provides detailed information about the dynamics of the structure of molecules, reaction state, and chemical environment. (163)

Nuclear Magnetic Resonance is a non-destructive spectroscopic method based on the magnetic properties of the atomic nucleus. Given nuclei within atoms are electrically charged and have a spin. When placed in an intense magnetic field, certain nuclei resonate at a characteristic frequency in the radiofrequency range of the electromagnetic spectrum. A measurable energy transfer can occur and can be used to generate an NMR spectrum. (164)

A slight variation in resonant frequency can give detailed information about the molecular structure in which the atom resides. The resonant frequencies of nuclei are measured and converted into an NMR spectrum that displays all the correct frequencies as peaks on a graph. Each peak height, known as signal intensity, represents nuclei numbers that resonate at each frequency. Furthermore, the more resonating nuclei, the higher the signal intensity. (163) The most common types of NMR are proton and carbon-^{13}NMR spectroscopy. Commun design of an NMR spectrometer with its principal components was represented in Figure 3-8.

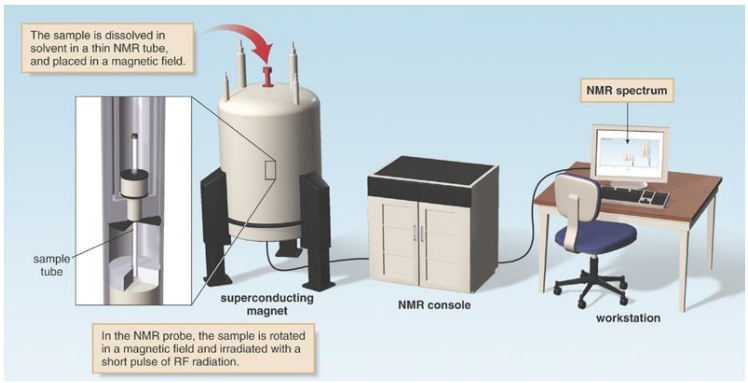

Figure 3-8 - General design of an NMR spectrometer with its principal components.
Source: PURCELL *et al.* (165)

3.9 Thermogravimetric analysis (TGA)

Thermogravimetric analysis (TGA) is an experimental technique involving the continuous weighing of material as a function of sample time or temperature up to 1000 °C. This thermal analysis method has been utilized to provide information about the kinetics of the thermal decomposition of samples to evaluate their thermal stability etc. (166) In addition, TGA has been performed to study factors, such as crystallinity effects, molecular weight, orientation, tacticity, and the substitution of hydrogen atoms, that affect the material's thermal stability. (166) TGA device includes a furnace, microbalance, temperature controller, and a data acquisition system. The sample mass is measured using microbalance while it is heated or cooled in the furnace, according to the predetermined program. (167-168)

The sample is typically heated in a crescent or decreasing temperature at a constant rate or an isothermal temperature. Moreover, it is possible to subject the sample to non-linear temperature

programs such as those used in sample controlled TGA experiments. The choice of temperature program will depend on the expected information. In addition, the atmosphere utilized in the TGA experiment is essential and can be reactive, oxidizing, or inert. (169) Results of TGA measurement are usually displayed under TGA curve form, which represents the plot of the percentage of mass as a function of temperature and/or time. An alternative and complementary presentation of the results consists of using the first derivative of the TGA curve (the differential thermogravimetric or DTG curve), respecting the temperature or the time. (166) This shows the changes in mass rate. Mass changes occur when the sample loses material or reacts with the surrounding atmosphere in several ways. This produces steps in the TGA curve or peaks in the DTG curve. Several effects can cause a sample to lose, or even gain, mass, making steps in the TGA curve. (166)

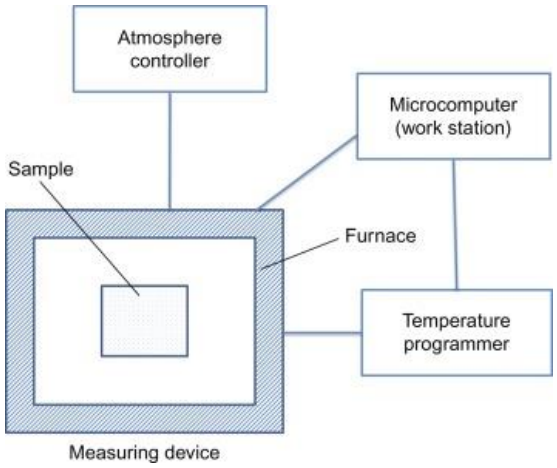

Figure 3-9 - Block diagram of a thermal analysis instrument.
Source: ABRAHAM *et al.* (170)

4 Chapter 4. Methodology

4.1 Chemical composition determination

The chemical characterization of untreated and pretreated LB was performed following two-step hydrolysis procedures using 72% (w/w) H_2SO_4 solution according to the protocol developed by NREL. (136) Chemical composition was determined, assuming LB was composed only of extractives, hemicellulose, cellulose lignin, and ash. All the measurements were conducted in triplicate biomass.

4.1.1 Raw material

In this work, the first project was carried out using Sugarcane (*Saccharum spp.*) culms (SC) of two different sugarcane varieties (LCP 85-384 and NA 78-724), termed SC384 and SC724, and two energy cane (INTA 05-3116, and INTA 05-3118) varieties, subsequently named EC3116 and EC3118 were used as raw materials. The second project was realized with leaves from sugarcane culms and energy cane culms previously used. Sugarcane bagasse was utilized for the third and fourth projects. Each LB was washed, dried, ground using a knife mill (20 mesh), and stored for future utilization.

4.1.2 Determination of extractive and ash contents of raw material

The extractives of raw material were removed by adding 3 g of LB and 300 ml of 1:1(v/v) cyclohexane/ethanol solvent mixture into an extraction thimble under reflux in a Soxhlet extraction apparatus (as shown in Figure 4-1) for 8 h, bags of filter papers containing the samples. The same cycle was repeated five times, replacing the cyclohexane–ethanol solution with water. Then, the samples were dried after extraction in an oven for 24h at 40°C, then at 105°C. Extractive content (%) was calculated through the following equations:

$$E_x(\%) = \frac{M_i - M_f}{M_i} \times 100\% \quad (3)$$

E_x (%) is the extractive content (%) of Raw material

Mi corresponds to the raw material mass initially weighed for extraction.

M_f represents the mass weighed after the extraction and drying step at 105 °C.

Ash contents of raw material were obtained by calcinating raw material in an oven for 4 h at three different temperatures: 1 h at 200 °C, 1 h at 400 °C, and 2 h at 800 °C. The ash content in this biomass can be determined considering the mass of biomass weighed for incineration (Minc) and the mass of ash M(Ash) obtained after incineration, as displayed in the following equation 6:

$$\% \text{ Ash} = \frac{\text{M(Ash)}}{\text{M}_{\text{inc}}} \times 100\ \% \qquad (4)$$

Figure 4-1 - Extraction from lignocellulosic biomass using Soxhlet equipment
Source: By the author

4.1.3 Two steps of acidic hydrolysis

Raw material without extractive was hydrolyzed with 72 % (v/v) H_2SO_4 solution for 7 minutes using a 1:10 (g/mL) biomass to solution ratio at 45°C under vigorous magnetic stirring, followed by dilution with water, up to 4% sulfuric acid solution. A secondary high-temperature (121°C) hydrolysis of the mixture was carried out by autoclaving for 30 minutes. Then, the slurry was

cooled at room temperature. The acid hydrolysate was separated from solid residues via filtration using a previously weighed filter paper.

4.1.4 Carbohydrate quantifications

Acid hydrolysate samples obtained previously were diluted and filtered using 0.45 µm filters (Millipore Filters) for high-performance liquid chromatography analysis. Sugars and degradation products, including glucose, xylose, arabinose, acetic acid, hydroxymethyl furfural, etc., were separated using high-performance liquid chromatography (HPLC) and detected with a refraction index detector coupled with a Biorad Aminex HPX-87 H column at 65 °C, using a 5 mM H_2SO_4 solution as a mobile phase at a flow rate of 0.6 mL/min^{-1}. Sugars and degraded products were identified and quantified by comparing with the glucose, xylose, acid acetic, furfural, acid formic, glucuronic acid, arabinose, mannose, and hydroxymethyl furfural standards. The obtained sugar and degraded product concentrations were utilized to quantify LB cellulose and hemicellulose content. The concentrations of released glucose, cellobiose, and HMF can be used to calculate the cellulose content. The concentrations of released xylose, arabinose, glucuronic acid, acetic acid, and furfural can determine the hemicellulose fraction, considering their respective conversion factors. Conversion factors of glucose, cellobiose and HMF were respectively 0.9, 0.95, and 1.29. Those for xylose, arabinose, acetic acid, and furfural were 0.88, 0.88, 0.72, and 1.37, respectively. (171) The glucose and xylose concentrations obtained after acid hydrolysis allow to quantify of cellulose and hemicellulose, respectively, according to the following equations:

$$\%\text{Hemicellulose} = \frac{C(\text{xylose}) \times V \times 0.88}{m} \quad (5)$$

$$\%\text{Cellulose} = \frac{C(\text{glucose}) \times V \times 0.9}{m} \quad (6)$$

The C(xylose) and C(glucose) represent, respectively, xylose and glucose concentrations (mg/ml) obtained after acidic hydrolysis, V (ml) represents the volume of the reaction mixture, and m (mg) means the weight of culm used for acidic hydrolysis. Thus, numbers 0.9 and 0.88 were the

conversion factors of glucose and xylose because of the addition of water molecules to the anhydroglucose residues in the cellulose and hemicellulose hydrolysis process.

Figure 4-2 - High-Performance Liquid chromatography (HPLC) equipment
Source: By the author

4.1.5 Quantification of lignin

The lignin fraction in raw material was calculated as the summation of acid-insoluble lignin and acid-soluble lignin.

4.1.5.1 Determination of soluble lignin

The soluble lignin was determined by analyzing light absorption at 280 nm by hydrolysate using a UV–visible spectrophotometer. The absorbance of the solution containing 5 ml aliquot of hydrolysate, which was adjusted to pH 12 using 6 M NaOH and diluted 20-fold, was read at 280 nm. The concentration was determined following the equations below:

$$C_{lig} = (A_{lig280} - A_{pd280})/\varepsilon_{lig} \quad (7)$$

Herein C_{lig} represents a concentration of soluble lignin, A_{lig280} represents the absorbance of sugar-degradation products (furfural and HMF):

$$A_{p280} = c_1\varepsilon_1 + c_2\varepsilon_2 \quad (8)$$

C_1 and C_2 correspond to concentrations of furfural and HMF, respectively whereas ε_1 and ε_2 represent absorptivity at 280 nm of furfural and HMF, respectively.

4.1.5.2 Determination of insoluble lignin

The lignin retained in filter paper, thoroughly washed with distilled water (1600 ml) to ensure the complete sulfate removal, was dried at room temperature, followed by a drying series at 105 °C for 2 h and weighing each time until weight stabilization. The ash contents in the insoluble lignin were obtained by calcinating solid residue in an oven for 4 h at different temperatures: 1 h at 200 °C, 1 h at 400 °C, and 2 h at 800 °C. Thus, insoluble lignin content was calculated as shown in the following equation:

$$\%\text{Insoluble lignin} = \frac{\mathrm{M_{ins-lig} - M_{lig-ash}}}{\mathrm{M_i}} \times 100\% \quad (9)$$

M_i: The raw material mass used for two-step acidic hydrolysis

$M_{ins\text{-}lig}$: The insoluble lignin mass obtained after drying at 105°C

Figure 4-3 - Autoclave utilized for Lignocellulosic Biomass Pretreatment (A), LHW Autoclaved SCB (B)
Source: By the author

4.2 Pretreatment stages

During this work, physical and chemical pretreatment was performed. Firstly, all the used LB have been submitted to particle reduction through grinding. Then, pretreatments were applied to LB following different configurations: Culm and leaves from Ecs and SCs were submitted to sequential acid- alkaline pretreatments, SCB was subjected to the sequential LHW – neutral /alkaline sulfonation for improving the monomeric sugar production after enzymatic hydrolysis.

4.2.1 Sequential acid-alkaline pretreatments (

Leaves from ECs and SCs were initially hydrolyzed with dilute acid (H_2SO_4 (1% v/v)) for 40 minutes in the autoclave at 121 °C. The ratio of biomass to liquid was maintained at 1:10 (grams of bagasse/mL of solution). At the end of pretreatment, the biomass was cooled at room temperature, and filtration separated a solid fraction from the hydrolysate. This material was washed with tap water to eliminate the excess acid before oven drying at 40 °C. A second pretreatment step was applied to a fraction of dilute acid pretreated leaves, using NaOH (1 % w/v) with a residence time of 40 minutes in an autoclave at 121 º. (more detailed in Chapter 5: published paper)

The same process of sequential acid -alkaline pretreatment was applied to the culms from Ecs and ECs using, this way, dilute H_2SO_4 (2% v/v)/ NaOH (2 % w/v) instead of H_2SO_4 (1% v/v)/ NaOH (1 % w/v). (More detailed in chapter 6: published paper).

4.2.2 LHW-sulfonation pretreatments

4.2.2.1 Liquid hot water pretreatment (LHW)

Raw SCB was submitted to liquid hot water pretreatment via boiling at 100ºC and autoclaving at 120ºC. Then, pretreatment time and enzyme loading effects on LHW pretreatment efficiency were evaluated. Indeed, LHW pretreatment was performed for 30, 60, and 120 min. Moreover, the pretreated sugarcane bagasse was hydrolyzed using 5mg/g, 10 mg/g, and 25 mg/g enzyme-to-substrate ratio.

4.2.2.2 Neutral/alkaline sulfonation

To emphasis the sulfonation effects, raw SCB was submitted to neutral sulfonation and LHW pretreated bagasse were subjected to neutral and alkaline sulfonation.

4.2.2.2.1 Neutral sulfonation

Raw material and LHW pretreated bagasse were sulfonated in an autoclave at 121°C for 2h, using sodium sulfite (Na_2SO_3) and Milli Q water at a 1:10 (g/mL) biomass to water ratio, using 0.16 g/g of sulfite de sodium to biomass weight ratio. The obtained residues were oven-dried at 40°C for 48 hours.

4.2.2.2.2 Alkaline sulfonation

LHW pretreated bagasse were sulfonated into alkaline media, mixing a 1:1 solution of 2% (w/v) NaOH and sodium sulfite (Na_2SO_3), using a 1:20 (g/mL) fiber to solution ratio at 121°C in the autoclave for 120 min and 0.16 g/g of sulfite de sodium to biomass weight. The mix was filtered, the lignin liquor was isolated, and the obtained residues were oven-dried for 48h at 40 °C.

4.3 Enzymatic hydrolysis performance

In all the projects, commercial cellulase enzymes Cellic CTec3 (Novozymes) were used for the untreated and treated samples' glucan conversion and xylan conversion. All single-step enzymatic pretreatment experiments were performed in 50 mM sodium citrate buffer (pH 5.0) at 50 °C, using a substrate to buffer ratio of 10 % (weight per volume). The reaction volume (10 mL) was conditioned in 250 ml Erlenmeyer flasks and kept in an orbital shaker at a constant shaking speed (180 rpm) for 72 h. Every 24 h, aliquots from the supernatant were taken, boiled in water for 10 min to inactive the enzyme, and centrifuged. The liquid fraction was collected to quantify soluble sugars, such as xylose and glucose. Glucan and xylan yields were calculated based on the release of glucose and xylose after enzymatic hydrolysis according to the following equations:

$$\mathrm{GY} = \frac{\mathrm{GC}\times\mathrm{V}\times 0.9}{\mathrm{m(glucan)}} \times 100\% \quad (10)$$

$$\mathrm{XY}(\%) = \frac{\mathrm{XC}\times\mathrm{V}\times 0.88}{\mathrm{m(xylan)}} \times 100\% \quad (11)$$

Where GC and XC are, respectively, the concentration of Release glucose (mg/ml) and xylose, V is the volume of enzymatic hydrolysis medium, 0.9 and 0.88 were, respectively, the conversion factors of glucose and xylose, m(glucan) and m(xylan) are respectively the weight (mg) of glucan and xylan in initial biomass.

Figure 4-4 - Incubator Shaker utilized for enzymatic hydrolysis
Source: By author

4.4 Nanocellulose production

The CNF isolation process from sugarcane bagasse was divided into three steps (Figure 4-2): pretreatment, partial enzymatic hydrolysis, and mechanical disintegration using ultrasonication. Firstly, SCB was subjected to one of two different types of pretreatments: one involving a delignification (or bleaching) step to obtain bleached bagasse (BB) samples (Route 1), which were sequentially sulfonated to obtain bleached-sulfonated bagasse (BSB) samples (Route 2). Then BB and BSB samples were hydrolyzed with two different enzymatic loadings resulting in the liberation of glucose in solution from remaining partially hydrolyzed solids. CNF was then obtained by sonication and filtration of the partially hydrolyzed solids.

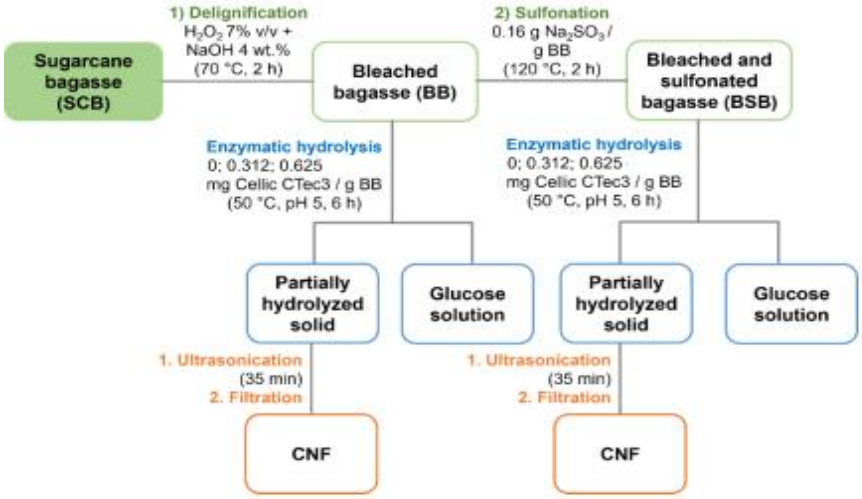

Figure 4-5 - Schematic representation of the CNF isolation process from sugarcane bagasse.
Source: By the author

4.4.1 Delignification

Dried and milled raw SCB was treated using a 1:1 solution of 4% (w/v) NaOH +7% (v/v) H_2O_2 using a 1:20 (g/mL) solid: liquid ratio at 70 °C for 2 h and under mechanical stirring at 120 rpm, Then, the solid fraction was recovered by filtration, washed with tap water until neutral pH, and oven-dried for 48 h at 40 °C.

4.4.2 Sulfonation

BB solid was sulfonated using 0.16 g of Na_2SO_3 per g of biomass in a 1:10 (g/mL) solid: liquid ratio for 2 h at 120 °C in an autoclave. Then, the BSB solid was separated by filtration and oven dried as described previously.

4.4.3 Enzymatic-assisted nanocellulose production

BB and BSB solids were hydrolyzed using the enzymatic cocktail Cellic CTec3 at 50 °C for 6 h in citrate buffer (50 mmol/L, pH = 5) at a solid: liquid ratio of 1:10 (g/mL). The reactions were performed using different enzyme loadings: 0 (control), 0.312, and 0.625 mg enzyme/g of the substrate. After the reaction period, hydrolyses were stopped by heating the reactions to 95 °C for 15 min and centrifuged at 3500 rpm for 20 minutes. An aliquot of the supernatant was collected

for glucose quantification, and the solids were stored at 4 °C without drying for ultrasonication (Figure 4-5).

4.4.4 Mechanical disintegration

The substrates, after enzymatic hydrolysis, were mechanically treated in a Branson Ultrasonics SonifierTM (Digital Sonifier 250 W) equipped with the 3.2-mm-diameter tip at 50% of amplitude for 35 min. Prior to ultrasonication, the concentration of substrate dispersions was adjusted to 5 g/L using deionized water. After ultrasonication, the distribution was filtered using 150 thread mesh to isolate CNF from the non-converted fibers.

4.5 Physicochemical characterizations

To emphasize the pretreatment effects on LB, structural and morphological analysis was carried out on untreated and treated samples. Changes in biomass crystallinity were investigated using X-ray diffraction (XRD). The structural analysis was performed using Nuclear Magnetic Resonance (NMR), Confocal Laser Scanning Microscopy (CLSM). Morphological analyses were done through Scanning Electronic Microscopy (SEM), TEM, and AFM techniques.

4.5.1 Scanning Electron Microscopy (SEM) performance

SEM analysis of culms and leaves was applied to investigate structural changes in the morphology of untreated and pretreated biomass. The dried samples were fixed on suitable stubs and then coated with Au in an SCD 050 sputter coater (Oerlikon-Balzers, Balzers, Liechtenstein). Following fixation, images were captured at different magnifications using a field emission electron microscope (Zeiss, SIGMA model).

4.5.2 Field-emission electron microscopy (FESEM)

Raw SCB samples, BB and BSB samples before and after enzymatic treatments were analyzed in an FEI. Quanta FEG 250 operating at 2 kV. Samples after enzymatic hydrolysis were freeze-dried, fixed on the sample holder with carbon tape, and then coated with an iridium film (*ca.* 5 nm) using a BALTEC MED 020 sputter coater (13.4 mA for 70 s). At least 20 images were obtained to ensure statistical analysis.

4.5.3 Atomic force microscopy (AFM.)

AFM analyzed CNF samples under environmental conditions in the non-contact mode in a Shimadzu SPM9600 microscope using silicon tips (NCHR Point probe, Nanoworld). Topography maps were obtained using a cantilever with a spring constant of 42 N/m and a nominal resonance of 318 kHz. The software Gwyddion 2.56 (gwyddion.net) was used for data treatment and particle measurements using the height image profiles (150 particles of each sample were measured to ensure the statistics). Samples were prepared by adding a drop (5 µL) of a nanoparticle dispersion (0.0025 wt.%) on a cleaved mica substrate, which was dried inside a desiccator for 4 h.

4.5.4 Transmission electron microscopy (TEM)

TEM analysis of CNF was performed in a Carl Zeiss LIBRA 120 equipment using a tungsten filament operating at 120 kV. Samples were prepared by adding a drop (5 µL) of nanoparticle dispersion (0.0025 wt.%) on a copper grid, followed by drying in a desiccator.

4.5.5 X-ray diffraction (XRD) performance

In order to follow crystallinity behavior during the pretreatments all raw materials (SCC, SCL and SCB) and pretreated samples was submitted to x-ray diffraction analysis. The X-ray diffractograms were recorded on a diffractometer RU200B (Rigaku, Japan) using copper radiation (λ = 1.54 Å) generated at an applied voltage of 45 kV and a current of 36 mA equipped with a graphite monochromator. To evaluate the crystallinity index, deconvolution method described by Park *et al.*. (2010) using the Peak fitting program (Peak Fit; www.systat.com) and Segal method (172,173). Thus, to separate amorphous and crystalline contributions to the diffraction spectrum by a curve-fitting process, a Peak fitting program (Peak Fit: www.systat.com) was used, and the amorphous peak was predicted to be at around 21.5º. The following equation (12) calculated the Segal CrI (%):

$$\mathrm{CrI} = \frac{I_{200} - I_{am}}{I_{200}} \qquad (12)$$

I_{200} is the total intensity of the (2 0 0) peak for cellulose at 22.7◦ peaks for cellulose I, and I am the amorphous intensity at 18◦.3 for cellulose I.

The crystallite sizes (D) were calculated following Scherrer equation (174,175) below:

$$D = \frac{K\lambda}{\beta \cos\theta} \quad (13)$$

Where K is the correction factor (0.9), λ is the wavelength of the X-ray radiation (1.54056 Å), β is the FWHM of the diffraction peak in radians, and Θ is the diffraction angle of the peaks.

4.5.6 Confocal laser scanning microscopy (CLSM) performance

CLSM was used to analyze the lignin autofluorescence of the untreated and treated culms, leaves and SCB samples. CLSM images were collected using a Zeiss LSM 780 confocal microscope equipped with a Coherent Chameleon laser (Tisapphire). Samples were immersed in water and analyzed with a Plan-Apochromat objective lens (20 X) in an excitation source for two-photon excitation (2P), as described previously by Coletta *et al.* (2013) and Santos *et al.* (2018) (176,177).

4.5.7 Low-field nuclear magnetic resonance (NMR) studies

The porosity and specific surfaces of untreated and pretreated SC leaves and SCB was investigated using Low-field nuclear magnetic resonance.

Porosity and water accessibility are intimately related to the enzyme accessibility to cellulose. Low-field nuclear magnetic resonance (NMR) is a physical technique that evaluates porosity and water accessibility in the samples. The excess water was removed by gently rubbing the samples with a paper towel, and the wet mass was measured. NMR experiments were carried out in samples previously dried at 80° C under an 800-mmHg vacuum for 5 hours and soaked with ultrapure water (MilliQ, Millipore Inc.) overnight. Then the samples were centrifuged with a rotation frequency of 1000 rpm for 1 minute and filtrated (Corning® Costar® Spin-X, 0.45 μm, nylon membrane). Relaxation measurements of 1H NMR were carried out using a CPMG (Carr-Purcell-Meiboom-Gill) sequence with the acquisition of 35,000 echoes and a permanent Bruker Minispec MQ-20 spectrometer (Bruker, Billerica, USA) operating at 0.47 T (20 MHz).

Data of NMR relaxation were analyzed by Inverse Laplace Transform (ILT), resulting in a distribution of transverse relaxation times (T2).(178-179). Echo times of 70 μs and recycle delay of 15 seconds. The contribution of each interstitial scale of the biomass was analyzed by deconvoluting T_2 distributions using logarithmic-Gaussian (log-Gaussian) functions. These experiments were conducted in duplicate, and the ILT was carried out on the CPMG decay given by the mean of the normalized data from these two experiments.

When a fluid is confined inside a pore, the interaction between the pore surface and the 1H nuclear spins of the fluid molecules imply a reduction of the observed transverse relaxation rate. T2, then T2 distribution of this fluid reflects its pore size distribution media qualitatively. This effect is directly dependent on the pore size. On the fast diffusion limit, the relation between T2 and the pore size is given in Equation3 (180-182)

$$\frac{1}{T_2} = \rho \left(\frac{S}{V}\right) = \frac{2\rho}{r}, \quad (14)$$

With ρ_2 the surface relaxivity, a constant that is often unknown, and S and V are pore surface and volume, respectively. When dealing with a complex pore structure, such as in lignocelluloses, the CPMG decay has a multiexponential behavior, described by a T2 distribution which is directly related to the pore size distribution

4.5.8 ^{13} C Solid-state NMR spectroscopy

^{13}C Solid-state NMR spectroscopy (^{13}C ssNMR) experiments on untreated and pretreated SCB were performed using a BRUKER Avance 3 Spectrometer operating at frequencies of 100.5 MHz and 400.0 MHz for ^{13}C and ^{1}H, respectively. A 7 mm, double resonance magic angle, spinning probe with frequency stability superior to 2 Hz was used. Ramped ^{1}H-^{13}C cross-polarization under magic angle spinning with RF amplitude varying between 80 – 100 % during 1 ms of contact time was performed as an excitation method. Total Suppression of Spinning Sidebands was applied along with Magic Angle Spinning of 4.5 kHz and high-power dipolar decoupling of 70 kHz (^{13}C CPMAS-TOSS). ^{13}C, and ^{1}H 90° pulse lengths of 3.5 and 4.0 μs, respectively, were typically used. All ssNMR measurements were performed using 2 s recycle delays.

4.5.9 Zeta potential (ζ-potential)

CNF ζ-potential was determined using a Zetasizer® 300 HS (Malvern, UK). All measurements were performed in triplicates with at least 10 scans each in backscattering (173°) mode. Samples were diluted to 0.5 wt.%, and the pH was adjusted to 7 before the analysis.

4.5.10 Conductometric titration

The acid groups in CNF were quantified by the conductometric titration method, as described by Katz, Beatson & Anthony (1984).

4.5.11 Thermogravimetric analysis (TGA)

TGA of the CNF was carried out in a PerkinElmer 4000 equipment under a nitrogen atmosphere at 50 mL min^{-1}. Samples with initial weight varying from 4 to 10 mg were placed in ceramic sample holders and heated from 30 °C to 600 °C, with a 20 °C min^{-1} heating rate.

4.5.12 Statistical analysis

Analysis of variance (ANOVA) and DGC multiple comparison tests(183) were used to analyze the effect of pretreatments on the chemical composition of EC and SC varieties, as well as the impact of pretreatments, hydrolysis time (24h, 48h, and 72h) and a various type, on the enzymatic hydrolysis yield obtained from SCL. Info starts software (184) was used for statistical analysis.

5 Chapter 5: Published paper

https://doi.org/10.1007/s12649-021-01528-5

ORIGI

Evaluating the Potential of Culms from Sugarcane and Energy Cane Varieties Grown in Argentina for Second-Generation Ethanol Production

Aissata Ousmane Kane[1] · Vanessa O. Arnoldi Pellergini[1] · Melissa C. Espírito Santo[1] · Balla Diop Ngom[2] · José M. García[3,4] · Alberto Acevedo[5] · Luis E. Erazzú[3] · Igor Polikarpov[1]

Received: 5 March 2021 / Accepted: 14 July 2021

Abstract

The efficient transformation of lignocellulosic biomass into fermentable sugars is essential for building bioeconomies. Sugarcane is an important agricultural crop in a number of Latin American countries, including Brazil and Argentina. Herein culms from two different sugarcane (SC384 and SC724) and two energy cane varieties (EC3116 and EC3118) bred in Argentina were evaluated for sustainable production of second-generation biofuels and green chemicals. Changes in the biomass crystallinity, structure, and morphology introduced by pretreatments were investigated using X-ray diffraction (DRX), confocal laser scanning microscopy (CLSM), and scanning electron microscopy (SEM) techniques. Enzymatic hydrolysis yields of untreated and pretreated sugarcane and energy cane culms were determined and correlated with physical analyses and chemical composition characterizations. Overall, after combined acid and alkali pretreatment, enzymatic convertibility was highly efficient for all studied sugarcane and energy cane varieties, reaching over 97% of theoretical conversion yields. High crystallinity indices and crystallite sizes of pretreated culms and SEM results and CLSM were consistent with the removal of lignin, solubilization of hemicellulose, and amorphous parts of lignocellulose imprinted by the pretreatments. High potential of culms from sugarcane and energy cane varieties cultivated in Argentina for sustainable production of renewable lignocellulosic sugars and their transformation into green chemicals and fuels was demonstrated.

* Igor Polikarpov
:
ipolikarpov@ifsc.usp.br

1 São Carlos Institute of Physics, University of São Paulo, Av. Trabalhador São-carlense, 400, São Carlos, SP 13566-590, Brazil

2 Faculté des Sciences et Techniques, Université Cheikh Anta Diop de Dakar (UCAD), B.P. 5005, Dakar-Fann Dakar, Senegal

3 Agricultural Experimental Station of Famaillá, National Institute of Agricultural Technology (INTA), Famaillá, Tucumán, Argentina

4 National Council of Scientific and Technical Research (CONICET), Ciudad Autónoma de Buenos Aires, Buenos Aires, Argentina

5 Institute of Soils, National Institute of Agricultural Technology (INTA), Castelar, Buenos Aires, Argentina

Published online: 26 July 2021

Vol.:(0123456789)1 3

Graphic Abstract

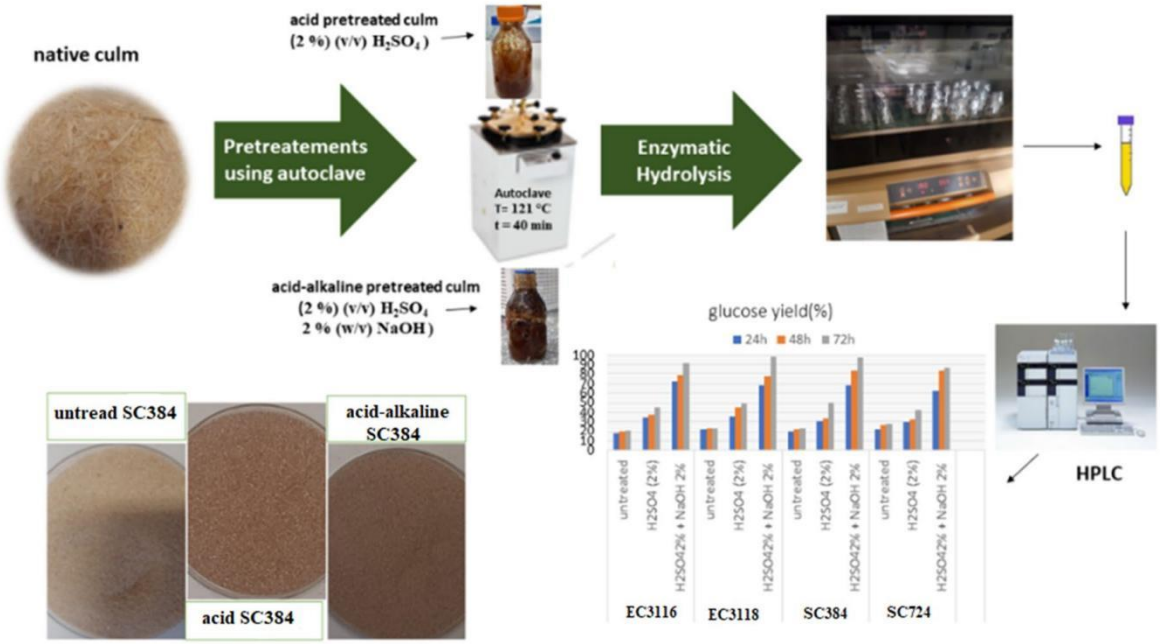

Keywords Culms · Sugarcane varieties · Acid and alkaline pretreatments · Enzymatic hydrolysis

Abbreviations
AFEX Ammonia fiber expansion
ANOVA Analysis of variance CrI Crystallinity index
DRX X-ray diffraction
CLSM Confocal laser scanning microscopy
EC Energy cane culm
EC3116 Energy cane variety INTA 05-3116
EC3118 Energy cane variety INTA 05-3118
EHY Enzymatic hydrolysis yields
GIMP GNU Image Manipulation Program
HPLC High-performance liquid chromatography
INTA National Institute of Agricultural Technology of Argentina
LPMOs Lytic polysaccharide monooxygenases
SC Sugarcane (Saccharum spp.) culm
SC384 Sugarcane variety LCP 85-384
SC724 Sugarcane variety NA 78-724
SEM Scanning electron microscopy

Statement of Novelty

Transitioning to a bioeconomy is not possible without efficient utilization of agricultural wastes and by-products. Applicability of the sugarcane and energy cane varieties grown in Argentina for second-generation bioethanol technologies remains largely unexplored. The potential of culms from two different sugarcane and two energy cane varieties grown in Argentina for sustainable production of biofuels was evaluated. Comprehensive structural and morphological investigations of untreated and pretreated cane varieties provided novel insights on the structural basis of their enzymatic digestibility. Excellent saccharification yields from the pretreated culms were achieved. These new findings hold a promise of exploring the studied types of sugarcane and energy cane for second-generation ethanol and green chemicals technologies.

Introduction

Increasing environmental impacts and growing greenhouse gas emissions motivate the development of alternative technologies for the transformation of agro-industrial wastes and by-products that are environmentally friendly, sustainable, and capable of reducing dependence on fossil fuels [1]. Therefore, the substitution of non-renewable carbon sources with underutilized biomass as a raw material for bioenergy and sustainable “green” chemical production is an exciting opportunity and a driving force for developing bio-economies [2]. The main compounds of plant biomass are cellulose, hemicellulose, and lignin, which form a complex and recalcitrant three-dimensional structure [3]. These three components represent around 90% of the dry biomass by weight [4].

Cellulose, the most abundant biopolymer of plant biomass (30–50 wt%), is the major component of the plant cells, mainly located in the secondary cell walls. It is a linear homopolymer with cellobiose as a repeating unit. Cellulose is semicrystalline with

intercalated ordered crystalline and disordered amorphous regions. Hemicelluloses are much more diverse linear or branched polysaccharides representing 20–35 wt% of the primary and secondary plant cell walls [5]. Finally, lignin is phenolic, branched, and hydrophobic biopolymer, which is built up by oxidative coupling of monolignols, which form a randomized structure in a tridimensional network by specific interunit linkages, such as β-O-4, β-5, and β-β [6] .

Among different biomass types, sugarcane is one of the most promising renewable resources for production of chemical precursors and second-generation biofuels [7]. The harvested part of the cane, known as culm, is divided longitudinally by a series of nodes (transversal septa) forming intercalated regions known as internodes, which plants use for sucrose storage. Both in Brazil and Argentina, bioethanol, produced by sugarcane sucrose fermentation, is already used to partially replace gasoline [8].

Within the last decades, a new sugarcane biotype alternative to the traditional high-sugar commercial sugarcane, known as energy cane, was put forward. Energy can biotype is based on promoting high biomass yield together with high-fiber culm content to enhance the entire energetic production of the crop. Breeding energy cane varieties is relatively new in most of the sugarcane producing countries e.g., no energy-cane varieties have been commercially released in Argentina so far. Therefore, only scarce information about their chemical composition and potential bioenergetic performance is currently available in the scientific literature [9].

Efficient transformation of recalcitrant sugarcane and energy cane into simple sugars is challenging because of the recalcitrance of the lignocellulosic biomass. Therefore, biochemical conversion of biomass into sugars comprises two main steps: pretreatment and enzymatic hydrolysis, followed by fermentation and/or catalytical upgrading to produce cellulosic ethanol and/or green chemicals [10]. Cellulose enzymatic hydrolysis involves the synergistic action of at least three types of enzymes endo-1,4-β-glucanases (EC 3.2.1.4), cellobiohydrolases (or exo-1,4-β-glucanases) (EC 3.2.1.91) and β-glucosidases (EC 3.2.1.21. Cellobiohydrolases and endo-1,4-ß-glucanases hydrolyze celluloses mostly into cellobiose and longer oligosaccharides, whereas ß-glucosidases hydrolyze soluble oligosaccharides into glucose [11]. Moreover, it was recently demonstrated that auxiliary activity enzymes such as lytic polysaccharide monooxygenases (LPMOs) that oxidatively nick cellulose chains and act in synergy with

cellulases have significant industrial importance for effective depolymerization of lignocellulosic biomass [12].

The efficiency of enzymatic hydrolysis critically depends on the pretreatment step, which aims to overcome the lignocellulosic biomass recalcitrance and enhance enzymatic convertibility [13]. Indeed, the major challenge in lignocellulosic biomass valorization resides in plant cell wall recalcitrance strongly related to the lignin content and distribution that interferes with the enzyme action by decreasing cellulose accessibility and causing unproductive adsorption [14]. Furthermore, pretreatments can introduce an increase in and partial depolymerization and solubilization of hemicelluloses and lignin [8].

Various mechanical, thermochemical, and biological pretreatment methods have been developed for overcoming the recalcitrance of lignocellulose towards enzymatic saccharification [15]. Thermochemical pretreatments are at the forefront of research, including dilute acid, dilute alkali, ammonia, oxidation reagents, organic solvent, ionic liquids, steam explosion, or ammonia fiber expansion (AFEX), among others [16]. The alkaline pretreatment involves using an alkali such as sodium hydroxide, calcium hydroxide (lime), potassium hydroxide, or ammonia resulting predominantly in structural and chemical changes of lignin and its release from the pretreated biomass. During the delignification process, the ether and ester bonds, as well as the ester and carbon-to-carbon (C–C) bonds in lignin molecules are cleaved, disrupting the structural linkage between lignin and carbohydrates [17], thus leading to the lignin structure disruption and the cellulose swelling. Additionally, alkaline pretreatment increases the internal surface area of the cellulose [18].

On the other hand, dilute acid pretreatments mainly result in the removal of hemicelluloses, which increases enzymatic digestibility of the pretreated biomass [19]. In this pretreatment, lignin also suffers chemical changes. A considerable disorder in lignin structure might occur, and its fragments tend to re-aggregate and re-precipitate at the surface of the pretreated biomass [5].

Although pretreatment technologies have significantly improved within the last years, this industrial step continues to be technologically challenging and expensive, representing more than 40% of the total processing cost of lignocellulosic ethanol [20, 21]. In addition, pretreatments might require the recycling of chemicals and disposal of waste solutions. The combined dilute acid–alkaline pretreatments were previously used for efficient solubilization of hemicellulose

and partial delignification of bagasse and other plant biomasses [22, 23].

Our current study aims to investigate the impacts of dilute acid and combined dilute acid and alkaline pretreatments on the structure, morphology, and composition of two different sugarcane varieties (LCP 85-384 and NA 78-724,) and two energy cane varieties (INTA 05-3116 and INTA 05-3118) and to evaluate their saccharification efficiencies. We also compare the enzymatic digestibility of the pretreated sugarcane and energy cane varieties in the context of sustainable second-generation sugar production.

LCP 85-384 is the prevailing planted variety in Tucumán [24, 25], the Argentine province that concentrates 73% of the sugarcane grown area in the country. NA 78-724 was used as a progenitor within the sugarcane breeding program of the National Institute of Agricultural Technology of Argentina (INTA). On the other hand, close to being released in Argentina, INTA 05-3116 and INTA 05-3118 varieties are energy cane biotypes developed to maximize the energy production from the entire biomass. The chemical characterization of these cultivars and evaluation of their performance for second-generation sugars production is crucial for identification of varieties that can be employed in the context of biorefineries to produce bioethanol and/or green chemical products.

Materials and Methods

Raw Material

Sugarcane (Saccharum spp.) culms (SCs) of two different sugarcane varieties (LCP 85-384 and NA 78-724), hereafter termed SC384 and SC724, and two energy cane (INTA 05-3116, and INTA 05-3118) varieties, hereafter called EC3116 and EC3118 were used as raw materials. Sugarcane varieties were selected because of their contrasting sugar/fiber ratios in culms and potentially different properties under pretreatment and enzymatic hydrolysis conditions.

Three SC samples of each variety were harvested from second-ratoon plants grown in sugarcane plots at the experimental field of INTA Famaillá Station (27°03′S, 65°25′W, 363 masl.). Each sample was composed of five 1-year grown culms. Leaves and culm tops were removed, and culms were shredded with a locally manufactured machine. Culms were washed using distilled water at 50 °C to remove free sugars and detachable particles and was dried at 40 °C for 48 h in an oven to remove moisture.

Brix and fiber percentages on a fresh weight basis in culms of SC384 were 17 and 11%; of SC724 were 18.5 and 14%; of EC3116 were

13.5 and 23%, and of EC3118 were 13 and 25%, respectively.

Pretreatment Methods

The combination of acid and alkaline pretreatments was used, following previously developed protocols [22, 26]. First, EC and SC samples were treated with aqueous 2% (v/v) H2SO4 and autoclaved at 121 °C and 1.05 bar of excess pressure for 40 min, using a 1:10 (g/mL) fiber to solution ratio. To separate solid residue from liquor, the mixture was filtered, and the resulting solid residue was rinsed with distilled water until neutral pH. Then, the solid residue was oven-dried at 40 °C for 48 h.

Subsequently, the diluted acid pretreated culms were treated with 2% (w/v) NaOH and again autoclaved at 121 °C and 1.05 bar excess pressure for 40 min, using a 1:10 (g/mL) solid to solution ratio. Finally, the mixture was filtered, and the residues were washed with Milli-Q water until neutral pH was reached and dried at 40 °C for 48 h.

Chemical Composition

The chemical composition of untreated and treated SCs and ECs was determined following two-steps hydrolysis procedures using 72% (w/w) H2SO4 solution as previously reported [27]. All the measurements were conducted in triplicates. Briefly, untreated culm was washed in cyclohexane–ethanol solution (1:1) for 8 h to remove extractives using Soxhlet equipment and bags of filter papers containing the samples. The same cycle was repeated five times, replacing the cyclohexane–ethanol solution with water. One gram of each culm without extractives, already dried and ground using knife-mill (20 mesh), was mixed with 10 ml of 72% (w/w) H2SO4 solution and kept in a thermostatic bath 45.0 °C for 7 min under vigorous magnetic stirring. Then, the reaction was transferred to an Erlenmeyer flask and diluted with 275 ml distilled water. The flasks covered with aluminum foil were autoclaved for 30 min at 1.05 atm excess of pressure to complete the acid hydrolysis. Following autoclaving, the mixture was filtered using a previously weighed filter paper. The filtrate was collected in a 500 ml volumetric flask completing the flask gauge line by washing the residue. The soluble lignin was determined by the analysis of light absorption at 280 nm by hydrolysate using a UV–visible spectrophotometer. The lignin retained in filter paper, thoroughly washed with distilled water (1600 ml) to ensure the complete sulfate removal, was dried at room temperature, followed by a drying series at 105 °C for 2 h and weighing each time until weight stabilization. The ash contents in the insoluble lignin were obtained by calcination

in an oven for 4 h at different temperatures: 1 h at 200 °C, 1 h at 400 °C, and 2 h at 800 °C. High-Performance Liquid Chromatography (HPLC) (Shimadzu) was used to analyze sugars in the hydrolysate using a refraction index detector coupled with a Biorad Aminex HPX-87 H column at 65 °C, and a 5 mM H2SO4 solution as a mobile phase at a flow rate of 0.6 mL/min. The glucose, xylose, acid acetic, furfural, acid formic, glucuronic acid, arabinose, and mannose and hydroxymethyl furfural standards were used. The glucose and xylose concentrations obtained after acid hydrolysis allow to quantify cellulose and hemicellulose, respectively according to the following equations:

$$\%\, Hemicellulose = \frac{C(xylose) \times V \times 0.88}{m} 100 \quad (1)$$

$$\%\, Cellulose = \frac{C(glucose) \cdot V \times 0.9}{m} \times 100 \quad (2)$$

The C(Xylose) and C(Hemicellulose) represent respectively xylose and hemicellulose concentrations (mg/ml) obtained after enzymatic hydrolysis, V (ml) represents the volume of the reaction mixture, and m (mg) means the weight of culm used for enzymatic hydrolysis. Thus, numbers 0.9 and 0.88 were respectively the conversion factors of glucose and xylose, due to the addition of water molecules to the anhydroglucose residues in the process of cellulose and xylan hydrolysis.

Enzymatic Hydrolysis

The enzymatic hydrolysis was performed with commercial enzymatic cocktail Cellic CTec3 at 5 mg of the enzyme mixture per g of substrate ratio (5 mg/g). Enzymatic hydrolysis assays of untreated and pretreated culms were conducted in triplicates during 72 h, and samples of hydrolysates were periodically (after 24 h, 48 h, and 72 h) collected from each hydrolyzed sample. They carried out in 50 mM sodium citrate buffer (pH 5.0), under constant stirring of 180 rpm at 50 °C using a substrate at 10% (w/v) concentration for the pretreated culms and at 5% (w/v) concentration for untreated culms to prevent drying of the untreated substrate during the hydrolysis. The released glucose quantity was measured by HPLC (Shimadzu) under previously described conditions. The cellulose enzymatic hydrolysis yield (EHY) was calculated considering the amount of released glucose (RG) in g/L and the cellulose percentage in the untreated and pretreated culm samples to Eq. 3:

$$HY = \frac{RG\ (g/L)}{BC\ (g/L) \times C\ (\%) \times 1.1} \quad (3)$$

The number 1.1 is a correction factor due to the addition of water molecules to the anhydroglucose residues in cellulose, BC

refers to biomass concentration, and C (%) is the cellulose content culm (g/g).

Scanning Electron Microscopy (SEM) Analyses

The Scanning Electron Microscope (model SIGMA) equipped with a Field Emission Gun (FEG) was used to obtain culm sample images at nanometer resolution. Pretreated and untreated culm samples were dried on aluminum stubs and coated with gold, using a sputter coater (SCD-050, Balzers). The analyses of the samples were carried out under vacuum, utilizing 5 kV as an acceleration voltage. For each sample, many images were produced in different regions to guarantee reliability of the results.

X-Ray Diffraction Studies

A diffractometer (Rigaku, Japan) using monochromatic radiation from a copper anode (1.5418 Å), operating at 45 kV and 36 mA and equipped with a graphite monochromator was utilized to collect data. The crystallinity index was evaluated both as described by Segal *et al*. [28], and Park *et al.* [29] respectively. Amorphous and crystalline contributions to the diffraction spectrum were separated by a curve-fitting process, in which a peak fitting program (Peak Fit; http://www.systat.com) was used. The amorphous peak was predicted to be at around 21.5°. The following equation allowed to calculate by the Segal crystallinity index (CrI, %):

$$CrI = \frac{I200 - Iam}{I200} \qquad (4)$$

I200 is the total intensity of the (2 0 0) peak for cellulose at 22.7° peaks for cellulose I, and Iam in the amorphous intensity at 18.3°.

The crystallite sizes (D) were calculated by the Scherrer equation [30] given below:

$$D = \frac{K\lambda}{\beta cos\theta} \qquad (5)$$

Here K is the correction factor (0.9), λ is the wavelength of the X-ray radiation (1.54056 Å), β is the full width at half maximum (FWHM) of the diffraction peak in radians, and θ is the diffraction angle of the peak.

Confocal Laser Scanning Microscopy

Confocal laser scanning microscopy (CLSM) was used to map lignin distribution in the samples and to obtain information on its molecular arrangement within the cell walls by measuring lignin fluorescence emission spectra, as previously described [31]. Pretreated and untreated samples were suspended in water and dropped on the cover slides. CLSM images were collected on the sample surfaces using a Plan Apochromat objective lens (20×, water immersion) and a Zeiss LSM 780 confocal microscope with a coherent chameleon laser (Tisapphire) as a

source for two-photon excitation. The images were obtained after at least three scans. Each pixel area was associated with the optical resolution of the lens (20×), with a lateral resolution of approximately 300 nm, and the total number of dots per image was 1024 × 1024.

Statistical Analysis

Analysis of variance (ANOVA) followed by DGC post hoc multiple comparison test ($p < 0.05$), was used to evaluate the effects of pretreatment (untreated, acid and acid alkaline), variety (SC384. SC724, EC3116 and EC3118) and pretreatment/variety interactions on the chemical composition of culms. Additionally, ANOVA and DGC test were used to determine statistical differences in the percentage enzymatic hydrolysis after 24, 48, and 72 h from untreated and pretreated culms of the four varieties. Statistical analysis was performed using a combined platform, including Infostat software and R software.

Results and Discussion

Chemical Composition Analysis

The chemical composition of untreated and pretreated sugarcane and energy canes is given in Table 1. Consistent with previous results [32, 33], the cellulose fraction was the highest in all four untreated culms, ranging from 40.3 to 43.6%. The measured cellulose content can vary according to culm types, their origin, varieties, and impacted by the analytic method used for its characterization [34]. However, overall, untreated SCs and ECs were not significantly different in terms of chemical composition. The range of hemicellulose fractions was the narrowest in untreated SCs and ECs, varying from 22.2 to 24.7% (Table 1). Their lignin content ranged from 25 to 28% (Table 1) which is consistent with the previous reports by Lima *et al.* [26] and Rezende *et al.* [22]. The pretreatments considerably increased the cellulose fractions in all culms. An increase in cellulose content is related to hemicellulose solubilization and the delignification of the culms. The acid pretreatment led to the removal of hemicellulose and lignin, respectively, on 48.17% ± 3.44 and 22.5% ± 7.7% on average, considering all the culms (Table 2). Besides, the cellulose fraction reached an average of 57.45 ± 2.96% (Table 1), confirming the efficacity of the dilute acid pretreatment step for hemicellulose solubilization. Indeed, acidic hydrolysis of lignocellulosic substrates causes catalysis of hemicellulose into various monomeric sugars (xylose, arabinose, etc.) [35]. In addition, a significant part of lignin was degraded in all culms with a maximum for energy cane varieties EC3116 (29.63%) and EC3118 (28.22%)

Table 1 Chemical composition culms (EC3116, EC3118, SC384, and SC724) untreated, and submitted to H 2SO4 (2%), H2SO4 2% + NaOH 2% for 40 min

Pretreatment	Variety	Composition (%)					
		Cellulose	Hemicellulose	Lignin	Ash	Extractives	Total
Untreated	EC3116	40.3 ± 0.3e	22.2 ± 0.3a	26 ± 1.4a	1.3 ± 0.2b	8.7 ± 1.5	98.8 ± 3.7
	EC3118	43.6 ± 0.5e	20.2 ± 1.0a	27.5 ± 0.5a	1.4 ± 0.3b	6.9 ± 1.3	96.3 ± 3.7
	SC384	42.0 ± 0.7e	21.9 ± 1.6a	24.4 ± 3.2a	1.7 ± 0.1a	8.3 ± 1.2	108.5 ± 9.5
	SC724	40.3 ± 0.3e	23.2 ± 0.2a	26.6 ± 1.1a	1.8 ± 0.3b	6.6 ± 0.8	100 ± 3.1
Dilute acid pretreated	EC3116	59.0 ± 0.6c	12.4 ± 6.0b	19.0 ± 0.5b	1.0 ± 0.01b		91.4 ± 7.1
	EC3118	60.0 ± 4.3c	13.1 ± 2.0b	20.1 ± 1.2b	1.3 ± 0.1b		94.5 ± 7.6
	SC384	53.5 ± 0.7d	12.3 ± 0.1b	20.8 ± 8.4b	3.4 ± 0.1a		90.0 ± 9.3
	SC724	55.9 ± 1.1d	11.8 ± 0.1b	21.4 ± 1.6b	2.8 ± 0.1b		91.5 ± 2.9
Combined acid alkaline pretreated	EC3116	79.8 ± 1.3a	4.3 ± 0.5c	12.0 ± 2.7c	0.6 ± 0.03b		96.7 ± 4.5
	EC3118	80.5 ± 0.6a	5.9 ± 2.2c	9.4 ± 2.9c	2.1 ± 1.3b		97.9 ± 7.0
	SC384	83.5 ± 2.0a	3.0 ± 0.8c	9.6 ± 4.5c	3.2 ± 2.4a		99.3 ± 9.7
	SC724	79.8 ± 1.3a	4.6 ± 2.7c	10.5 ± 2.7c	0.5 ± 0.1b		92.2 ± 7.8
Summary of ANOVA							
Pretreatment		***	***	***	ns		
Variety		ns	ns	ns	**		
Pretreatment: Variety		**	ns	ns	ns		

Acid: H2SO4 (2%)

Acid–alkaline: H2SO4 2% + NaOH 2% ns non-significant

***Significant at < 0.001 **Significant at < 0.01

Different letters within columns indicate significant differences for DGC post hoc multiple comparison test ($p < 0.05$)

Table 2. Hemicellulose and lignin fractions removed after diluting acid and combined acid–alkaline pretreatment of EC3116, EC3118, SC384, and SC724

	Acid pretreatment	Acid–alkaline pretreatment	Acid pretreatment	Acid–alkaline pretreatment
EC3116	44.14	80.63	29.63	55.56
EC3118	46.96	76.11	28.21	66.43
SC384	49.38	87.65	16.80	62.00
SC724	52.23	81.38	14.40	58.00
Average	48.2 ± 3.4	81.0 ± 4.7	22.5 ± 7.8	60.0 ± 4.8

The combined acid–alkaline pretreatment resulted in the samples with the cellulose fraction reaching 80.15 ± 2.79%, on average (Table 1), while hemicellulose and lignin release was increased up to 81.0 ± 4.75% and 60.0 ± 4.76 respectively (Table 2). Thus, the combined acid–alkaline was highly efficient in the solubilization of hemicellulose and lignin under applied conditions. Furthermore, these chemical composition results are consistent with previously published studies that reported cellulose content to increase to 83.4%, with 86.9% hemicellulose removal [22]. Overall, the applied combined acid–alkaline pretreatment was efficient for cellulose isolation and can also be exploited for hemicellulose recovery (up to 87.65% for SC384; Table 2).

ANOVA revealed statistically significant differences for cellulose ($p < 0.001$), hemicellulose ($p < 0.001$), and lignin contents ($p < 0.001$) because of the applied pretreatments, but no differences were found for ash content ($p = 0.5$), which was dependent on culm ($p < 0.01$).

X-Ray Diffraction Analysis

The crystallinity indices (CrIs) and the average crystallite sizes of culm samples were calculated based on XRD experiments (Table 3). Two different approaches, Segal, and deconvolution methods were used to calculate the CrIs. Even though slight differences were observed between both approaches, the values of Segal-based CrIs paralleled the values of CrIs determined using a deconvolution procedure (Table 3). The CrIs of the untreated and pretreated culm samples

increased after each pretreatment step (Table 3), presumably because of amorphous hemicellulose and lignin removal [36]. As a result, a relative fraction of the crystalline cellulose is increased within the pretreated culm samples [37]. Therefore, crystallinity changes can be mainly

Material	Crystallinity Index (%)a		Crystallite size (nm)b
	Segal method	Deconvolution	

	untreated	45.8 ± 0.7	49.0 ± 1.6	3.1 ± 0.02
EC3116	H2SO4 (2%)	51.9 ± 0.3	52.5 ± 1.7	3.2 ± 0.03
	H2SO4 2% + NaOH 2%	53.0 ± 0.01	53.6 ± 4.4	3.6 ± 0.2
	untreated	45.0 ± 0.5	47.7 ± 0.9	3.0 ± 0.03
EC3118	H2SO4 (2%)	44.6 ± 0.2	52.7 ± 1.3	3.1 ± 0.3
	H2SO4 1% + NaOH 2%	52.8 ± 2.5	58.9 ± 2.7	3.9 ± 0.1
	untreated	44.1 ± 1.7	49.0 ± 8.3	2.4 ± 0.3
SC384	H2SO4 (2%)	51.8 ± 0.02	54.7 ± 0.4	3.2 ± 0.2
	H2SO4 1% + NaOH 2%	54.0 ± 2.5	58.0± 0.05	3.8 ± 0.2
	untreated	32.4 ± 1.1	49.0 ± 3.7	2.3 ± 0.2
SC724	H2SO4 (1%)	42.7 ± 0.7	54.2 ± 3.1	2.9 ± 0.2
	H2SO4 2% + NaOH 2%	45.1 ± 0.1	54.9 ± 0.03	3.7 ± 0.3

Table 3 Crystallinity index (%) and crystallite sizes of untreated and treated energy cane (EC3116 and EC3118) and sugarcane varieties (SC384 and SC724)

[a]Crystallinity indexes were determined according to [28]

[b] Crystallite sizes (D) were calculated by the Scherrer equation [30]

attributed to solubilization of the amorphous fractions of culms. The alkaline pretreatment might also lead to swelling of the cellulose fibers. A consecutive drying step can cause hornification .

and recrystallization of the cellulose fibers, thus increasing cellulose crystallinity and crystallite sizes [38]. Indeed, average crystallite sizes increased significantly after the combined pretreatment (Table 3).

and recrystallization of the cellulose fibers, thus increasing cellulose crystallinity and crystallite sizes [38]. Indeed, average crystallite sizes increased significantly after the combined pretreatment (Table 3).

The crystallinity indices obtained by the Segal method varied between 32.4 and 45.8% for all the raw biomasses and increased (45.1–54.0%) for the pretreated culms (Table 3), in line with the previously published studies [22, 39]. Additionally, the high crystallinity index was accompanied by elevated enzymatic hydrolysis yields (EC3118 acid–alkaline EHY: 98.7% and CrI: 58.9%; SC384 acid–alkaline EHY: 92.2% and CrI: 58.0%). These results are consistent with the results of Bernardinelli *et al*. [40]. Although it is challenging to conclude that high crystallinity directly correlates with improved enzymatic digestion, a combined effect of lignin removal and resulting biomass modification, accompanied by the collapse of cellulose microfibrils into bigger crystallites and higher overall crystallinity, is probably a reason of

improved enzymatic hydrolysis. Therefore, the enhanced hydrolytic yields are probably related to modified chemical composition and altered ultrastructure of the remaining SC biomass, which favors enzymatic accessibility and lessens unproductive absorption of the enzymes on the remaining lignin [39, 41].

Morphological Changes During Pretreatment

The Scanning Electron Microscopy (SEM) was used to evaluate the surface morphology of untreated and pretreated culms (Figs. 1, 2, and 3). The untreated culms (ECs and SCs) exhibited a compact and well-ordered structure due to the interconnection between cellulose and hemicellulose biopolymers embedded in a lignin matrix. Native EC3116, EC3118, and SC724 were made up of parallel stripes consistent with cellulose fibers coated with lignin on their surfaces (Fig. 1a, b, and d). Untreated SC384 revealed pores on its surface (Fig. 1c). Similar fibers of native lignocellulosic biomass from sugarcane bagasse were previously reported [42].

SEM images of culms obtained after dilute acid pretreatment are given in Fig. 2. Relatively separate parallel bands with rough surfaces were observed in all culms. These results reflect the diluted acid pretreatment effect of removing hemicellulose from culms, allowing the lignin reorganization on the surface of lignocellulosic biomass. Furthermore, after acid–alkaline pretreatment of ECs and SCs, wholly separated and opened smooth surface cellulosic fibers were observed, particularly in the studied energy cane culm samples (Fig. 3a and d). Thus, SEM images

of untreated and pretreated culms illustrate the combined acid–alkaline pretreatment efficiency on ECs and SCs, confirming. solubilization of lignin and hemicellulose [22, 26].

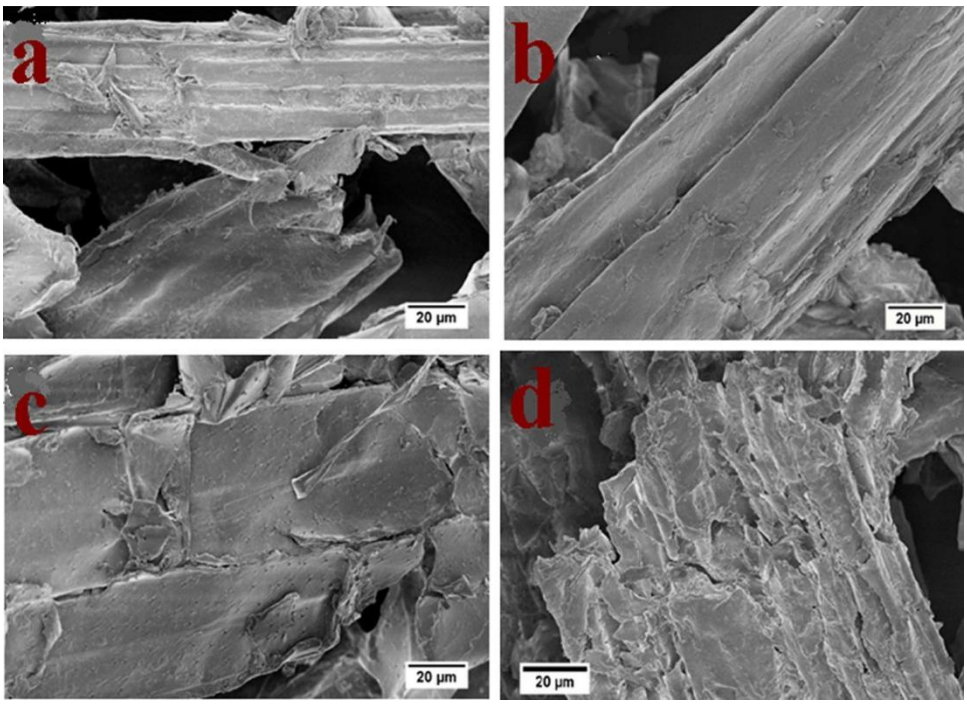

Fig. 1 SEM images of untreated sugarcane and energy cane culms: a Energy cane culms EC3116; b energy cane culms EC3118; c sugarcane culms SC384; d sugarcane culms SC724. The figures were processed using the GNU Image Manipulation Program (GIMP) (https:// www. gimp. org/)

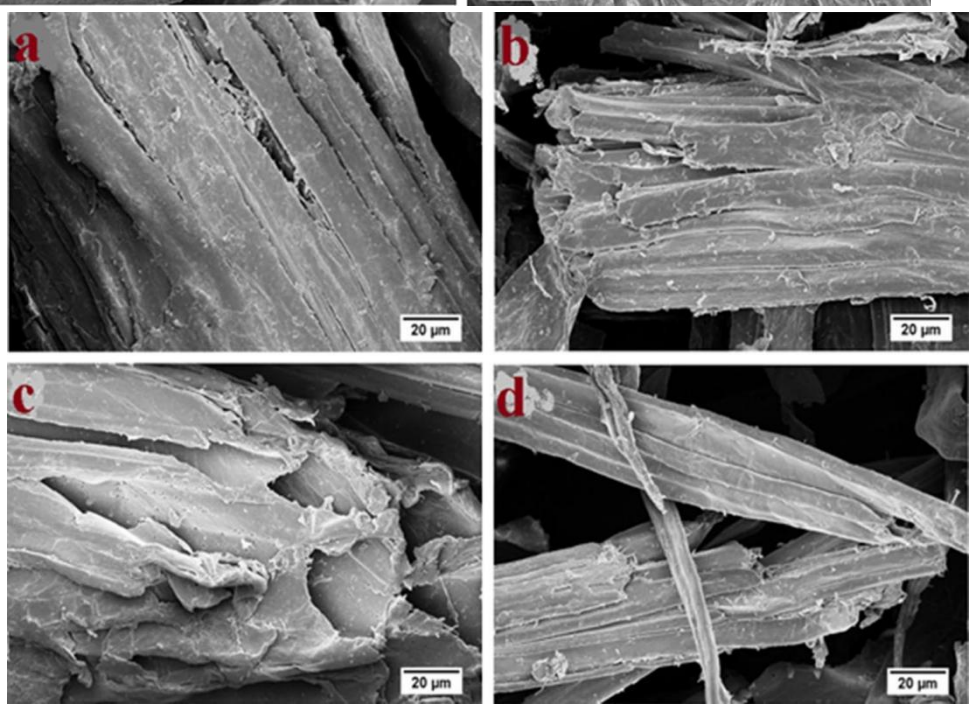

Fig. 2 SEM images of sugarcane and energy cane culms submitted to dilute acid pretreatment. a Energy cane culms EC3116; b energy cane culms EC3118; c sugarcane culms SC384; d sugarcane culms SC724. The figures were processed using the GNU Image Manipulation Program (GIMP) (https:// www. gimp. org/

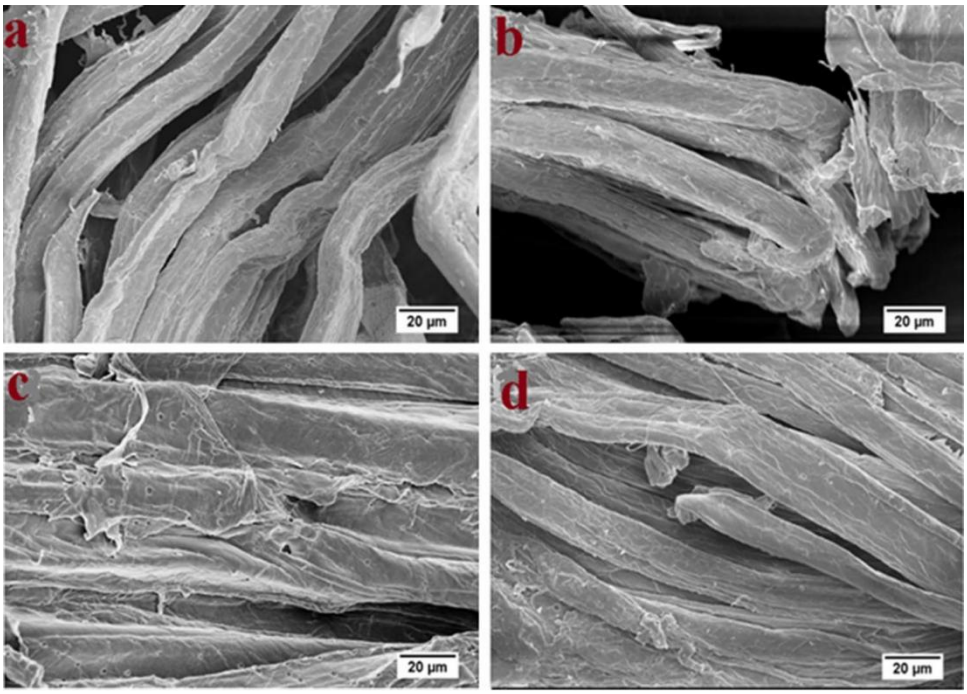

Fig. 3 SEM images of sugarcane and energy cane culms submitted to combined acid– alkali pretreatment. a Energy cane culms EC3116; b energy cane culms EC3118; c sugarcane culms SC384; d sugarcane culms SC724. The figures were processed using the GNU Image Manipulation Program (GIMP) (https:// www. gimp. org/)

Confocal Laser Scanning Microscopy Images

Confocal laser scanning microscopy (CLSM) was used to determine lignin distribution within the substrates. Confocal images of the raw culms (Fig. 4) showed mainly fluorescence in a blue spectral region (400–500 nm). Indeed, plant cell walls can exhibit autofluorescence, and lignin is the predominant fluorophore in plant biomass [43]. The lignin substructures define the color and fluorescent properties of its emission, and untreated native sugarcane lignin emits fluorescence in the blue region of the electromagnetic spectrum [33].

Confocal images of all pretreated culms (ECs and SCs) representative for the biomass area reveal changes in lignin autofluorescence color. The

fluorescence emission shifts from blue (400–500 nm) to yellowish green (500–550 nm) for the acid pretreated culms (Fig. 5) and to green for acid–alkaline pretreated culms (Fig. 6).

Lignin has a broad fluorescence emission spectrum and can be excited by UV and visible light. The lignin multimodal autofluorescence characteristic indicates multiple fluorescent structures within the lignin macromolecule [44].

During the acid pretreatment, a large part of hemicellulose was solubilized (Table 2), resulting in improved accessibility of the

substrates to enzymatic hydrolysis (Fig. 7). This pretreatment was also accompanied by partial solubilization of the lignin fraction (Table 2)

Because of its hydrophobic nature, lignin may be extruded by the pretreatment and recondense on the substrate surface. Therefore, the acid pretreatment led to rearrangement and increase of heterogeneity of lignin distribution, resulting in emission to the yellowish green range (500–550 nm) (Fig. 5) [41].

Consecutive alkaline pretreatment, resulting in lignin fragmentation and solubilization [45] resulted in more homogeneous lignin fluorescence in the green wavelength range (Fig. 6), which can also be associated to lower remaining lignin concentration in the samples (Table 1) [33].

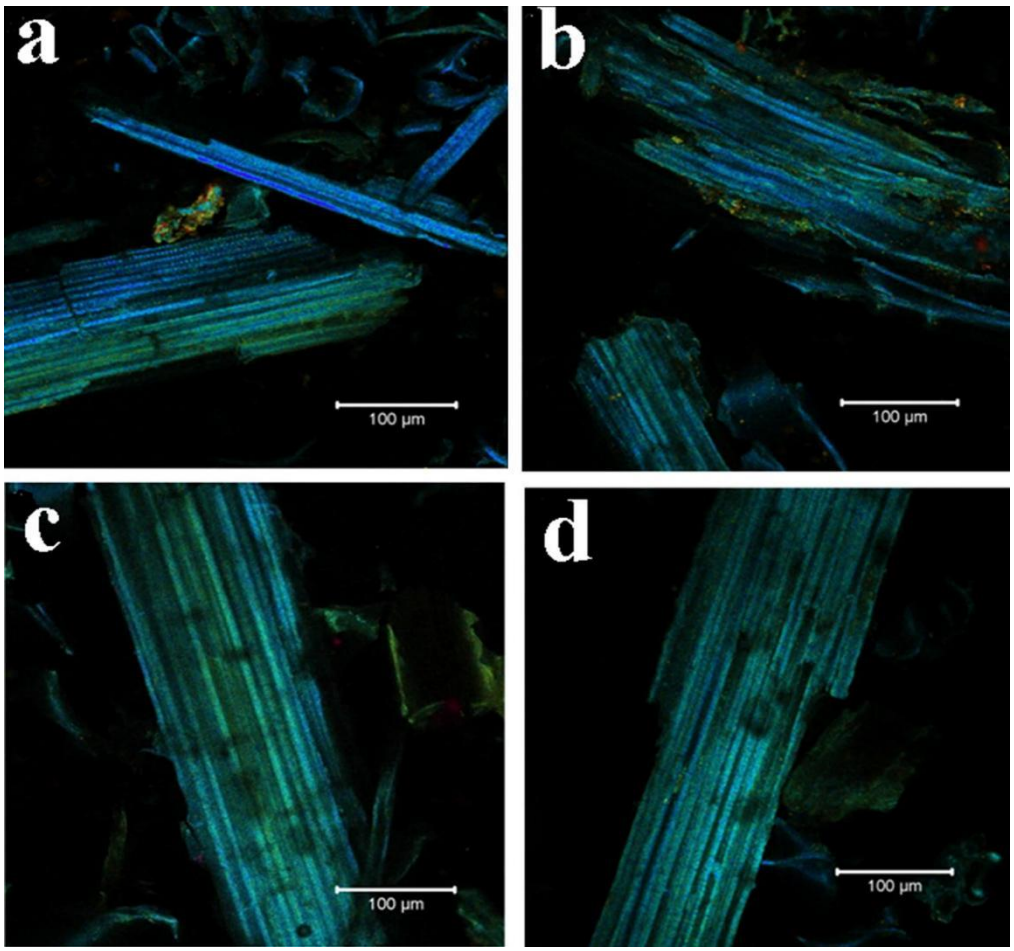

Fig 4. Confocal images of untreated SC. a Energy cane culms EC3116; b energy cane culms EC3118; c sugarcane culms SC384; d sugarcane culms SC724

Enzymatic Hydrolysis Yields

Enzymatic hydrolysis experiments of untreated and pretreated ECs and SCs revealed that all

pretreatments induced a significant increase in glucose release after saccharification for each culm (Fig. 7). Importantly, a single diluted acid pretreatment step turned energy cane samples more susceptible to enzymatic hydrolysis, with high rates and yields of glucose release (Fig. 7), which can be related to stronger hemicellulose solubilization and significant removal of lignin from these samples. Combined acid–alkali pretreatment considerably increased enzymatic hydrolysis efficiency of all culm samples, reaching an average of 93.6% after 72 h (Fig. 7).

In comparison, the maximum saccharification obtained with the untreated culms is 27.7% for SC724. This increase in efficiency is correlated with delignification after the alkaline pretreatment step (Table 2). A high yield of glucose was obtained with SC724. (86%), EC3116 (92%), EC3118 (97.8%), SC384 (97.2%), which respectively suffered maximum delignification of 58%, 55%, 62%,

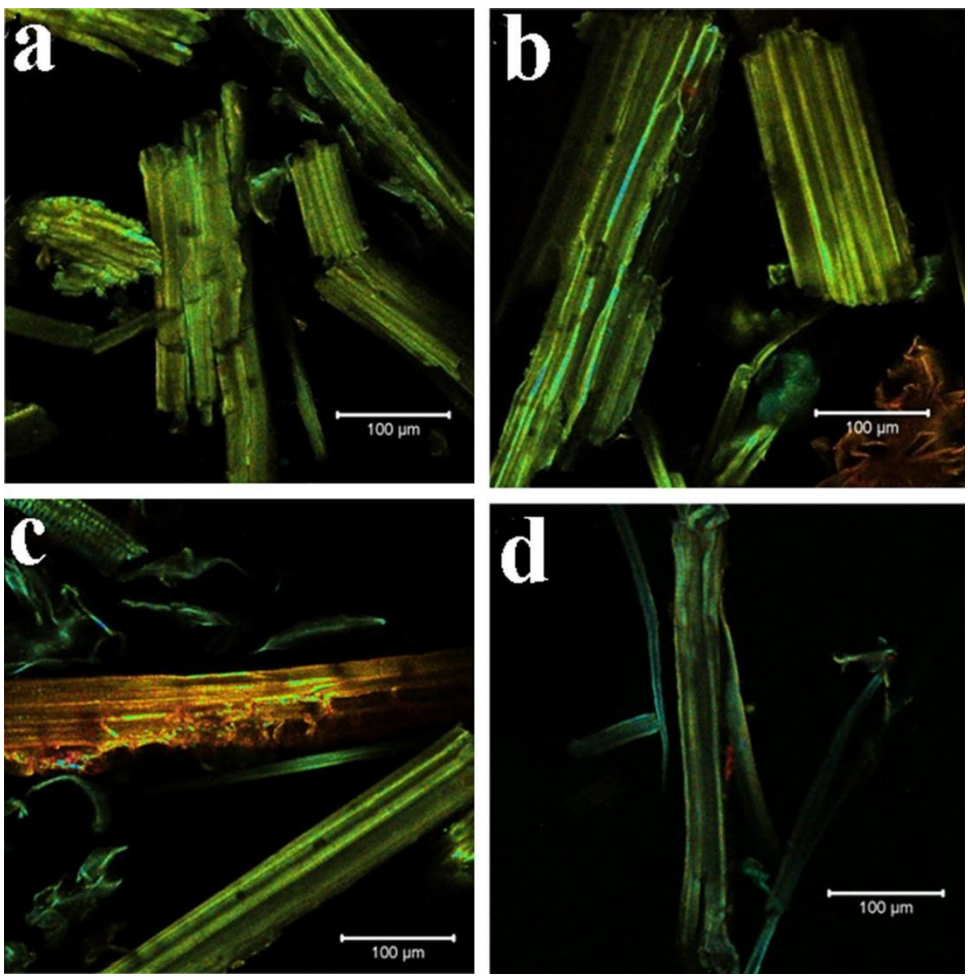

Fig.5 Confocal images of SC submitted to dilute acid pretreatment. a Energy cane culms EC3116; b energy cane culms EC3118; c sugarcane culms SC384; d sugarcane culms SC724

66.2% after combined acid–alkaline pretreatment (Fig. 1; Table 2). Additionally, the glucose yield obtained with the different culms pretreated with dilute acid practically doubled after the combined pretreatment. The hemicellulose solubilization can also positively influence enzymatic saccharification. During acid pretreatment, hemicellulose solubilization involves lignocellulosic biomass reorganization, which improves the cellulase access to cellulose in the enzymatic hydrolysis process [46, 47]. Under conditions applied in the current study, the hemicellulose solubilization was effective with an average of 81.0 ± 4.75% considering all culms and a maximum of 87.65% with SC384 (Table 2).

The observed saccharification of untreated and pretreated culms can be compared to saccharification of other lignocellulosic biomasses. Robak *et al*. [48] submitted rye straw to dilute acid pretreatment with various sulfuric acid concentrations (0.5–2.0% (w/v)). In different cases, the maximum cellulose saccharification rate (69%) was reached with straw pretreated with 2.0% (w/v) H2SO4. Noparat *et al.* [49] investigate the enzymatic digestibility of dilute acid pretreated oil palm trunk biomass at high temperature. The diluted acid pretreatment with 3% H2SO4 at 180 °C for 40 min reached an 80% enzymatic hydrolysis. Similarly, to what was found in our studies, these efficiencies were correlated with complete hemicellulose solubilization. Combined pretreatments generally allow increasing sugar recoveries, with additional advantages such as avoiding the formation of inhibitory products, for example. Yang *et al.*. [50] investigated the enzymatic saccharification of bamboo residues submitted to two-step pretreatments (2% NaOH + steam explosion pretreatment). Their results confirmed better efficiency of the two-step pretreatment as compared to the one-step pretreatments. The highest enzymatic hydrolysis yield of 78.9% was obtained after combined pretreatment as compared to 47% after alkaline pretreatment. The latter allowed a delignification of 50% confirming its efficiency to remove lignin from biomass. Therefore, our results show similar or better cellulose enzymatic hydrolysis yields as compared to other types of lignocellulosic biomass and demonstrate potential of studied SC varieties grown in Argentina for second-generation bioethanol production.

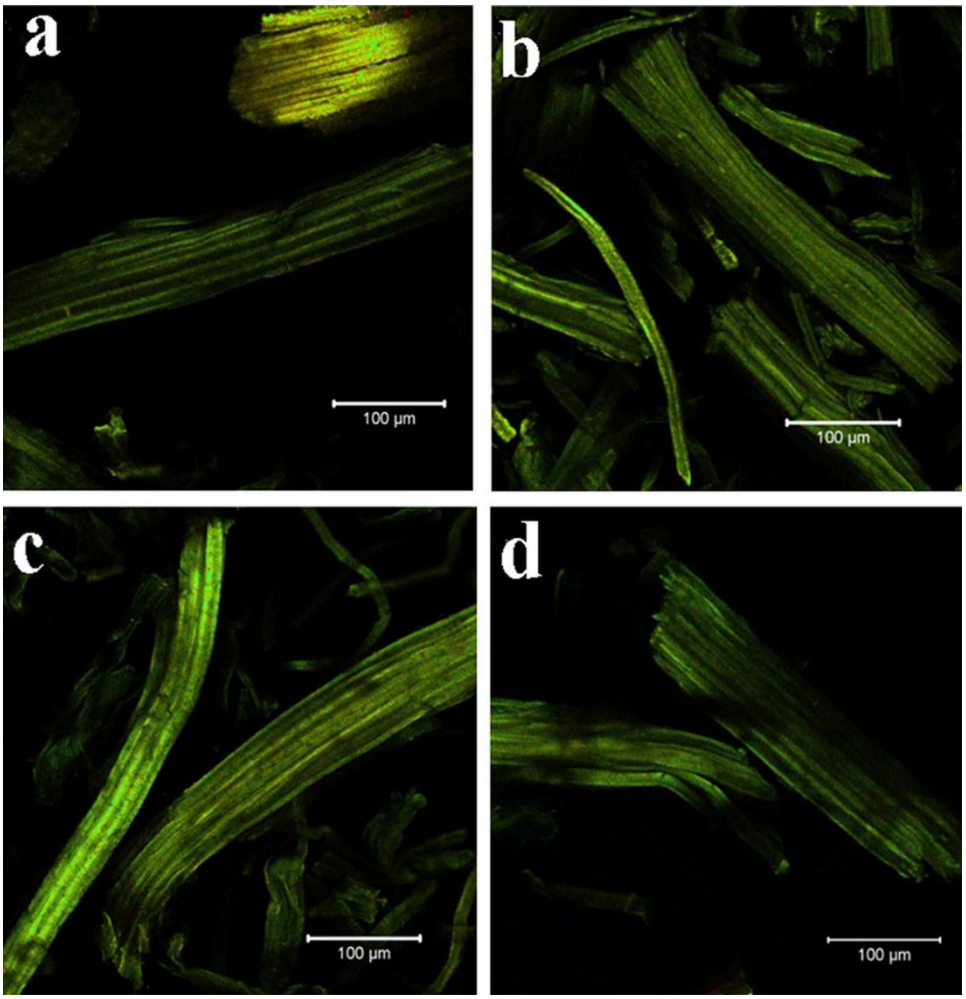

Fig 6. Confocal images of SC submitted to combined acid alkali pretreatment. a Energy cane culms EC3116; b energy cane culms EC3118; c sugarcane culms LCP SC384; d sugarcane culms SC724

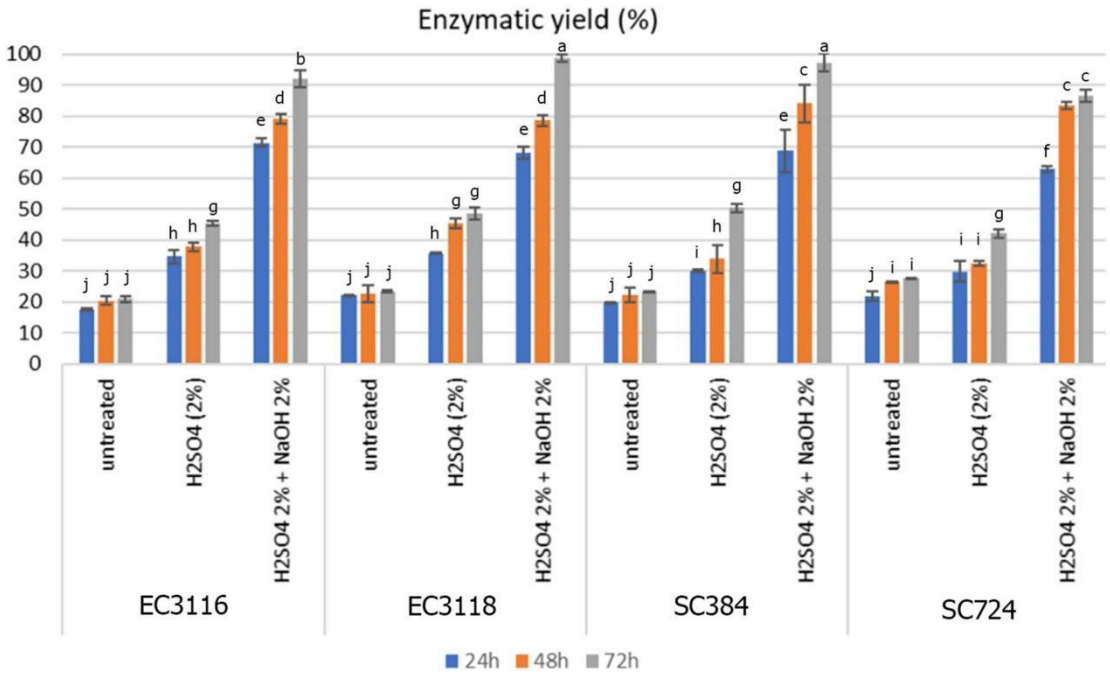

Fig. 7 Glucose yield obtained by enzymatic hydrolysis after 24, 48, and 72 h from untreated and pretreated sugarcane culms of INTA 05-3116 (EC3118), INTA 05-3118 (EC3116), LCP 85-384 (SC384), and NA 78-724 (SC724) varieties. The measurements were made in triplicates. Bars show the standard deviations between the three measurements

Conclusions

In the present study, culms from two different sugarcane and two different energy cane varieties grown in Argentina underwent dilute acid and combined acid–alkaline treatments to evaluate their enzymatic digestibility. Their chemical composition was determined, and their morphology, crystallinity, and lignin distribution were investigated using X-ray diffraction, confocal laser scanning microscopy, and scanning electron microscopy. Combined acid–alkali pretreatment accounted for the highest enzymatic hydrolysis efficiency across all four genotypes, followed by the diluted acid pretreatment which

demonstrated that the enzymatic hydrolysis was more efficient in the energy canes than in the sugarcane varieties. Culm structure changes after each pretreatment were clearly visible in confocal microscopy images, which also reported changes in lignin autofluorescence emission. Scanning electron microscopy analysis demonstrated well-separated cellulose fibers after acid–alkaline pretreatments, consistent with the removal of amorphous hemicellulose and lignin. The subtraction of amorphous fractions from the culms explains their increasing crystallinity after pretreatments.

Our results provide perspectives for the application of all studied sugarcane and energy cane varieties for cellulosic ethanol production, with exceptionally high yields obtained from energy cane EC3118 and sugarcane SC384 under applied experimental conditions. Additionally, the high hemicellulose solubilization, reaching 87.5%, was also achieved.

NA 78-724 (SC724) varieties. The measurements were made in triplicates. Bars show the standard deviations between the three measurements

Author Contributions AOK: Formal analysis; Investigation; Methodology; Writing—original draft; VOAP: Conceptualization; Data curation; Formal analysis; Investigation; Methodology; Project administration; Validation; Writing—original draft; MCES: Formal analysis; Investigation; Methodology; Writing—original draft; BDN: Supervision; Writing—original draft. JMG: Formal analysis; Investigation; Methodology; Writing—original draft; AA: Formal analysis; Investigation; Methodology; Writing—original draft. LEE: Formal analysis; Investigation; Methodology; Writing—original draft; IP: Conceptualization; Formal analysis; Funding acquisition; Investigation; Methodology; Resources; Supervision; Validation; Writing—original draft; Writing—review & editing.

Funding This work was supported by Fundação de Amparo à Pesquisa do Estado de São Paulo (FAPESP) via Grant 2015/13684-0, by Conselho Nacional de Desenvolvimento Científico e Tecnológico (CNPq) via Grants 423693/2016-6 and 303988/2016-9, by Instituto Nacional de Tecnología Agropecuaria (INTA) via Grant PNAIyAV 2019-PE-E6-I114-001, and by Ministry of Science and Technology of Argentina via Grant PICT 2016-1670. This work was also supported by CAPES (Coordenação de Aperfeiçoamento de Pessoal de Nível Superior) via a PhD fellowship to AOK. JMG has a fellowship from
Consejo Nacional de Investigaciones Científicas y Técnicas (CONICET). We thank the field team of INTA Sugarcane Breeding Program for its technical assistance.

Data Availability The data will be made available on request.

Declarations

Conflict of interest the authors declare that they have no conflict of interest.

References

1. Auxenfans, T., Terryn, C., Paës, G.: Seeing biomass recalcitrance through fluorescence. Sci. Rep. **7**, 10 (2017). https:// doi. org/ 10. 1038/ s41598- 017- 08740- 1ï
2. Fatma, S., Hameed, A., Noman, M., Ahmed, T., Sohail, I., Shahid, M., Tariq, M., Tabassum, R.: Lignocellulosic biomass: a sustainable bioenergy source for future. Protein Pept. Lett. **25**, 1–16 (2018). https:// doi. org/ 10. 2174/ 09298 66525 66618 01221 44504
3. Kucharska, K., Rybarczyk, P., Hołowacz, I., Łukajtis, R., Glinka, M., Kamiński, M.: Pretreatment of lignocellulosic materials as substrates for fermentation processes. Molecules. **23**, 1–32 (2018). https:// doi. org/ 10. 3390/ molec ules2 31129 37
4. Ranzi, E., Debiagi, P.E.A., Frassoldati, A.: Mathematical modeling of fast biomass pyrolysis and bio-oil formation. Note I: kinetic mechanism of biomass pyrolysis. ACS Sustain. Chem. Eng. **5**, 2867–2881 (2017). https://d oi.org/1 0 .1021 /a cssuschem eng. 6b030 96
5. Schmatz, A.A., Salazar-Bryam, A.M., Contiero, J., Sant'Anna, C., Brienzo, M.: Pseudo-lignin content decreased with hemicellulose and lignin removal, improving cellulose accessibility, and enzymatic digestibility. Bioenergy Res. **14**, 106–121 (2020). https:// doi. org/ 10. 1007/ s12155- 020- 10187-8
6. Rinaldi, R., Woodward, R.T., Ferrini, P., Rivera, H.J.E.: Ligninfirst biorefining of lignocellulose: the impact of process severity on the uniformity of lignin oil composition. J. Braz. Chem. Soc. **30**, 479–491 (2019). https://d oi.org/1 0 .21577/0 103 -5053.2 018 0 231

7. Bordonal, R., de Carvalho, O., Lal, J.L.N., de Figueiredo, R., de Oliveira, E.B., la Scala, B.G.: Sustainability of sugarcane production in Brazil. A review. Agron. Sustain. Dev. **38**, 1–23 (2018). https:// doi. org/ 10. 1007/ s13593- 018-0490-x
8. Bhalla, A., Cai, C.M., Xu, F., Singh, S.K., Bansal, N., Phongpreecha, T., Dutta, T., Foster, C.E., Kumar, R., Simmons, B.A., Singh, S., Wyman, C.E., Hegg, E.L., Hodge, D.B.: Performance of three delignifying pretreatments on hardwoods: hydrolysis yields, comprehensive mass balances, and lignin properties. Biotechnol. Biofuels **12**, 213 (2019). https://d oi.org/1 0 .1186 /s 13068-019-1546- 0
9. Matsuoka, S., Kennedy, A.J., dos Santos, E.G.D., Tomazela, A.L., Rubio, L.C.S.: Energy cane: its concept, development, characteristics, and prospects. Adv. Bot. **2014**, 1–13 (2014). https://d oi.org/ 10. 1155/ 2014/ 597275
10. Borand, M.N., Karaosmanoğlu, F.: Biorefinery applications: a review effects of organosolv pretreatment conditions for lignocellulosic biomass in biorefinery applications: a review. Renew. Sustain. Energy **10**, 1–23 (2018). https://d oi.org/1 0 .1063/1.5 025 8 76
11. Ogier, J.C., Ballerini, D., Leygue, J.P., Rigal, L., Pourquié, J.: Production d'éthanol à partir de biomasse lignocellulosique. Oil Gas Sci. Technol. **54**, 67–94 (1999). https://d oi.org/1 0 .2516 /o gst: 19990 04
12. Rani Singhania, R., Dixit, P., Kumar Patel, A., Shekher Giri, B., Kuo, C.-H., Chen, C.-W., di Dong, C.: Role and significance of lytic polysaccharide monooxygenases (LPMOs) in lignocellulose deconstruction. Bioresour. Technol. **335**, 125261 (2021). https:// doi. org/ 10. 1016/j. biort ech. 2021. 125261
13. . Silveira, M.H.L., Morais, A.R.C., da Costa Lopes, A.M., Olekszyszen, D.N., Bogel-Łukasik, R., Andreaus, J., Ramos, P.: Current pretreatment technologies for the development of cellulosic ethanol and biorefineries. ChemSusChem **8**, 3366–3390 (2015). https:// doi. org/ 10. 1002/ cssc. 20150 0282
14. Li, X., Li, M., Pu, Y., Ragauskas, A.J., Klett, A.S., Thies, M., Zheng, Y.: Inhibitory effects of lignin on enzymatic hydrolysis: the role of lignin chemistry and molecular weight. Renew. Energy **123**, 664–674 (2018). https:// doi. org/ 10. 1016/j. renene. 2018. 02.079
15. 15. Das, P.: Novel pretreatment techniques for extraction of fermentable sugars from natural waste materials for bio ethanol production. Int. J. Environ. Sci. Nat.Resour. **7**, 74–80 (2017). https://d oi. org/ 10. 19080/ ijesnr. 2017. 07. 555713
16. Chen, J., Adjallé, K., Barnabé, S., Perrier, M., Paris, J.: Mechanical and thermal pretreatment processes for increasing sugar production from woody biomass via enzymatic hydrolysis. Waste Biomass Valoriz. **10**, 2057–2065 (2019). https://d oi.org/1 0 .1007 / s12649- 018-0217-x

16 Xu, L., Zhang, S.-J., Zhong, C., Li, B.-Z., Yuan, Y.-J.: Alkalibased pretreatment-facilitated lignin valorization: a review. Ind. Eng. Chem. Res. **59**, 16923–16938 (2020). https:// doi. org/ 10.1021/ acs. iecr. 0c014 56

17 Sarkar, N., Ghosh, S.K., Bannerjee, S., Aikat, K.: Bioethanol production from agricultural wastes: an overview. Renew. Energy **37**, 19–27 (2012). https:// doi. org/ 10. 1016/j. renene. 2011. 06. 045

18 Li, J., Wei, X., Wang, Q., Chen, J., Chang, G., Kong, L., Su, J., Liu, Y.: Homogeneous isolation of nanocellulose from sugarcane bagasse by high pressure homogenization. Carbohydr. Polym. **90**, 1609–1613 (2012). https://d oi.org/1 0 .1016 /j.c arbpol.2 012 .07.0 3 8

19 Sindhu, R., Binod, P., Pandey, A.: Biological pretreatment of lignocellulosic biomass—an overview. Bioresour. Technol. **199**,76–82 (2016). https:// doi. org/ 10. 1016/j. biort ech. 2015. 08. 030

20 . Hodgson-Kratky, K., Papa, G., Rodriguez, A., Stavila, V., Simmons, B., Botha, F., Furtado, A., Henry, R.: Relationship between sugarcane culm and leaf biomass composition and saccharification efficiency. Biotechnol. Biofuels **12**, 247 (2019). https://d oi.org/1 0 . 1186/ s13068- 019- 1588-3

22. Rezende, C.A., de Lima, M., Maziero, P., Deazevedo, E., Garcia, W., Polikarpov, I.: Chemical and morphological characterization of sugarcane bagasse submitted to a delignification process for enhanced enzymatic digestibility. Biotechnol. Biofuels **4**, 54 (2011). https:// doi. org/ 10. 1186/ 1754- 6834-4- 54
23. Tsuchida, J.E., Rezende, C.A., de Oliveira-Silva, R., Lima, M.A., D'Eurydice, M.N., Polikarpov, I., Bonagamba, T.J.: Nuclear magnetic resonance investigation of water accessibility in cellulose of pretreated sugarcane bagasse. Biotechnol. Biofuels **7**, 1–13 (2014). https://d oi.org/1 0 .1186 /s 13068-014-0 127- 5
24. Acevedo, A., Tejedor, M.T., Erazzú, L.E., Cabada, S., Sopena, R.: Pedigree comparison highlights genetic similarities and potential industrial values of sugarcane cultivars. Euphytica **213**, 2–16 (2017). https:// doi. org/ 10. 1007/ s10681- 017- 1908-2
25. Racedo, J., Gutiérrez, L., Perera, M.F., Ostengo, S., Pardo, E.M., Cuenya, M.I., Welin, B., Castagnaro, A.P.: Genome-wide association mapping of quantitative traits in a breeding

population of sugarcane. BMC Plant Biol. **16**, 142 (2016). https://d oi. org/ 10. 1186/ s12870- 016- 0829-x

26. Lima, M.A., da Silva, H.K.P., Bragatto, J., Rezende, C.A., Bernardinelli, O.D., DeAzevedo, E.R., Gomez, L.D.,McQueenMason, S.J., Labate, C.A., Polikarpov, I.: Effects of pretreatment on morphology, chemical composition and enzymatic digestibility of eucalyptus bark: a potentially valuable source of fermentable sugars for biofuel production—part 1. Biotechnol. Biofuels **6**, 75 (2013). https:// doi. org/ 10. 1186/ 1754- 6834-6- 75
27 . Rocha, G.J., de Martin, M., Soares, C., Souto Maior, I.B., Baudel, A.M., Moraes, H.M., de Abreu, C.A.: Dilute mixed-acid pretreatment of sugarcane bagasse for ethanol production. Biomass Bioenergy **35**, 663–670 (2011). https:// doi. org/ 10.1 016/j. biomb ioe. 2010. 10. 018
28. Segal, L., Creely, J.J., Martin, A.E., Conrad, C.M.: An empirical method for estimating the degree of crystallinity of native cellulose using the X-ray diffractometer. Text. Res. J. **29**, 786–794 (1959). https:// doi. org/ 10. 1177/ 00405 17559 02901 003
29 . Park, S., Baker, J.O., Himmel, M.E., Parilla, P.A., Johnson, D.K.: Cellulose crystallinity index: measurement techniques and their impact on interpreting cellulase performance. Biotechnol. Biofuels **3**, 1–10 (2010). https:// doi. org/ 10. 1186/ 1754- 6834-3- 10
30. Langford, J.I., Wilson, A.J.C.: Scherrer after sixty years: a survey and some new results in the determination of crystallite size. J. Appl. Crystallogr. **11**, 102–113 (1978). https:// doi. org/ 10. 1107/ s0021 88987 80128 44
31. Santos, F.A., de Queiroz, J.H., Colodette, J.L., Manfredi, M., Queiroz, M.E.L.R., Caldas, C.S., Soares, F.E.F.: Otimização do pré-tratamento hidrotérmico da palha de cana-de-açúcar visando à produção de etanol celulósico. Quim. Nova **37**, 56–62 (2014). https:// doi. org/ 10. 1590/ S0100- 40422 01400 01000 11
32 . Cao, W., Sun, C., Liu, R., Yin, R., Wu, X.: Comparison of the effects of five pretreatment methods on enhancing the enzymatic digestibility and ethanol production from sweet sorghum bagasse. Bioresour. Technol. **111**, 215–221 (2012). https:// doi. org/ 10. 1016/j. biort ech. 2012. 02. 034
33. Coletta, V.C., Rezende, C.A., da Conceição, F.R., Polikarpov, I., Guimarães, F.E.G.: Mapping the lignin distribution in pretreated sugarcane bagasse by confocal and fluorescence lifetime imaging microscopy. Biotechnol. Biofuels **6**, 1–10 (2013). https://d oi.org/ 10. 1186/ 1754- 6834-6- 43
34. Chandel, A.K., Antunes, F.A.F., Anjos, V., Bell, M.J.V., Rodrigues, L.N., Polikarpov, I., de Azevedo, E.R., Bernardinelli, O.D., Rosa, C.A., Pagnocca, F.C., da Silva, S.S.: Multi-scale structural and chemical analysis of sugarcane bagasse in the process of sequential acid-base pretreatment and ethanol produc-tion by *Scheffersomyces shehatae* and *Saccharomyces cerevi-siae*. Biotechnol. Biofuels **7**, 63 (2014). https:// doi. org/ 10. 1186/ USMANE KANE 1754- 6834-7- 63
35. Bensah, E.C., Mensah, M.: Chemical pretreatment methods for the production of cellulosic ethanol: technologies and innovations. Int. J. Chem. Eng. **1**, 1–21 (2013). https:// doi. org/ 10. 1155/ 2013/ 719607
36. Zheng, Q., Zhou, T., Wang, Y., Cao, X., Wu, S., Zhao, M., Wang, H., Xu, M., Zheng, B., Zheng, J., Guan, X.: Pretreatment of wheat straw leads to structural changes and improved enzymatic hydrolysis. Sci. Rep. **8**, 1–9 (2018). https://d oi.org/1 0 .1038 / s41598- 018- 19517-5
37. Haque, M.A., Barman, D.N., Kang, T.H., Kim, M.K., Kim, J., Kim, H., Yun, H.D.: Effect of dilute alkali on structural features and enzymatic hydrolysis of barley straw (*Hordeum vulgare*) at boiling temperature with low residence time. J. Microbiol. Biotechnol. **22**, 1681–1691 (2012). https://d oi.org/1 0 .4014 /j mb.1206. 06058
38. Brienzo, M., Ferreira, S., Vicentim, M.P., de Souza, W., Sant'Anna, C.: Comparison study on the biomass recalcitrance of different tissue fractions of sugarcane culm. Bioenergy Res. **7**, 1454–1465 (2014). https:// doi. org/ 10. 1007/ s12155- 014- 9487-8
39. Santos, M., Rezende, C.A., Bernardinelli, O.D., Pereira, N., Curvelo, A.A.S., Eduardo, R., Guimarães, F.E.G., Polikarpov, I.: Structural and compositional changes in sugarcane bagasse subjected to hydrothermal and organosolv pretreatments and their impacts on enzymatic hydrolysis. Ind. Crops Prod. **113**, 64–74 (2018). https:// doi. org/ 10. 1016/j. indcr op. 2018. 01. 014
40. Bernardinelli, O.D., Lima, M.A., Rezende, C.A., Polikarpov, I., Ribeiro, E.: Quantitative 13 C MultiCP solid state NMR as a tool for evaluation of cellulose crystallinity index measured directly inside sugarcane biomass. Biotechnol. Biofuels **8**, 1–11 (2015). https:// doi. org/ 10. 1186/ s13068- 015- 0292-1
41. Santos, M., Brito, E., Eduardo, F., Guimaraes, G., Ribeiro, E., Paro, G., Henrique, E., de Oliveira, V., Pellegrini, A., Kumar, A., Henrique, M., Silveira, L., Polikarpov, I.: Multifaceted characterization of sugarcane bagasse under different steam explosion severity conditions leading to distinct enzymatic hydrolysis yields. Ind. Crops Prod. **139**, 111542 (2019). https:// doi. org/ 10. 1016/j. indcr op. 2019. 111542
42. Simão, J.A., Carmona, V.B., Marconcini, J.M., Mattoso, L.H.C., Barsberg, S.T., Sanadi, A.R.: Effect of fiber treatment condition and coupling agent on the mechanical and thermal properties in highly filled composites of sugarcane bagasse fiber/ PP. Mater. Res. **19**, 746–751 (2016). https:// doi. org/ 10. 1590/ 1980- 5373- MR- 2015- 0609
43. Donaldson, L., Williams, N.: Imaging and spectroscopy of natural fluorophores in pine

needles. Plants **7**, 1–16 (2018). https:// doi. org/ 10. 3390/ plant s7010 010

44. Donaldson, L.: Softwood and hardwood lignin fluorescence spectra of wood cell walls in different mounting media. IAWA J. **34**, 3–19 (2013). https:// doi. org/ 10. 1163/ 22941 932- 00000 002
45. Thite, V.S., Nerurkar, A.S.: Valorization of sugarcane bagasse by chemical pretreatment and enzyme mediated deconstruction. Sci. Rep. **9**, 1–14 (2019). https://d oi.org/1 0 .1038 /s 41598-019-5 2347- 7
46. Chen, W.H., Tu, Y.J., Sheen, H.K.: Disruption of sugarcane bagasse lignocellulosic structure by means of dilute sulfuric acid pretreatment with microwave-assisted heating. Appl. Energy. **88**, 2726–2734 (2011). https:// doi. org/ 10. 1016/j. apene rgy. 2011. 02. 027
47. Wilkinson, S., Smart, K.A., Cook, D.J.: A comparison of dilute acid- and alkali-catalyzed hydrothermal pretreatments for bioethanol production from brewers' spent grains. J. Am. Soc. Brew. Chem. **72**, 143–153 (2014). https:// doi. org/ 10. 1094/ ASBCJ- 2014- 0327- 02
48. Robak, K., Balcerek, M., Dziekońska-Kubczak, U., Dziugan, P.: Effect of dilute acid pretreatment on the saccharification and fermentation of rye straw. Biotechnol. Prog. **35**, e2789 (2019). https:// doi. org/ 10. 1002/ btpr. 2789
49. Noparat, P., Prasertsan, P., O-Thong, S., Pan, X.: Dilute acid pretreatment of oil palm trunk biomass at high temperature for enzymatic hydrolysis. Energy Procedia. **79**, 924–929 (2015). https:// doi. org/ 10. 1016/j. egypro. 2015. 11. 588
50. Yang, J., Xu, H., Jiang, J., Zhang, N., Xie, J., Zhao, J., Wei, M.: Enhanced enzymatic hydrolysis and structure properties of bamboo by moderate two-step pretreatment. Appl. Biochem. Biotechnol. **193**, 1011–1022 (2021). https:// doi. org/ 10. 1007/ s12010- 020- 03472-x

6 Chapter 6: Published paper

Biocatalysis and Agricultural Biotechnology 45 (2022) 102485

Contents lists ScienceDir

Biocatalysis and Agricultural Biotechnology

journal www.elsevier.com/locate

Leaves from four different sugarcane varieties as potential renewable feedstocks for second-generation ethanol production: Pretreatments, chemical composition, physical structure, and enzymatic hydrolysis yields

Melissa C. Espírito Santo [a] Aissata Ousmane Kane [a], Vanessa O.A. Pellegrini [a], Force Tefo Thema [b], Jos´e M. García [c,d], Alberto Acevedo [e], Luis E. Erazzú [c], Francisco E.G. Guimaraes [a], Eduardo R. deAzevedo [a], Igor Polikarpov [a,*]

[a] *Sao Carlos Institute of Physics, University of S˜ao Paulo, Av. Trabalhador São-carlense, 400, Pq. Arnoldo Schmidt, Sao Carlos, SP, 13566-590, ˜ Brazil*

[b] *Botswana University of Agriculture and Natural Resources (BUAN), Gaborone, Botswana*

[c] *Agricultural Experimental Station of Famailla, National Institute of Agricultural Technology (INTA), Famaill´ a, Tucum´ an, Argentina ´* [d] *National Council of Scientific and Technical Research (CONICET), Ciudad Autonoma de Buenos Aires, Buenos Aires, Argentina ´* [e] *Institute of Soils, National Institute of Agricultural Technology (INTA), Castelar, Buenos Aires, Argentina*

ARTICLE INFO

Keywords:
Sugarcane leaves
Sugarcane biotypes
Physical structure
Enzymatic hydrolysis
Second-generation ethanol

ABSTRACT

Development of Bioeconomy is impossible without establishing efficient technologies of lignocellulosic biomass valorization via transformation into fermentable sugars. Sugarcane is a valuable agricultural crop in several Asian, African, and Latin American countries. Here, leaves from two sugarcane and two energy cane varieties were evaluated for sustainable production of second-generation sugars, and their enzymatic hydrolysis yields were compared. Structural, morphological, and chemical composition changes in sugar and energy cane leaves submitted to acid, and acid-alkaline pretreatments were analyzed using X-ray diffraction, scanning electron microscopy, confocal laser microscopy, high-performance liquid chromatography, and low-field solid-state NMR techniques. Enzymatic hydrolysis assays were conducted to evaluate saccharification yields of untreated and pretreated leaves. Jointly, our results revealed the significant potential of leaves from two commercial sugar cane cultivars currently bred in Argentina as possible lignocellulose substrates for the 2G ethanol industry.

https://doi.org/10.1016/j.bcab.2022.102485
Received 30 April 2022; Accepted 5 September 2022
Available online 15 September 2022

Abbreviations: ANOVA, Analysis of variance; CLSM, Confocal Laser Scanning Microscopy; CrI, Crystallinity Index; CPMAS, Cross-Polarization Magic-Angle Spinning; CPMG, Carr-Purcell Meiboom-Gill; EC, Energy cane; HPLC, High-Performance Liquid Chromatography; INTA, National Institute of Agricultural Technology of Argentina; NMR, Nuclear Magnetic Resonance; SC, Sugar cane; SCB, Sugar Cane Bagasse; SCL, Sugar Cane Leaves; SEM, Scanning Electron Microscopy; XRD, X-ray diffraction.

* Corresponding author.
E-mail address: ipolikarpov@ifsc.usp.br (I. Polikarpov).

https://doi.org/10.1016/j.bcab.2022.102485
Received 30 April 2022; Accepted 5 September 2022
Available online 15 September 2022

1. Introduction

Lignocellulosic residues from agricultural production represent a renewable and abundant resource for producing second- generation biofuels, sustainable materials, and green chemicals. In subtropical and tropical zones, the use of sugarcane for sugar and first-generation (1G) ethanol production generates three types of abundant lignocellulosic residues: sugarcane bagasse, sugar cane leaves, and tops (the upper immature portion of the stalks) (Canilha *et al.*., 2012). Sugar cane bagasse is obtained after sugarcane stalks are crashed at the mills, whereas leaves and tops are frequently left at the fields in the process of sugar cane harvesting. Although the second-generation (2G) ethanol industry based on sugar cane bagasse as a source of carbohydrates has become a reality, an addition of the remaining sugarcane residues (sugar cane leaves and tops) could greatly increase the amount of lignocellulosic material available for 2G ethanol production without the need of expansion to newly cultivated areas (Martins *et al.*., 2016; Roozeboom *et al.*., 2019).

The three main constituents of lignocellulosic biomass are cellulose, hemicellulose, and lignin. These main fractions could be found in different proportions depending on several factors, including crop variety, environmental conditions (climate, location, physical and chemical soil composition), growth habit, and use of fertilizers can be significantly different for sugar cane bagasse and sugar cane leaves (De Souza *et al.*., 2013; Ferreira-Leitao *et al.*., 2010˜). One of the biggest challenges that biorefinery faces is the availability of suitable raw materials. In this context, the sugar cane leaves can be considered as a source of renewable carbon, poorly explored by the sugarcane agroindustry.

Although sugar cane leaves have a somewhat different chemical composition and morphology than sugar cane bagasse, their joint processing is more challenging. It is possible to reduce lignocellulose recalcitrance through the optimization of biomass pretreatments, leading to increased enzymatic hydrolysis yields and more efficient use of the biomass (Galbe and Zacchi, 2012; Lima *et al.*., 2013). Acid and alkaline pretreatments of sugar cane leaves have been previously studied (Alvira *et al.*., 2010; Baruah *et al.*., 2018; Kumar and Sharma, 2017); however, structural and chemical features of sugar cane leaves that could affect pretreatment efficiencies have not been yet thoroughly investigated. The hemicellulose fraction is hydrolyzed at low pHs and acid conditions, while the cellulose and lignin fractions are less affected. On the other hand, lignin solubilization occurs at basic pHs (Galbe and Wallberg, 2019; Kumar and Sharma, 2017). Furthermore, cell wall recalcitrance is a complex trait controlled by diverse factors, including sugarcane genetic background.

In the present study, we analyze changes in the chemical composition and physical structure of leaves from two sugarcane commercial varieties (SC384 85–384 and NA 78–724) and two energy cane biotypes recently developed in Argentina (INTA 05–3116 and INTA 05–3118), submitted to acid and acid-alkaline pretreatments. Subsequent enzymatic hydrolysis assays were conducted to compare the side-by-side saccharification potential of untreated and pretreated leaves from the studied sugarcane and energy cane cultivars. The physical structure and morphology of sugar and energy canes from studied varieties were analyzed using X-ray diffraction, scanning electron microscopy, confocal laser microscopy, and low-field solid-state NMR techniques. Jointly, the results of our studies reveal the leaves from commercial sugarcane cultivars SC384 85–384 and NA 78–724 have a significant potential to be used as lignocellulose substrates for the 2G ethanol industry.

2. Materials and methods

2.1. Biomass

The raw material consisted of sugarcane (Saccharum spp.) leaves from two commercial varieties, LCP 384 85–384 (hereafter SC384) and NA 78–724 (SC724) currently bred in Argentina, and two recently developed energy cane biotypes, INTA 05–3116 (EC3116) and INTA 05–3118 (EC3118). SC384 is the prevailing planted variety in Tucuman (´ Acevedo *et al.*., 2017; Racedo *et al.*., 2016), the Argentine province which concentrates 73% of the sugarcane growth area in the country. SC724 was used as a progenitor within the National Institute of Agricultural Technology of

Argentina (INTA). EC3116 and EC3118 varieties are close to be released in Argentina and have been developed to maximize the energy production from the entire biomass. Sugar and energy canes were collected at the experimental field of INTA, Famailla Research Station, Tucum´ an, Argentina (27´ ◦03′S, 65◦25′W, 363 masl.) from plots growing at the second-ratoon crop. Biomass samples were size reduced using a knife mill (Wiley) and passed through a 20-mesh sieve. Then, they were dried in a convection oven at 40 ◦C and stored at room temperature in airtight plastic zip-lock bags until further use.

2.2. Pretreatment conditions

ECs and SCs were initially hydrolyzed with dilute H_2SO_4 (1% v/v) for 40 min in the autoclave at 121 ◦C. The ratio of biomass to liquid was maintained at 1:10 (grams of bagasse/mL of solution). At the end of pretreatment, the biomass was cooled at room temperature, and a solid fraction was separated from the hydrolysate by filtration. This material was washed with tap water to eliminate the excess acid before oven drying at 40 ◦C. A second pretreatment step was applied to a fraction of dilute acid pretreated leaves, using NaOH (1% w/v) with a residence time of 40 min in an autoclave at 121 ◦C.

2.3. Compositional analysis

A heating balance (Shimadzu; Kyoto, Japan) was used to determine the leave humidity contents. Chemical compositions of raw and pretreated samples were determined as described by Rocha *et al.* (2011) (Rocha *et al.*., 2011) with some modifications detailed in Santo *et al*. (2018).

Briefly, untreated, and pretreated samples (ECs and SCs) (2 g) were hydrolyzed with 72% (v/v) H2SO4 for 7 min at 45 ◦C. After the first hydrolysis, the acid was diluted to a 4% concentration, and the second hydrolysis was carried out by autoclaving the reaction mixture at 121 ◦C for 30 min. The solid residue that remained after filtration was used to determine the acid-insoluble lignin, and the liquid fraction was filtered with 0.45 μ filters (Millipore Filters) for high-performance liquid chromatography analysis (HPLC; Shimadzu LC-10). The mobile phase was diluted H2SO4 (5.10–3 mol/L) with a 0.6 ml/min flow rate in the Aminex column (HPX-87H, 300.0 × 7.8 mm Bio-Rad - Hercules, CA, USA). The temperature of oven was maintained at 65 ◦C, and the sugars were detected using a Refractive Index (RI) detector. Glucose, xylose, and arabinose were used as standards for HPLC analysis.

Raw material before acid concentration hydrolysis extractives were removed using a 1:1 cyclohexane/ethanol solvent mixture under reflux in a Soxhlet apparatus for 8 h, followed by water

extraction. The glucose and xylose concentrations obtained after acid and acid-alkaline hydrolysis were used to quantify cellulose and hemicellulose content, respectively, according to the following equations:

$$\%\text{Hemicellulose} = \frac{\text{C(xylose)}\times\text{V}\times 0.88}{\text{m}} \qquad \text{equation (1)}$$

$$\%\text{Cellulose} = \frac{\text{C(glucose)}\times\text{V}\times 0.9}{\text{m}} \qquad \text{equation (2)}$$

Here, the C(Xylose) and C(Hemicellulose) stand, respectively, for xylose and hemicellulose concentrations (mg/ml) obtained after enzymatic hydrolysis, V(ml) is the volume of the reaction mixture, and m (mg) is the weight of leaves used for enzymatic hydrolysis. 0.9 and 0.88 represent respectively the conversion factors of glucose and xylose, which consider the addition of water molecules to the anhydroglucose residues in the process of cellulose and xylan hydrolysis.

2.4. Determination of glucan conversion yields

Commercial cellulase enzymes Cellic CTec3 (Novozymes, Sigma–Aldrich, St. Louis, MO) were used for glucan conversion in the untreated and treated samples. Enzymatic saccharification of the samples was performed in 50 mM sodium citrate buffer (pH 5.0) at 50 ◦C with shaking (180 rpm) for 72 h, using a sample to solution ratio of 10% (weight per volume). The applied enzymatic dosage was 5 mg of enzyme per g of sample. According to published data, Cellic CTec3 activity is 165.2 ± 5.1 FPU/g of product (Suna *et al.*., 2015), therefore the applied enzymatic loadings roughly corresponded to 0.83 ± 0.03 FPU per g of biomass samples. Since glucan content in studied sugar and energy cane biotypes varied between 32% and 44% (Table 1), this corresponded to enzymatic loadings of 1.9–2.6 FPU per g of glucan in the studied samples. Enzymatic reaction samples were retrieved after 24, 48 and 72 h of hydrolysis, centrifuged to remove the unhydrolyzed residues and incubated at 100 ◦C for 10 min to deactivate the enzymes. Next, the hydrolysates were filtered through 0.45 μm syringe filters and their glucose concentrations were determined by HPLC under the same condition used for compositional analysis (see above). The glucan conversion yields were calculated as a ratio between the glucose released during enzymatic hydrolysis and the total amount of glucose which could be obtained from the complete hydrolysis of cellulose in each sample.

2.5. Scanning electron microscopy (SEM)

SEM analysis was applied to investigate structural changes in the morphology of untreated and pretreated leaves. The dried samples were fixed on suitable stubs and then coated with Au in a SCD 050 sputter coater (Oerlikon-Balzers, Balzers, Liechtenstein). Following fixation, images were

captured at different magnifications using a field emission electron microscope (Zeiss, SIGMA model).

2.6. X-ray diffraction (XRD) analysis

The X-ray diffractograms were recorded on a diffractometer RU200B (Rigaku, Japan) using copper radiation (λ =1.54 Å) generated at an applied voltage of 45 kV and a current of 36 mA. To evaluate the crystallinity index in each sample deconvolution of the XRD diffractograms using Peak fitting program (Peak Fit; www.systat.com) was performed as described by Park *et al.* (2010) and Bernardinelli *et al.* (2015) (Bernardinelli *et al.*, 2015; Park *et al.*, 2010). Following Scherrer equation was applied to calculate average crystallite sizes (Monshi *et al.*., 2012; Scherrer, 1912).

$$D = \frac{K\lambda}{\beta cos\theta} \qquad \text{Equation (3)}$$

here K is the correction factor (0.9), λ is the wavelength of the X-ray radiation (1.54056 Å), β is the full width on the half maximum (FWHM) of the diffraction peak in radians, and Θ is the diffraction angle of the peak.

2.7. Confocal laser scanning microscopy (CLSM)

CLSM was used to analyze the lignin autofluorescence of the untreated and treated ECs and ECs samples. CLSM images were collected using a Zeiss LSM 780 confocal microscope equipped with a Coherent Chameleon laser (Tisapphire). Samples were immersed in water and analyzed with a Plan-Apochromat objective lens (20×) in an excitation source for two-photon excitation (2P), as described previously (Coletta *et al.*., 2013; Santos *et al.*., 2018).

2.8. Low-field nuclear magnetic resonance (NMR) studies

Porosity and water accessibility are intimately related to the enzyme accessibility to cellulose. Low-field nuclear magnetic resonance (NMR) is a physical technique that allows evaluation of porosity and water accessibility in the samples. NMR experiments were carried out in samples previously dried at 80 ◦C, under an 800-mmHg vacuum for 5 h and soaked with ultrapure water (MilliQ, Millipore Inc.) overnight. Then the samples were centrifuged with a rotation frequency of 1000 rpm for 1 min and filtrated (Corning®

Costar® Spin-X, 0.45 μm, nylon membrane). Relaxation measurements of 1H NMR were carried out using a CPMG (Carr-Purcell- Meiboom-Gill) sequence with the acquisition of 35,000 echoes and a permanent Bruker Minispec MQ-20 spectrometer (Bruker, Billerica, USA) operating at 0.47 T (20 MHz).

Datas of NMR relaxation were analyzed by Inverse Laplace Transform (ILT), resulting in a distribution of transverse relaxation times (T2) (Borgia *et al.*., 1998; Provencher, 1982). Echo times of 70 μs and recycle delay of 15 s. The contribution of each interstitial scale of the biomass was analyzed by deconvoluting T2 distributions using logarithmic-Gaussian (log-Gaussian) functions. These experiments were conducted in duplicate, and the ILT was carried out on the CPMG decay given by the mean of the normalized data from these two experiments.

When a fluid is confined inside a pore, the interaction between the pore surface and the 1H nuclear spins of the fluid molecules imply a reduction of the observed transverse relaxation rate. T2, then T2 distribution of this fluid reflects its pore size distribution media qualitatively. This effect is directly dependent on the pore size. On the fast diffusion limit, the relation between T2 and the pore size is given in Equation3 (Brownstein and Tarr, 1979; Capitani *et al.*., 2012)

$$\frac{1}{T_2} = \rho \frac{S}{V} = \frac{2\rho}{r} \qquad \text{Equation (4)}$$

where ρ is the surface relaxivity dependent on the porous matrix, and S and V are the pore surface area and volume, respectively.

2.9. 13C solid-state NMR spectroscopy

Solid-state NMR spectroscopy experiments of raw and treated samples were acquired using a Varian Unity Inova spectrometer (Varian, Palo Alto, USA) operating at 100.5 MHz and 400.0 MHz for 13C and 1H, respectively. A Jakobsen probe 7 mm double resonance with sample rotation pneumatic system built around the magic angle spinning probe with a frequency stability superior to 2 Hz was used for data collection. Ramped cross-polarization with RF amplitude varying between 80 and 100% during a contact time of 1 ms was performed as an excitation method (13C CPMAS). Magic angle spinning of 10 kHz, high power dipolar decoupling of 70 kHz, 13C, and 1H 90◦ pulse durations of 3.5 and 4.0 s, respectively, were typically used. All 13C ssNMR measurements were performed using 2 s recycle delays.

2.10. Statistical analysis

Analysis of variance (ANOVA) and DGC multiple comparison test (Di Rienzo *et al.*., 2002) were used to analyze the effect of pretreatments on the chemical composition of EC and SC varieties, as well as the effect of pretreatments, hydrolysis time (24h, 48h and 72h) and a variety type, on the enzymatic hydrolysis yield obtained from SCL. Info starts software v. 2020 (Di Rienzo *et al.*., 2020) was used for statistical analysis.

3. Results and discussion

3.1. Acid and acid-alkaline pretreatments increase cellulose content in the leaf varieties

Chemical composition of the SCL samples from commercial varieties and EC biotypes are given in Table 1. ANOVA revealed statistically significant differences in the amount of cellulose and ash content in untreated SCL from commercial cultivars (SC384 and SC724) as compared to the energy cane cultivars (EC3116 and EC3118) (Table 1). Both SC384 and SC724 have significantly higher cellulose content (about 43%) than leaves from energy cane genotypes (EC3116 and EC3118, maximum of 35%), indicating that from a biorefinery point of view, high glucan content materials such as SC384 and SC724 SCL might be preferable for lignocellulosic ethanol production. Levels of hemicellulose and lignin did not have statistically significant deviations in untreated leaves across analyzed genotypes (Table 1). Nevertheless, the lignin and hemicellulose removal levels varied among samples and depended on the applied pretreatments (Table 1). Therefore, the final chemical composition results might be related to the structural characteristics of each sample.

An increase in lignin and cellulose after acid pretreatment is related to the solubilization of the hemicellulose fraction (Table 1). This process makes cellulose more accessible to the enzymes and facilitates their enzymatic hydrolysis (Rocha *et al.*., 2011; Rezende *et al.*., 2011). The strongest enrichment of the cellulose fraction occurred in SCL EC3118 sample, where the cellulose content after acid pretreatment increased to 58% from the initial 31% as determined for the native sample. In all samples, most of the hemicellulose fraction was removed using the dilute acid pretreatment conditions (Table 1). In addition, relative percentage of lignin in the samples increased slightly after the dilute acid pretreatment mostly due to the removal of hemicelluloses. A part of the remaining hemicellulose fractions was further removed in the subsequent alkaline pretreatment steps using 1% NaOH, which mostly resulted in lignin solubilization (Jackson, 1977; Rezende *et al.*., 2011). Consistently, the cellulose content considerably increased after two-step pretreatment (H2SO4 1% + NaOH 1%). Overall, two-step pretreatment (H2SO4 1% + NaOH 1%) of SCL from commercial SC724 and SC384 varieties led to pretreated biomass with higher content of cellulose and lower concentration of lignin as compared to recently developed EC3116 and EC3118 varieties. For example, in SCL SC724 samples, the cellulose fraction was increased from an initial 43% to circa 72% after the applied two-step pretreatment, whereas lignin fraction decreased from 14.5% to 9.9%.

However, chemical compositional analysis alone does not provide information on the complex structure of the lignocellulosic materials and changes in the physical structure of the sugar and

energy canes imprinted by applied pretreatments. Therefore, we applied a set of physical techniques and methods to shed light on the physical structure of the SCL from studied sugar and energy cane varieties and changes introduced in these lignocellulosic materials by applied pretreatments.

Table 1. Chemical composition of untreated sugar and energy cane leave samples, and the samples submitted to dilute acid pretreatment (H2SO4 1%) and combined acid + alkaline pretreatment (H2SO4 1% + NaOH 1%).

Sample	Cellulose (%)	Hemicellulose (%)	Ash (%)	Lignin (%)	Extractives (%)	Total (%)
Untreated						
SCL_EC3116	35.5±2.1f	23.0±1.3a	7.6±0.4c	14.4±0.2d	12.4±1.5a	92.8±5.6
SCL_EC3118	31.6±1.2g	22.8±1.4a	7.8±0.9c	15.7±0.9d	13.8±1.7a	91.6±1.8
SCL_SC384	43.9±1.4e	24.4±0.6a	5.6±1.1d	13.4±0.6d	12.7±1.3a	100.0±3.8
SCL_SC724	42.8±1.8e	24.4±0.7a	4.5±0.1d	14.5±0.7d	13.9±1.1a	100.1±2.8
IDilute acid pretreated						
SCL_EC3116	53.0±0.8d	8.9±0.1c	11.6±0.1a	22.6±2.4b		96.1±3.3
SCL_EC3118	57.8±1.5c	11.6±0.7b	11.3±0.1a	20.9±0.5b		101.3±1.6
SCL_SC384	57.0±1.9c	8.3±0.2c	11.5±0.4a	20.6±1.6b		97.2±3.7
SCL_ SC724	52.7±0.9d	8.1±0.1c	10.8±0.3a	25.6±0.4a		97.1±0.7
Acid+alkali pretreated						
SCL_EC3116	60.3±0.2c	8.3±0.1c	11.2±0.4a	17.8±0.7c		97.4±1.2
SCL_EC3118	64.1±1.8b	7.1±0.4d	10.7±0.3a	14.5±0.6d		96.3±3.0
SCL_SC384	68.8±2.1a	5.6±0.9d	9.3±0.6b	7.5±0.5e		91.2±3.0
SCL_SC724	72.2±2.0a	6.7±0.6d	8.5±0.0c	9.9±0.5e		97.2±1.9
	Summary of ANOVA					

SCL	***	ns	***	***	ns
Treatment	***	***	***	***	
SCL: treatment	***	**	*	***	

*** significant at <0.001, ** significant at <0.01, ** significant at <0.05, ns = no significant. Different letters within columns indicate significant differences for DGC test ($p < 0.05$). SCL: Sugar Cane Leaves.
Dilute acid: H_2SO_4 (1%).
Acid þ alkali: H_2SO_4 1% + NaOH 1%.

3.2. Both dilute acid and combined acid and alkali pretreatments lead to the separation of fibers

Morphological changes in leaves after dilute acid and two-step (dilute acid and alkali) pretreatments were examined by scanning electron microscopy (SEM) to evaluate structural modification introduced in pretreated sugar and energy-cane leave samples in comparison to raw materials. Fig. 1 shows the scanning electron micrographs of raw sugar and energy cane samples. All the studied samples have a compact rigid structure. The images of the untreated leaves revealed that the fiber bundles are covered by a dense surface layer irrespective of the sample while morphological analysis of the pretreated materials showed that this surface layer is being gradually removed by each pretreatment step (Figs. 2 and 3).

Partial deconstruction of the natural rigid structure of the plant cell walls with exposure and separation of fiber bundles is observed after acid pretreatment (Fig. 2). This is consistent with previous studies of SCB which demonstrated that dilute acid pretreatment can cause separation of the cellulose bundles loosening the fibrous network (Chandel *et al.*, 2014; Rezende *et al.*, 2011). However, degree of cellulose bundles separation of SC and EC leaves caused by dilute acid pretreatment was clearly superior to that observed for sugarcane bagasse (Chandel *et al.*, 2014; Rezende *et al.*, 2011) and for eucalyptus bark (Lima *et al.*., 2013). The reason for that is not completely clear but might be related to different physiological role and chemical composition of these different biomasses. Importantly, sugarcane bagasse is significantly more lignified than SC and EC leaves. Indeed, lignin fraction in SC bagasse was reposted as 22%–29% (Rezende *et al.*, 2011; Lima *et al*., 2013; Santo *et al*., 2018) whereas SC and EC leaves lignin content varied

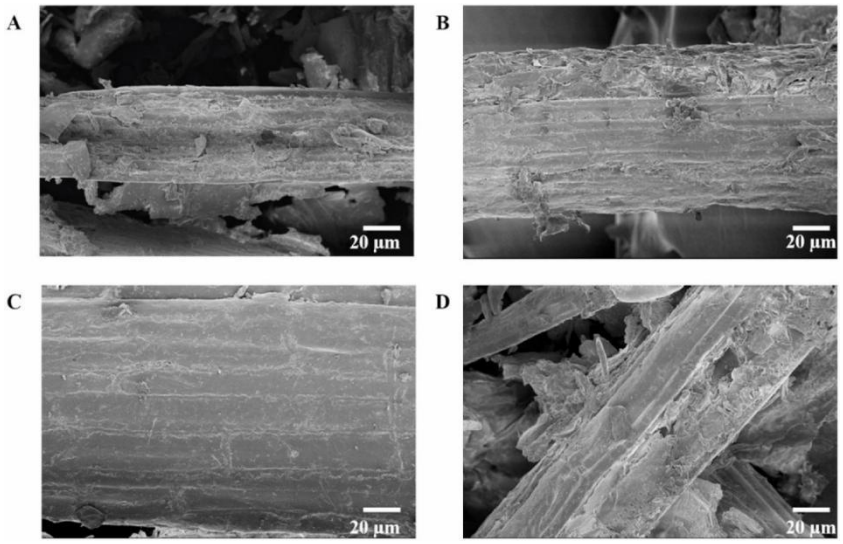

Fig. 1. Surface images of untreated sugar and energy cane leaves obtained by scanning electron microscopy. (A) EC3116; (B) EC3118; (C) SC384; (D) SC724 cultivars.

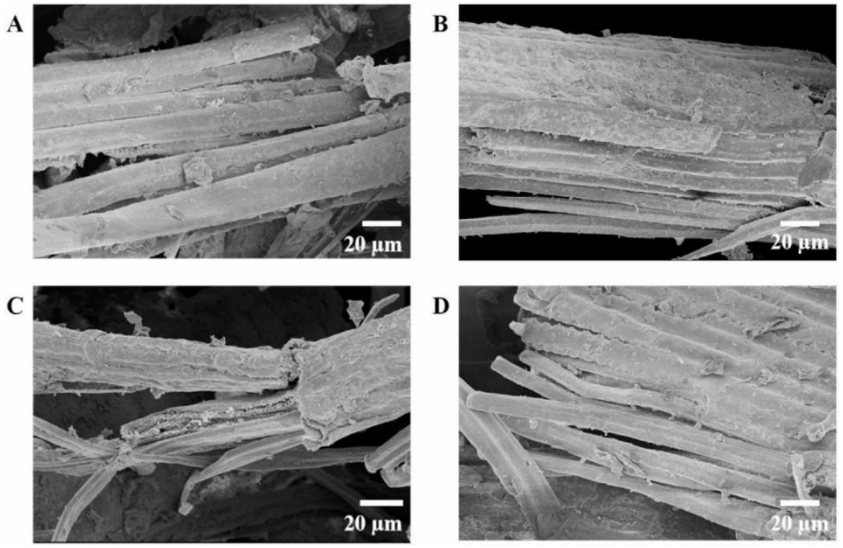

Fig. 2. Scanning electron microscopy surface images of leaves from (A) EC3116; (B) EC3118; (C) SC384 and (D) SC724 varieties after diluting sulfuric acid (H2SO4 1% (v/v)) pretreatment.

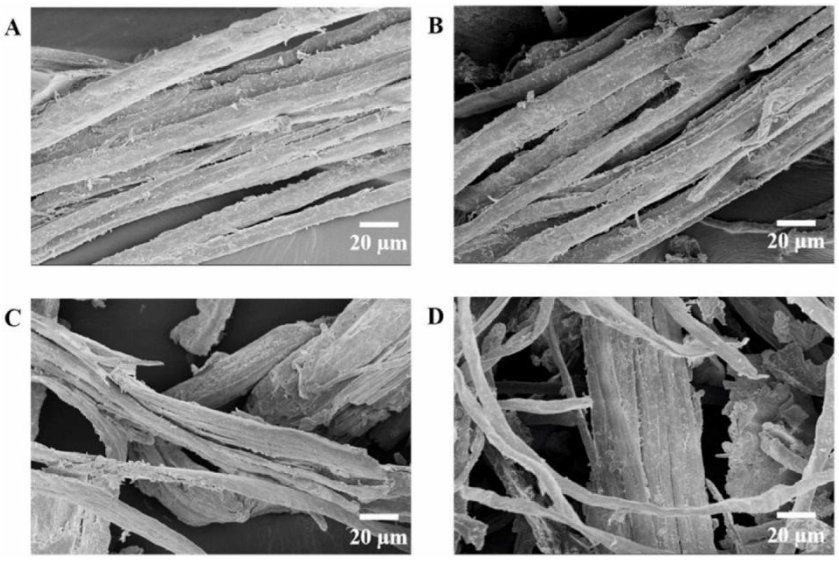

Fig. 3. Scanning electron microscopy surface images of the leaves from (A) EC3116; (B) EC3118; (C) SC384 and (D) SC724 submitted to combined acid + alkaline pretreatment (H2SO4 1% + NaOH 1%).

between 14% and 17% (Table 1). The latter numbers are consistent with previous characterization of SC leaves composition with a lignin fraction reported to be 16% (Jutakanoke *et al.*, 2012). Indeed, pretreated sugar and energy cane leaves display a less cohesive and more fractured structure after the dilute acid pretreatment (Fig. 2).

After the two-steps of pretreatment, the structuring of the cellulose bundles is even more evident. The bundles lose their tightly packed assembly (Fig. 1) and are more separated from each other (Fig. 3). This is a result of the delignification process provoked by the alkaline pretreatment. Lignin acts as an adhesive material in the cell wall structure, limiting access to the cellulose bundles, and when it is removed, the cellulose fibers become more separated and looser (Rezende *et al.*., 2011; Lima *et al.*, 2013).

Significantly, combined dilute acid followed by alkaline pretreatment of SC and EC leaves applied in this study led to a similar lignin content as for SC bagasse subjected to similar combined acid + alkaline pretreatment (Rezende *et al.*, 2011).

3.3. Confocal laser scanning microscopy (CLSM)

Next, CLSM was used to characterize and map the lignin arrangement in sugar and energy cane cell walls before and after of applied pretreatments. Fig. 4 shows CLSM images of unpretreated SC and EC leaves samples. Emission contribution in the red spectral region is attributed to chlorophyll in the chloroplasts (Hutzler *et al.*, 1998), as seen in all images of CLSM (Fig. 4A–D). In primary rye leaves, the blue autofluorescence has contributions from lignin and is covalently

bound to its ferulic acids (Schmitz *et al*., 1996). Furthermore, Lichtenthal and Schweiger (1998) (Lichtenthaler and Schweiger, 1998) demonstrated that different kinds of leaves of green plants exhibited blue-green fluorescence emission and in sugarcane the blue-green fluorescence was generally several times higher than the red chlorophyll fluorescence, corroborating our results (Fig. 4). Overall, CLSM images of unpretreated SC and EC leaves samples are like those obtained for untreated SC bagasse (Coletta *et al.*, 2013; Santo *et al.*, 2018), except for strong red autofluorescence of chlorophyll observed in SC and EC leaves samples (Fig. 4). Since chlorophyll is essential for photosynthesis in plants which mostly occurs in leaves, its presence in EC and SC leaves samples is not surprising.

Autofluorescence emission changes dramatically after the pretreatments indicating that the natural lignin arrangement in the untreated leaves has been strongly modified by the dilute sulfuric acid and alkali catalyzed pretreatments (Figs. 5 and 6). It is important to notice that Figs. 5 and 6 show the true-color images resulting from the pixel-by-pixel overlapping of the spectrally resolved lignin auto emission light (Coletta *et al*., 2013).

Following thermo-chemical pretreatment with dilute sulfuric acid, the predominant autofluorescence of the leaf cell walls turns green and pink- red (Fig. 5).

Dilute acid pretreatment results in a considerable disorder in lignin arrangement provoked by the removal of xylan. Lignin fragments in the residual biomass tend to reorganize, causing remarkable redistribution of aggregated lignin (Liu and Wyman, 2003; Coletta *et al*.., 2013). It reflects spectral changes that report on rearrangements of condensed lignin in the pretreated plant cell wall. In the pretreated sugar and energy cane samples (Figs. 5 and 6), the outermost region emits green-yellowish light characteristic of this reorganization (Coletta *et al.*, 2013; Espírito Santo *et al*., 2019). Pink and red color emission is characteristic of chlorophyll (Markou, 2015). The chlorophyll is degraded by alkaline treatment (Mínguez-Mosquera and Gandul-Rojas, 1995). Consistent with this fact, no significant pink or red color emission contribution is observed after the two-step pretreatment (Fig. 6). Shifts in lignin autofluorescence emission color observed for SC and EC leaves samples (Fig. 6) are consistent to the changes in color of SC bagasse autofluorescence CLMS images of pretreated SC bagasse samples reported in previous studies (Coletta *et al.*, 2013; Espírito Santo *et al.*, 2019).

3.4. Low-field nuclear magnetic resonance

Lignocellulosic pretreatments may have diverse effects on the biomass structure and chemical composition, for instance, through the total surface area alteration of the substrate and/or the sample porosity changes, which could directly influence the access of enzymes to the substrate, thus playing a fundamental role in the efficiency of enzymatic hydrolysis (Tsuchida *et al*., 2014a).Water accessibility to polysaccharides of the plant cell walls can be a good approximation of enzyme accessibility to their polysaccharide

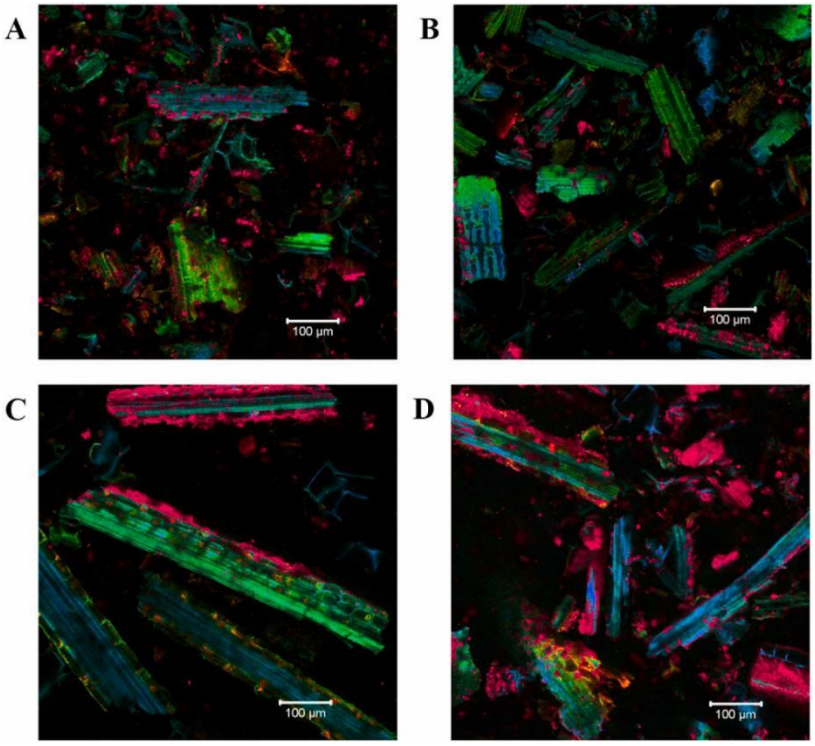

Fig. 4. Confocal laser scanning microscopy images of untreated sugarcane and energy cane leaves (A) EC3116; (B) EC3118; (C) SC384; (D) SC724.

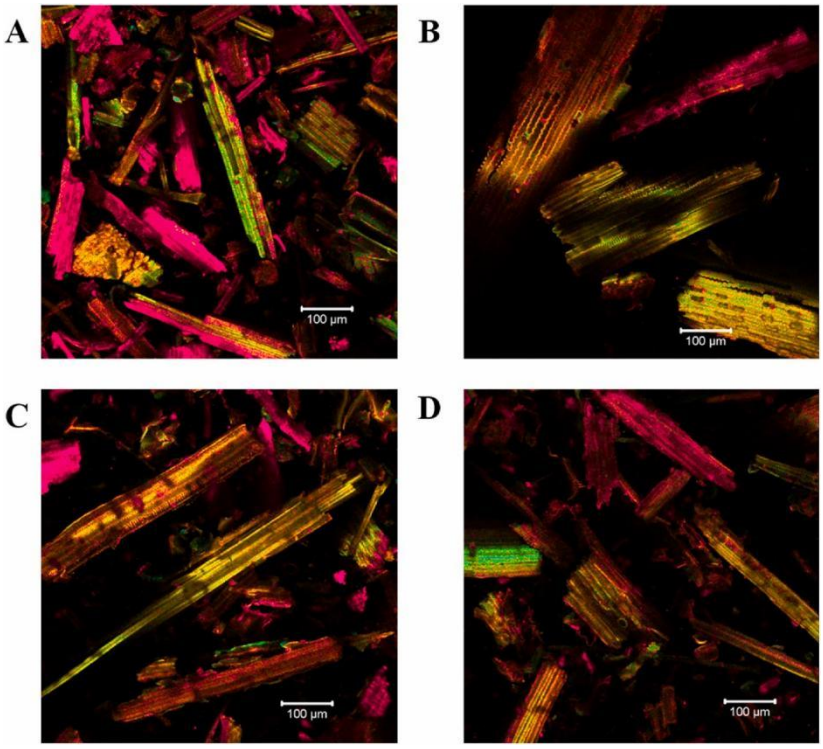

Fig. 5. Confocal laser scanning microscopy images of sugar and energy cane leaves. The studied varieties (A) EC3116; (B) EC3118; (C) SC384 and (D) SC724 after diluting sulfuric acid (H2SO4 1% (v/v)) pretreatment. substrates (Kane *et al*.., 2022; Tsuchida *et al*.., 2014a). To estimate the water accessibility, low field ssNMR was applied in our studies.

For lignocellulosic biomass, three different length scales are observed: first related to pores at microfibril surfaces (shortest T2 values, about 1 ms); second related to distances within the lignin-hemicellulose matrix on the surface of the fibers (tens of milliseconds), and the third one, characteristic of small luminal pores or between the fibers (hundreds of milliseconds) (Santo *et al*.., 2018; Espírito Santo *et al*., 2019). Each of these components is deconvoluted from the T2 distributions by log-Gaussian functions, and their relative contribution indicates the amount of solvent in the respective interstitial scale. Thus, by measuring the T2 distributions for samples which underwent different pretreatments, it is possible to assess how the microstructure of the biomass is modified at different scales.

To remove the bulk water and get a good reproducibility on the T2 distributions, we have abdicated to control the amount of biomass and water in each measurement. Thus, we can only assess the proportion of water on each microstructure of the leaf samples given by the respective relative area on the distributions (Fig. 7). For all samples, the relative area of the smallest component related to pores on microfibril surfaces is not significant compared to the other two components. Moreover, these small components showed themselves particularly sensitive to the regularization parameter

of the ILT procedure) (Borgia *et al*., 1998; Provencher, 1982) and therefore were not considered in our data analysis. As a general trend for all groups of the EC and SC samples after the applications of the pretreatments, an increase in the relative areas related to the largest pore scale was observed indicating that the removal of hemicellulose and lignin fractions result in an increase of water accessibility within the larger pores. Such effect is stronger in the leaf samples of the groups SCL_EC3118, SCL_SC384 and SCL_SC724, which, after the combined effects of the dilute acid and alkaline pretreatments show an increase of the areas of luminal pores of 31 ± 6%, 30 ± 10%, and 53 ± 8%, respectively. All relative areas obtained from the deconvolutions are shown in Table 2.

There is a direct relation between the sizes of pores and T2, however the surface relaxivity constant being unknown impedes us to estimate the actual pore sizes for the interstitial scales observed in our experiments. Thus, the variations observed on the central T2 values of each component in the T2 distributions shown in Fig. 7 are a combined effect of modifications both on the pore sizes and the surface relaxivity of the pores, caused by the changes in the composition of the leave samples due to the removal of hemicelluloses and lignin after pretreatments. The later changes will modify the affinity of interactions between the pore surfaces and water molecules.

The three distinct T2 distributions associated with the different water environments show SCL_EC3118, SCL_SC384, and SCL_SC724 samples a steady decrease in T2 constants characteristic of waters interacting with the cell walls (Table 2) and simultaneous increase in a fraction of water molecules within the lumen pores. These facts can be partially explained by the lignin removal, particularly after alkali pretreatment (NaOH 1%), which results in the pretreated sample with greater hydrophilicity. Indeed, partial removal of highly hydrophobic lignin molecules renders the pretreated leaves more water-accessible and hydrophilic (Tsuchida *et al.*, 2014a). This

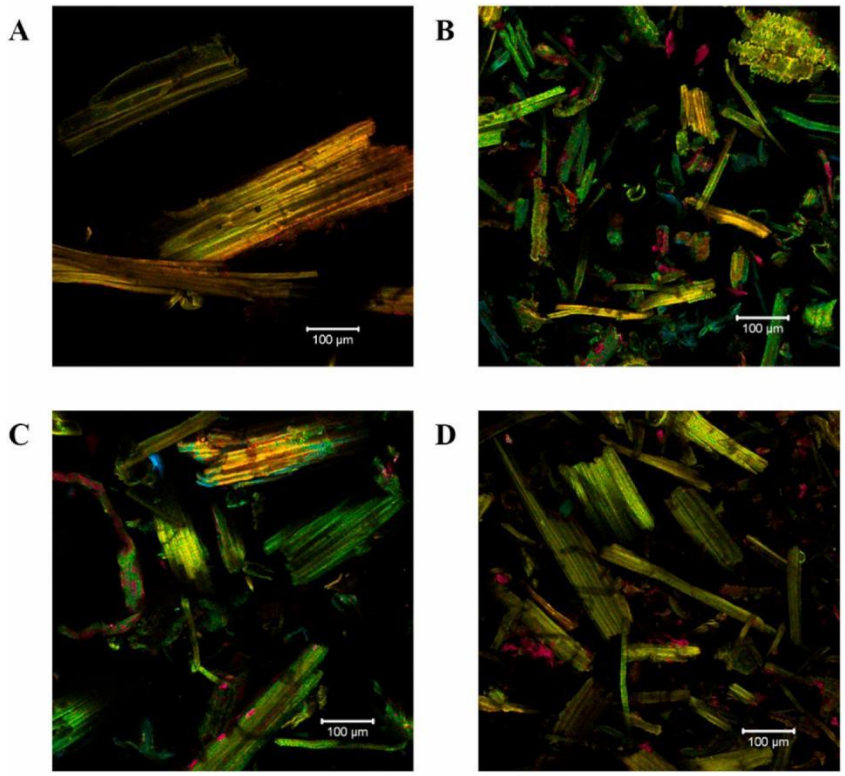

Fig. 6. Confocal laser scanning microscopy images of leaves from (A) EC3116; (B) EC3118; (C) SC384; (D) SC724 submitted to combined dilute acid + alkaline pretreatment (H2SO4 1% + NaOH 1%).

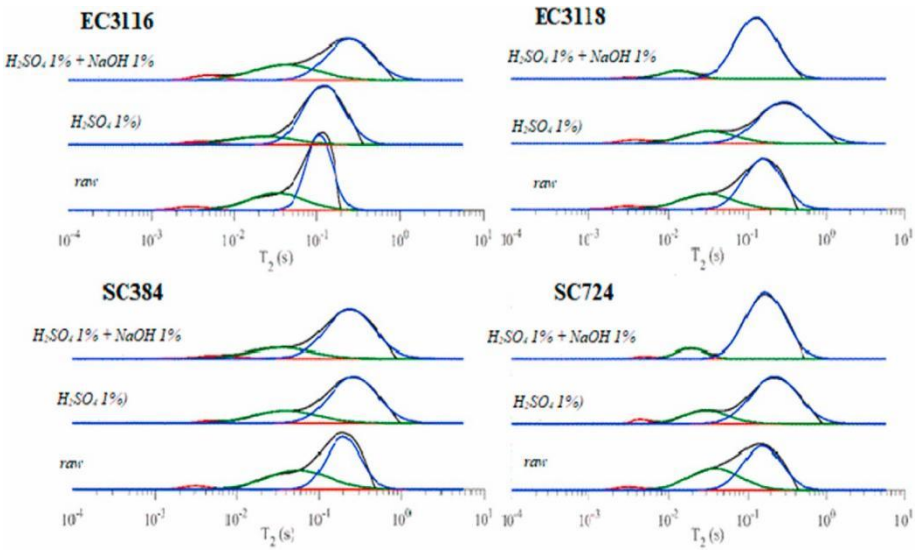

Fig. 7. T2 distributions for sugar and energy leaf samples (EC3116; EC3118; SC384; SC724) untreated and submitted to dilute acid pretreatment (H2SO4 1%) and combined acid -alkaline pretreatment (H2SO4 1% + NaOH 1%). The solid black lines represent the distributions, whereas the components associated with each interstitial scale are shown in red (microfibril surfaces), green (cell wall) and blue (lumens). (For interpretation of the references to color in this figure legend, the reader is referred to the Web version of this article.)

presumably explains an increase of water accessibility in the larger luminal pores, particularly after the two-stage pretreatments in SCL_EC3118, SCL_SC384, and SCL_ SC724 samples (Fig. 7 and Table 2).

The T2 distribution for SCL_EC3116 sample after two-step pretreatment (H2SO4 1% + NaOH 1%) differed from the other similarly pretreated sugar cane and energy cane samples (Table 1). T2 analysis points out that the lignin fraction remaining in this sample after the two-step pretreatment is higher than in other SCL samples. This is consistent with the sugar and energy cane chemical composition analysis (Table 1). Therefore, an apparent decrease in the lumen porosity of SCL_EC3116 could be related to lignin redistribution within the cell wall (Donohoe *et al.*, 2008; Santos *et al.*, 2018).

Table 2. Relative areas for the four different groups of untreated sugar and energy cane leaves, and sugar and energy cane leaves submitted to dilute acid pretreatment (H2SO4 1%) and combined acid-alkaline pretreatment (H2SO4 1% + NaOH 1%).

Sample	Pretreatment	Inner microfiber	Cell wall	Lumen
SCL_EC3116	None	0.04 ± 0.02	0.31 ± 0.06	0.64 ± 0.05
	H2SO4 1%	0.03 ± 0.04	0.17 ± 0.08	0.80 ± 0.05
	H2SO4 1% + NaOH 1%	0.05 ± 0.01	0.33 ± 0.03	0.62 ± 0.03
SCL_EC3118	None	0.04 ± 0.02	0.29 ± 0.03	0.68 ± 0.03
	H2SO4 1%	0.04 ± 0.01	0.22 ± 0.01	0.74 ± 0.01
	H2SO4 1% + NaOH 1%	0.01 ± 0.01	0.10 ± 0.01	0.89 ± 0.02
SCL_SC384	None	0.03 ± 0.01	0.39 ± 0.05	0.58 ± 0.04
	H2SO4 1%	0.02 ± 0.01	0.26 ± 0.02	0.72 ± 0.02
	H2SO4 1% + NaOH 1%	0.03 ± 0.04	0.20 ± 0.06	0.76 ± 0.03
SCL_ SC724	None	0.03 ± 0.01	0.39 ± 0.04	0.58 ± 0.03
	H2SO4 1%	0.03 ± 0.01	0.21 ± 0.02	0.77 ± 0.02
	H2SO4 1% + NaOH 1%	0.02 ± 0.01	0.10 ± 0.01	0.89 ± 0.02

T2 distribution associated with the water molecules bound to cellulose surfaces inside the cell walls decreased for SCL_EC3118, SCL_SC384, and SCL_SC724 samples (Table 2), indicating that the pretreatments severely modified these regions. Our SEM investigation of the pretreated samples (Fig. 3) clearly indicate the compact structure of leaves is lost because of the applied pretreatments and the cellulose bundles separate creating much bigger interstitial water-accessible spaces, which in our T2 analyses manifest themselves as apparent “lumen” volumes. Separation of cellulose bundles and an increase in their accessibility to enzymes typically result in higher enzymatic hydrolysis yields (Kane *et al..*, 2022; Weiss *et al.*, 2017; Rezende *et al.*, 2011), which indicates higher potential susceptibility of SCL_EC3116 samples to the enzymatic degradation.

3.5.X-ray diffraction analysis

To investigate changes of crystallinity index and crystallite size, XRD analysis was performed on raw and pretreated SCL samples (Table 3). The crystallinity index (CrI) and average crystallite sizes are frequently associated with modifications in lignocellulose structure after physicochemical pretreatments, therefore it has been considered one of the most relevant factors determining enzymatic hydrolysis yields (Brar *et al.*., 2020; Kim *et al*., 2003).

Crystallinity indexes in all the studied samples increased after each pretreatment for all the studied samples but SCL_SC724 (Table 3). In the latter case, initial crystallinity of the untreated sample was quite high and practically remained the same after applied pretreatments (Table 3). After the two-step pretreatments CrIs of all the samples reached 52%–54% level, which are characteristic of well-pretreated and hydrolytically accessible lignocellulosic samples (Brar *et al.*., 2020; Kane *et al*., 2022).

The observed increase in CrIs in the samples subjected to the applied pretreatments is directly related to the enrichment in the cellulose fraction caused by the pretreatments. Furthermore, the average crystallite size of the SCL samples steadily increased with the applied pretreatments being smallest for raw, untreated samples and highest for the samples subjected to two-step pretreatments (Table 3). Interestingly, the SC724 genotype after two-step pretreatment has the biggest average crystallite size (3.7 ± 0.2 nm), which correlates well with one of the highest cellulose contents and one of the lowest fractions of hemicellulose and lignin within this SCL variety (Table 1). Taken together, all these results may indicate that observed increases in the average dimensions of cellulose crystallites closely follow changes in SCL chemical composition (cf. Tables 1 and 3). The same phenomenon has been described previously for SC bagasse (Driemeier *et al.*, 2012; Santo *et al.*., 2018) and was attributed to the removal of hemicelluloses and lignin, that act as intercrystallite spacers, thus allowing for direct interfacing between cellulose crystallites upon drying. This enables co-crystallization and hornification of the samples, resulting in larger crystallites (Driemeier *et al.*, 2012; Santo *et al.*, 2018; Kane *et al.*, 2022).

3.6. Enzymatic hydrolysis assays

To verify how differences in chemical composition and physical structure of each sample demonstrated by physical techniques and chemical analyses impacted the enzymatic degradation, enzymatic hydrolysis assays were performed with commercial enzymatic Cellic CTec3 (Novozymes, Sigma–Aldrich, St. Louis, MO) on the studied SCL samples (Table 4). The enzymatic hydrolysis efficiency was evaluated by measuring the total amount of released glucose

after 24h,48h and 72h (Table 4). The enzymatic hydrolysis yields (i. e., percentage of cellulose conversion to glucose) were calculated for each sample before and after the pretreatment.

Enzymatic hydrolysis of untreated samples highlights the difference between the cultivars in the conversion of leaves into fermentable sugars, related to cellulose accessibility in these samples which is an essential factor for bioethanol production. SCL_SC724 and SCL_EC3116 samples show the highest enzymatic hydrolysis yields for untreated raw materials, which is however quite small (about 37–38%, Table 4). Overall, enzymatic hydrolysis yields on the pretreated SCL samples were the best for sugarcane cultivars. Indeed, following dilute acid pretreatment (H2SO4 1%), SCL_SC724 and SCL_SC384 samples reveal better performance than the other two genotypes leading to 56.6% and 53.8% of maximum theoretical yield after 76 h of enzymatic hydrolysis as computed based of the cellulose composition in the leaves of the respected cultivars (Table 4). This is particularly significant because the cellulose fraction in the leaves of these two biotypes is significantly higher as compared to EC cultivar leaves (Table 1).

The same trend prevailed after the two-step sequential pretreatment: SCL from SC384 variety accounted for the highest enzymatic hydrolysis yields, followed by SCL from SC724 cultivar. In this case enzymatic hydrolysis yields after 76h reached 82.1% and 91.2% for SC724 and SC384 cultivars, respectively. This trend correlates with higher cellulose and lower lignin contents in these two SC cultivars subjected to two-step acid-alkaline pretreatment. The obtained enzymatic hydrolysis yields favorable correlate with the enzymatic hydrolysis yields of other plant biomasses. For example, combined consecutive dilute acid (1%) followed by alkaline (NaOH 1%) pretreatment of eucalyptus bark of Eucaliptus grandis x urophylla led to 60% of enzymatic hydrolysis yield whereas the bark of Eucaliptus grandis rendered only 21% after 48h of enzymatic hydrolysis using 25 FPU of Accellerase 1500 (Genencor, Denmark) supplemented with 12.5 BGU of beta-glucosidase from Aspergillus Niger (Novozyme 188; Novozymes, Denmark) per gram biomass (Lima *et al.*, 2013).

Table 3. Crystallinity Index (%) and crystallite sizes of untreated sugar and energy cane leaves and sugar and energy cane leaves submitted to dilute acid pretreatment (H2SO4 1%) and combined acid -alkaline pretreatment (H2SO4 1% + NaOH 1%).

Sample	Pretreatment	CrI (%) a	Crystallite size b (nm)
SCL_EC3116	None	43.5 ± 4.0	2.7 ± 0.1
	H2SO4 1%	47.4 ± 0.2	2.9 ± 0.2
	H2SO4 1% + NaOH 1%	52.2 ± 2.7	3.1 ± 0.3
SCL_EC3118	None	45.8 ± 1.3	2.5 ± 0.2
	H2SO4 1%	52.8 ± 1.4	3.2 ± 0.2
	H2SO4 1% + NaOH 1%	51.9 ± 2.9	3.2 ± 0.1
SCL_SC384	None	42.7 ± 2.7	2.8 ± 0.3
	H2SO4 1%	47.9 ± 0.7	3.0 ± 0.1
	H2SO4 1% + NaOH 1%	52.3 ± 5.9	3.1 ± 0.2
SCL_SC724	None	54.6 ± 0.5	2.5 ± 0.5
	H2SO4 1%	53.3 ± 0.1	3.0 ± 0.1
	H2SO4 1% + NaOH 1%	54.5 ± 0.8	3.7 ± 0.2

[a] Crystallinity indexes were determined using Peak fitting program (Peak Fit; www.systat.com).
[b] Crystallite size were determined using Scherrer equation.

Table 4. Enzymatic hydrolysis yield during 24, 48 and 72 h of untreated sugar and energy cane leaves and sugar and energy cane leaves submitted to dilute acid pretreatment (H2SO4 1%) and combined acid -alkaline pretreatment (H2SO4 1% + NaOH 1%).

Treatment	SCL_EC3116	SCL_EC3118	SCL_SC384	SCL_SC724
Untreated 24h	31.6 ± 0.2c	22.4 ± 1.5a	22.9 ± 2.3a	31.3 ± 0.3c
Untreated 48h	36.0 ± 1.4c	24.0 ± 1.0a	27.3 ± 2.8b	34.7 ± 0.6c
Untreated 72h	38.2 ± 0.2d	32.0 ± 0.5c	33.9 ± 0.2c	37.4 ± 1.1d
Acid 24h	39.1 ± 1.9d	42.3 ± 1.2d	40.2 ± 0.8d	40.7 ± 0.6d
Acid 48h	45.1 ± 2.0e	47.4 ± 0.1f	42.8 ± 1.6d	52.8 ± 3.0g
Acid 72h	50.3 ± 4.2f	51.0 ± 0.4f	53.8 ± 0.4g	56.6 ± 1.6h
Acid + alkaline 24h	45.1 ± 2.5e	48.8 ± 1.4f	58.1 ± 0.0h	64.9 ± 0.4i
Acid + alkaline 48h	65.2 ± 0.5i	53.5 ± 1.1g	73.3 ± 0.1j	71.9 ± 0.1j
Acid + alkaline 72h	72.2 ± 4.7j	60.7 ± 1.2h	91.2 ± 0.1l	82.1 ± 0.2k

Different letters indicate significant differences for DGC test ($p < 0.05$). SCL: Sugar Cane Leave.
Acid: H2SO4 (1%).
Acid + alkaline: H2SO4 1% + NaOH 1%.

Sequential acid and alkaline pretreatment of rice straw with 1% (v/w) H2SO4 at 125 ◦C and 1.25% NaOH at 90 ◦C for 10 min followed by enzymatic hydrolysis with 25 FPU/g with Accelerase 1500 (Danisco, Rochester, NY) for 72h resulted in enzymatic hydrolysis yield of 70.9% (Weerasai *et al.*., 2014). Finally sequential pretreatment of wheat straw with dilute sulfuric acid and dilute sodium hydroxide under optimized conditions followed by enzymatic hydrolysis with 14 FPU/g rendered 0.709 of theoretically possible glucose yield (Sanchez *et al*., 2015).

Furthermore, our XRD studies demonstrated that cellulose SCL_SC724 cultivar has higher crystallinity and bigger cellulose crystallites, characteristics typically associated with higher enzymatic digestibility (Brar *et al*., 2020; Kane *et al*., 2022). Furthermore, pretreatments of SCL from the same cultivar led to the strongest morphological rearrangement as revealed by the low field NMR experiments. This might indicate that commercial cultivars SC724 and SC384 could be promising sugarcane germplasms for 2G bioethanol production based on lignocellulosic biomass from sugar cane leaves.

4. Conclusions

In our work a range of chemical and physical techniques have been employed to investigate the chemical composition and physical structure changes in leaves from commercial sugar and energy cane varieties impacted by dilute acid and two-step acid + alkaline pretreatments. Our chemical composition analyses demonstrated that cellulose fraction of sugarcane leaves is significantly higher than that of energy cane leaves. Dilute acid and combined acid + alkaline pretreatments enhanced cellulose content in the pretreated sugar and energy cane leaves and led to the progressive separation and loosening of the cellulose fibers. This effect was strong for dilute acid pretreatment and that further intensified by the delignification process promoted by the alkaline pretreatment. Glucan enrichment and lignin depletion in pretreated materials seem to be critical in explaining enhancements of glucan accessibility and enzymatic hydrolysis. Overall, the data from our physical studies and enzymatic hydrolysis essays jointly indicate that two commercial sugarcane cultivars, SC384 85–384 and NA 78–724 currently bred in Argentina are promising germplasms when 2G bioethanol production from sugarcane leaves is considered.

Declaration of competing interest

The authors declare that they have no known competing financial interests or personal relationships that could have appeared to influence the work reported in this paper.

Acknowledgments

This work was supported by Fundaçao de Amparo ˜ a Pesquisa do Estado de S` ao Paulo (FAPESP) via grant 15/13684-0, by Conselho ˜ Nacional de Desenvolvimento Científico e Tecnologico (CNPq) via grants 423693/2016-6 and 303988/2016-9, by Instituto Nacional ´ de Tecnología Agropecuaria (INTA) via grant PNAIyAV 2019-PE-E6-I114-001, and by Ministry of Science and Technology of Argentina via grant PICT 2016-1670. This work was also supported by

Coordenaçao de Aperfeiçoamento de Pessoal de Nível Superior (CAPES) ˜ via a PhD fellowship to AOK. JMG has a fellowship from Consejo Nacional de Investigaciones Científicas y T´ecnicas (CONICET). We also thank the field team of INTA Sugarcane Breeding Program for its technical assistance.

References

Acevedo, A., Tejedor, M.T., Erazzú, L.E., Cabada, S., Sopena, R., 2017. Pedigree comparison highlights genetic similarities and potential industrial values of sugarcane cultivars. Euphytica 213, 2–16. https://doi.org/10.1007/s10681-017-1908-2.

Alvira, P., Tomas-Pej´ o, E., Ballesteros, M., Negro, M.J., 2010. Pretreatment technologies for an efficient bioethanol production process based on enzymatic hydrolysis: ´ a review. Bioresour. Technol. 101, 4851–4861. https://doi.org/10.1016/j.biortech.2009.11.093.

Baruah, J., Nath, B.K., Sharma, R., Kumar, S., Deka, R.C., Baruah, D.C., Kalita, E., 2018. Recent trends in the pretreatment of lignocellulosic biomass for value-added products. Front. Energy Res. 6, 141. https://doi.org/10.3389/fenrg.2018.00141.

Bernardinelli, O.D., Lima, M.A., Rezende, C.A., Polikarpov, I., Ribeiro, E., 2015. Quantitative 13 C MultiCP solid - state NMR as a tool for evaluation of cellulose crystallinity index measured directly inside sugarcane biomass. Biotechnol. Biofuels 8, 1–11. https://doi.org/10.1186/s13068-015-0292-1.

Borgia, G.C., Brown, R.J.S., Fantazzini, P., 1998. Uniform-penalty inversion of multiexponential decay data. J. Magn. Reson. 132, 65–77. https://doi.org/10.1006/ jmre.1998.1387.

Brar, K.K., Espirito Santo, M.C., Pellegrini, V.O.A., De Azevedo, E.R., Guimaraes, F.E.C., Polikarpov, I., Chadha, B.S., 2020. Enhanced hydrolysis of hydrothermally and autohydrolytically treated sugarcane bagasse and understanding the structural changes leading to improved saccharification. Biomass Bioenergy 139, 105639. https://doi.org/10.1016/J.biombioe.2020.105639.

Brownstein, K.R., Tarr, C.E., 1979. Importance of classical diffusion in NMR studies of water in biological cells. Phys. Rev. 19, 2446–2453. https://doi.org/10.1103/ PhysRevA.19.2446.

Canilha, L., Chandel, A.K., Suzane Dos Santos Milessi, T., Antunes, F.A.F., Luiz Da Costa Freitas, W., das Graças Almeida Felipe, M., da Silva, S.S., 2012. Bioconversion of sugarcane biomass into ethanol: an overview about composition, pretreatment methods, detoxification of hydrolysates, enzymatic saccharification, and ethanol fermentation. J. Biomed. Biotechnol. 2012, 1–15. https://doi.org/10.1155/2012/989572.

Capitani, D., di Tullio, V., Proietti, N., 2012. Nuclear magnetic resonance to characterize and monitor cultural heritage. Prog. Nucl. Magn. Reson. Spectrosc. 64, 29–69. https://doi.org/10.1016/j.pnmrs.2011.11.001.

Chandel, A.K., Antunes, F.A.F., Anjos, V., Bell, M.J.V., Rodrigues, L.N., Polikarpov, I., de Azevedo, E.R., Bernardinelli, O.D., Rosa, C.A., Pagnocca, F.C., da Silva, S.S., 2014. Multi-scale structural and chemical analysis of sugarcane bagasse in the process of sequential acid-base pretreatment and ethanol production by Scheffersomyces shehatae and Saccharomyces cerevisiae. Biotechnol. Biofuels 7, 63. https://doi.org/10.1186/1754-6834-7-63.

Coletta, V.C., Rezende, C.A., da Conceiçao, F.R., Polikarpov, I., Guimar˜ aes, F.E.G., 2013. Mapping the lignin distribution in pretreated sugarcane bagasse by confocal ˜ and fluorescence lifetime imaging microscopy. Biotechnol. Biofuels 6, 1–10. https://doi.org/10.1186/1754-6834-6-43.

De Souza, A.P., Leite, D.C.C., Pattathil, S., Hahn, M.G., Buckeridge, M.S., 2013. Composition and structure of sugarcane cell wall polysaccharides: implications for second-generation bioethanol production. Bioenergy Research 6, 564–579. https://doi.org/10.1007/S12155-012-9268-1.

Di Rienzo, J.A., Casanoves, F., Balzarini, M.G., Gonzalez, L., Tablada, M., Robledo, C.W., 2020. InfoStat Version 2020. Centro de Transferencia InfoStat, FCA, ´ Universidad Nacional de Cordoba, Argentina. URL. ´ http://www.infostat.com.ar.

Di Rienzo, J.A., Guzman, A.W., Casanoves, F., 2002. A multiple-comparisons method based on the distribution of the root node distance of a binary tree. J. Agric. Biol. ´ Environ. Stat. 7 (2 7), 129–142. https://doi.org/10.1198/10857110260141193, 2002.

Donohoe, B.S., Decker, S.R., Tucker, M.P., Himmel, M.E., Vinzant, T.B., 2008. Visualizing lignin coalescence and migration through maize cell walls following thermochemical pretreatment. Biotechnol. Bioeng. 101, 913–925. https://doi.org/10.1002/bit.21959.

Driemeier, C., Santos, W.D., Buckeridge, M.S., 2012. Cellulose crystals in fibrovascular bundles of sugarcane culms: orientation, size, distortion, and variability. Cellulose 19, 1507–1515. https://doi.org/10.1007/s10570-012-9743-z.

Espírito Santo, M.C. do, Cardoso, E.B., Guimaraes, F.E.G., deAzevedo, E.R., Cunha, G.P. da, Novotny, E.H., Pellegrini, V. de O.A., Chandel, A.K., Silveira, M.H.L., Polikarpov, I., 2019. Multifaceted characterization of sugarcane bagasse under different steam explosion severity conditions leading to distinct enzymatic hydrolysis yields. Ind. Crop. Prod. 139, 111542 https://doi.org/10.1016/j.indcrop.2019.111542.

Ferreira-Leitao, V., Perrone, C.C., Rodrigues, J., Franke, A.P.M.H., MacRelli, S., Zacchi, G., 2010. An approach to the utilisation of CO2as impregnating agent in steam ˜ pretreatment of sugar cane bagasse and leaves for ethanol production. Biotechnol. Biofuels 3, 1–8. https://doi.org/10.1186/1754-6834-3-7.

Galbe, M., Wallberg, O., 2019. Pretreatment for biorefineries: a review of common methods for efficient utilisation of lignocellulosic materials. Biotechnol. Biofuels 12, 1–26. https://doi.org/10.1186/s13068-019-1634-1.

Galbe, M., Zacchi, G., 2012. Pretreatment: the key to efficient utilization of lignocellulosic materials. Biomass Bioenergy 46, 70–78. https://doi.org/10.1016/j. biombioe.2012.03.026.

Hutzler, P., Fischbach, R., Heller, W., Jungblut, T.P., Reuber, S., Schmitz, R., Veit, M., Weissenbock, G., Schnitzler, J.P., 1998. Tissue localization of phenolic ¨ compounds in plants by confocal laser scanning microscopy. J. Exp. Bot. 49, 953–965. https://doi.org/10.1093/jxb/49.323.953.

Jackson, M.G., 1977. Review article: the alkali treatment of straws. Anim. Feed Sci. Technol. 2, 105–130. https://doi.org/10.1016/0377-8401(77)90013-X.

Kane, A.O., Pellergini, V.O.A., Espirito Santo, M.C., Ngom, B.D., García, J.M., Acevedo, A., Erazzú, L.E., Polikarpov, I., 2022. Evaluating the potential of culms from sugarcane and energy cane varieties grown in Argentina for second-generation ethanol production. Waste and Biomass Valorization 13, 329–343. https://doi.org/ 10.1007/s12649-021-01528-5.

Kim, T.H., Kim, J.S., Sunwoo, C., Lee, Y.Y., 2003. Pretreatment of corn stover by aqueous ammonia. Bioresour. Technol. 90, 39–47. https://doi.org/10.1016/S0960- 8524(03)00097-X.

Kumar, A.K., Sharma, S., 2017. Recent updates on different methods of pretreatment of lignocellulosic feedstocks: a review. Bioresources and Bioprocessing 4 (1 4), 1–1, 2017 20179. https://doi.org/10.1186/S40643-017-0137-9 .

Lichtenthaler, H.K., Schweiger, J., 1998. Cell wall bound ferulic acid, the major substance of the blue-green fluorescence emission of plants. J. Plant Physiol. 152, 272–282. https://doi.org/10.1016/S0176-1617(98)80142-9.

Lima, M.A., da Silva, H.K.P., Bragatto, J., Rezende, C.A., Bernardinelli, O.D., DeAzevedo, E.R., Gomez, L.D., McQueen-Mason, S.J., Labate, C.A., Polikarpov, I., 2013. Effects of pretreatment on morphology, chemical composition and enzymatic digestibility of eucalyptus bark: a potentially valuable source of fermentable sugars for biofuel production – part 1. Biotechnol. Biofuels 6, 75. https://doi.org/10.1186/1754-6834-6-75.

Liu, C., Wyman, C.E., 2003. The effect of flow rate of compressed hot water on xylan, lignin, and total mass removal from corn stover. Ind. Eng. Chem. Res. 42, 5409–5416. https://doi.org/10.1021/ie030458k.

Markou, G., 2015. Effect of various colors of light-emitting diodes (LEDs) on the biomass composition of arthrospira platensis cultivated in semi-continuous mode. Appl. Biochem. Biotechnol. https://doi.org/10.1007/s12010-014-0727-3.

Martins, M.T.B., de Souza, W.R., da Cunha, B.A.D.B., Basso, M.F., de Oliveira, N.G., Vinecky, F., Martins, P.K., de Oliveira, P.A., Arenque-Musa, B.C., de Souza, A.P., Buckeridge, M.S., Kobayashi, A.K., Quirino, B.F., Molinari, H.B.C., 2016. Characterization of sugarcane (Saccharum spp.) leaf senescence: implications for biofuel production. Biotechnol. Biofuels 9, 1–17. https://doi.org/10.1186/S13068-016-0568-0.

Mínguez-Mosquera, M.I., Gandul-Rojas, B., 1995. High-performance liquid chromatographic study of alkaline treatment of chlorophyll. J. Chromatogr. A 690, 161–176. https://doi.org/10.1016/0021-9673(94)00924-X.

Monshi, A., Foroughi, M.R., Monshi, M.R., Monshi, A., Foroughi, M.R., Monshi, M.R., 2012. Modified scherrer equation to estimate more accurately nano-crystallite size using XRD. World J. Nano Sci. Eng. 2, 154–160. https://doi.org/10.4236/wjnse.2012.23020.

Park, S., Baker, J.O., Himmel, M.E., Parilla, P.A., Johnson, D.K., 2010. Cellulose crystallinity index: measurement techniques and their impact on interpreting cellulase performance. Biotechnol. Biofuels 3, 1–10. https://doi.org/10.1186/1754-6834-3-10.

Provencher, S.W., 1982. A constrained regularization method for inverting data represented by linear algebraic or integral equations. Comput. Phys. Commun. 27, 213–227. https://doi.org/10.1016/0010-4655(82)90173-4.

Racedo, J., Guti´errez, L., Perera, M.F., Ostengo, S., Pardo, E.M., Cuenya, M.I., Welin, B., Castagnaro, A.P., 2016. Genome-wide association mapping of quantitative traits in a breeding population of sugarcane. BMC Plant Biol. 16, 142. https://doi.org/10.1186/s12870-016-0829-x.

Rezende, C.A., de Lima, M., Maziero, P., Deazevedo, E., Garcia, W., Polikarpov, I., Garcia, W., Maziero, P., Rezende, C.A., 2011. Chemical and morphological characterization of sugarcane bagasse submitted to a delignification process for enhanced enzymatic digestibility. Biotechnol. Biofuels 4, 54. https://doi.org/ 10.1186/1754-6834-4-54.

Rocha, G.J. de M., Martin, C., Soares, I.B., Souto Maior, A.M., Baudel, H.M., Moraes de Abreu, C.A., 2011. Dilute mixed-acid pretreatment of sugarcane bagasse for ethanol production. Biomass Bioenergy 35, 663–670. https://doi.org/10.1016/j.biombioe.2010.10.018.

Roozeboom, K.L., Wang, D., McGowan, A.R., Propheter, J.L., Staggenborg, S.A., Rice, C.W., 2019. Long-term biomass and potential ethanol yields of annual and perennial biofuel crops. Agron. J. 111, 74–83. https://doi.org/10.2134/AGRONJ2018.03.0172.

Santo, M.E., Rezende, C.A., Bernardinelli, O.D., Pereira, N., Curvelo, A.A.S., Eduardo, R., Guimaraes, F.E.G., Polikarpov, I., 2018. Industrial Crops ˜ & Products Structural and compositional changes in sugarcane bagasse subjected to hydrothermal and organosolv pretreatments and their impacts on enzymatic hydrolysis. Ind. Crop. Prod. 113, 64–74. https://doi.org/10.1016/j.indcrop.2018.01.014.

Sanchez, A., Gil, J.C., Rojas-Rejon, O.A., de Alba, A.P., Medina, A., Flores, R., Puente, R., 2015. Sequential pretreatment strategies under mild conditions for efficient ´ enzymatic hydrolysis of wheat straw. Bioproc. Biosyst. Eng. 38 (6), 1127–1141. https://doi.org/10.1007/s00449-015-1355-1.

Santos, V.T. de O., Siqueira, G., Milagres, A.M.F., Ferraz, A., 2018. Role of hemicellulose removal during dilute acid pretreatment on the cellulose accessibility and enzymatic hydrolysis of compositionally diverse sugarcane hybrids. Ind. Crop. Prod. 111, 722. https://doi.org/10.1016/j.indcrop.2017.11.053.

Scherrer, P., 1912. Bestimmung der inneren Struktur und der Gro¨ße von Kolloidteilchen mittels Rontgenstrahlen. Kolloidchemie Ein Lehrbuch 2, 387¨ -409. https:// doi.org/10.1007/978-3-662-33915-2_7.

Schmitz, R., Reuber, S., Veit, M., Weissenbock, G., 1996. Comparison of soluble and insoluble hydroxycinnamic acids (HCAs) with soluble flavonoids with regard to UV protection of rye primary leaves. In: Plant Physiol. Biochem. Special Issue. 10th FESPP Congress, Florence, pp. 309–310.

Suna, F.F., Honga, J., Hub, J., Saddler, J.N., Fang, Xu, Zhanga, Z., Shena, S., 2015. Accessory enzymes influence cellulase hydrolysis of the model substrate and the realistic lignocellulosic biomass. Enzym. Microb. Technol. 79, 42–48. https://doi.org/10.1016/j.enzmictec.2015.06.020.

Tsuchida, J.E., Rezende, C.A., de Oliveira-Silva, R., Lima, M.A., D'Eurydice, M.N., Polikarpov, I., Bonagamba, T.J., 2014a. Nuclear magnetic resonance investigation of water accessibility in cellulose of pretreated sugarcane bagasse. Biotechnol. Biofuels 7, 1–13. https://doi.org/10.1186/s13068-014-0127-5.

Weerasai, K., Suriyachai, N., Poonsrisawat, A., Arnthong, J., Unrean, P., Laosiripojana, N., Champreda, V., 2014. Sequential acid and alkaline pretreatment of rice straw for bioethanol fermentation. Bioresources 9 (4), 5988–6001.

Weiss, S., Xu, Z.Z., Peddada, S., Amir, A., Bittinger, K., Gonzalez, A., Lozupone, C., Zaneveld, J.R., Vazquez-Baeza, Y., Birmingham, A., Hyde, E.R., Knight, R., 2017. ´ Normalization and microbial differential abundance strategies depend upon data characteristics. Microbiome 5. https://doi.org/10.1186/S40168-017-0237-Y.

7 Chapter 7 Results and discussion

7.1 Optimization of the production of fermentable sugars via a combination of liquid hot water and sulfonated pretreatments of sugarcane bagasse

7.1.1 Chemical composition analysis

Chemical compositions of native and pretreated sugarcane bagasse were obtained after analyzing data from HPLC, UV visible, and gravimetrically measuring solid residues in the crucible. Native sugarcane bagasse consists mainly of 42.3 ± 0.1% cellulose, 24.9 ± 1.7 % hemicelluloses, and 20.4 ± 0.7 % lignin (Table 1). After boiling and /or autoclaving, overall, there was no significant modification in sugarcane bagasse composition (Table 1). There was a slight increase in hemicellulose and lignin fraction for both LHW pretreatments and an enhancement in cellulose fraction for the biomass samples after autoclaving with pretreatment times (30, 60, and 120 min). Preservation of the bagasse composition after LHW pretreatment can be explained by the relatively low temperature (100ºC to 120 ºC) of pretreatment. Indeed, the LHW pretreatments can simply disturb biomass structure, allowing lignin relocalization in the substrate at low temperatures. Consequently, disruption of lignocellulose structure can facilitate enzyme access to cellulose and enhance substrate saccharification without hemicellulose solubilization. (185) In addition, some researchers reported that hemicellulose starts to dissolve at a temperature above 150ºC. (186,187) Conversely, compositional analysis of neutral and alkaline sulfonated samples revealed an increase in cellulose fraction (Table 1). The neutral sulfonation of LHW pretreated bagasse provoked an increase in cellulose and hemicellulose fraction and slight delignification (3.2% for autoclaved and sulfonated bagasse (ASB) and 17.2% for boiled and sulfonated bagasse (BSB), as shown in Table 8. Boiled and sulfonated biomass reached 50.2 ± 1.8 % cellulose content when sulfonation was done in a neutral solution and 65.9 ± 1.0% of cellulose when the reaction was performed in alkaline conditions. The sulfonation of autoclaved bagasse increased cellulose fraction to 47.1 ± 1.5 % when performed under neutral conditions and to 65.4 ± 0.1 % in an alkaline medium. The cellulose fraction enhancements after pretreatments can be correlated with lignin removal, which reached 69.1 ± 1.6 % for boiled and alkaline sulfonated bagasse (BASB) and 71.4 ± 2.2 % for autoclaved and alkaline sulfonated bagasse (AASB). During alkaline pretreatment, alkali is expected to cleave hydrolysable linkages in lignin and glycosidic bonds of polysaccharides, causing a degree of

polymerization and crystallinity reduction, swelling the fibers, as well as disrupting the lignin structure. In addition, alkaline saponification of acetyl and uronic ester bonds also improves the polysaccharides' enzymatic accessibility polysaccharides, allowing effective delignification, as found in our previous works (99,188). NaOH penetrates the interface between lignin and polysaccharides, cleaves ester bonds between them, and promotes lignin solubilization(189). Furthermore, alkaline media has known to be also efficient in improving the sulfonation of lignin (190-191) Moreover, most hemicellulose has been retained in the solid fractions after pretreatments (Table 1), permitting high substrate yields and minimizing the formation of fermentation inhibitors such as hydroxymethylfurfural (HMF), furfural, etc. (192) The low pretreatment severity (120ºC) can explain considerable hemicellulose retention.

Table 1 - Chemical composition of native bagasse (NB), liquid hot water pretreated bagasse (boiled bagasse (BB) and autoclaved bagasse (AB)) during 30-, 60-, and 120-min. as well as the chemical composition of sulfonated native Bagasse (Sulfonated Bagasse: SB) and neutral /alkaline sulfonated liquid hot water pretreated sugar cane bagasse for 60 min: (boiled and sulfonated bagasse (BSB), autoclaved and sulfonated bagasse (ASB), boiled, and alkaline sulfonated bagasse (BASB), and autoclaved and alkaline sulfonated bagasse (AASB)).

SCB	pretreatment time	Cellulose	Hemicellulose	Lignin	Ash	extractive	Total
NB	0 min	42.30 ± 0.13	24.91 ± 1.70	20.42 ± 0.70	0.97 ± 0.15	7.31 ± 0.04	95.91 ± 2.72
	30 min	42.75 ± 0.51	28.65 ± 0.34	21.54 ± 0.41	1.05 ± 0.01		93.98 ±1.27
BB	60 min	42.84 ± 0.25	28.65 ± 0.34	21.05 ± 0.44	1.16 ± 0.25		93.7 ± 1.28
	120 min	42.39 ± 0.25	28.63 ± 0.10	21.64 ± 2.61	0.59 ± 0.04		93.25 ± 3.0
	30 min	45.9 ± 0.25	29.27 ± 0.17	21.71 ± 2.44	0.59 ± 0.16		97.97 ± 3.02
AB	60 min	45.23 ± 0.70	27.99 ± 0.06	21.52 ± 2.03	0.53 ± 0.10		95.27 ± 2.79
	120 min	46.22 ± 0.57	28.43 ± 0.66	21.09 ± 1.86	0.58 ± 0.33		96.3 ± 3.42

sulfonation of native biomass (NB), BB (60min) and AB (60 min)

	sulfonation time	Cellulose	Hemicellulose	lignin	Ash		removed lignin
SB	120 min	43.59 ± 0.19	28.36 ± 0.62	22.97 ±0.23	1.94 ± 0.42	96.47± 1.7	
BSB	120 min	50.17 ± 1.84	30.71 ± 0.87	16.8 ± 1.11	1.3 ± 1.0	98.98 ± 4.81	17.72 ± 2.55
BASB	120 min	65.94 ± 1.01	25.47 ± 0.14	6.3 ± 0.41	2.1 ± 1.1	99.81± 2.66	69.14 ± 1.55
ASB	120 min	47.0 7 ± 1.46	29.12 ± 1.74	19.72 + 0.33	1.66 ± 0.19	97.57 ± 3.72	3.42 ± 2.22
AASB	120 min	65.43 ± 0.14	26.92 ± 0.21	5.85 ± 0.21	1.52 ± 0.8	99.72 ± 1.36	71.35 ± 2.15

BB (60 min): Boiled Bagasse for 60 min, AB (60min): Autoclaved Bagasse for 60 min

7.1.2 Confocal result

Confocal laser scanning microscopy (CLSM) reports on structural changes introduced by pretreatment in bagasse samples by measuring lignin autofluorescence signals. Indeed, lignin autofluorescence intensity effectively predicted saccharification efficiency and assessed the recalcitrance of lignocellulosic biomass. (193–195) Confocal images of native bagasse (NB) showed fluorescence in the greenish-blue spectral region (Figure 7-1). Traces of red fluorescence emission were also noted, indicating chlorophyll in the untreated sugarcane bagasse (196). Images obtained from LHW pretreated bagasse confirmed slight modifications in the observed lignin autofluorescence emission, with the maximum emission always in the greenish-blue region of electromagnetic spectra (Figure 7-1). This is consistent with little changes in the chemical composition of the samples during this pretreatment stage (Table 1). Confocal images of the neutral/alkaline sulfonated reveal lignin autofluorescence color changes (Figure 7-1), from greenish blue to green (500–550 nm) for the sulfonated bagasse. Structural reorganization of lignin during pretreatments can explain differences in autofluorescence. (197) During sulfonation, lignin in the substrate was chemically modified (partially sulfonated) (198), thus, leading to the shift in autofluorescence of lignin to the green spectral zone. The differences in intensities of green fluorescence signals for sulfonated sugarcane bagasse samples could be due to the differences in lignin removal. Previous studies correlated strong green fluorescence to the minor lignin concentration in the pretreated substrate. (199) Therefore, more intense autofluorescence of alkaline sulfonated bagasse samples correlates with massive lignin removal during alkaline sulfonation pretreatment. (199)

Changes in lignin autofluorescence imprinted by applied hot water pretreatments and neutral/alkaline sulfonation differ from the acid and alkaline pretreatments studied in previous works**.** (99,200) Dilute acid and combined acid/alkaline catalyzed pretreatments led to much stronger spectral shifts in lignin autofluorescence and characteristic shifts to the yellow and red regions of the electromagnetic spectrum, indicating condensation of lignin particles. (201) Dilute acid pretreatments also introduced extrusion and reprecipitation of the condensed lignin at the surface of the biomass samples, manifesting itself by characteristic sphere-like lignin particles, emitting dark-red fluorescence at the surface of lignocellulose. (202) This could be partly attributed

to lower temperatures, pretreatment severity, and chemical modifications introduced by biomass sulfonation.

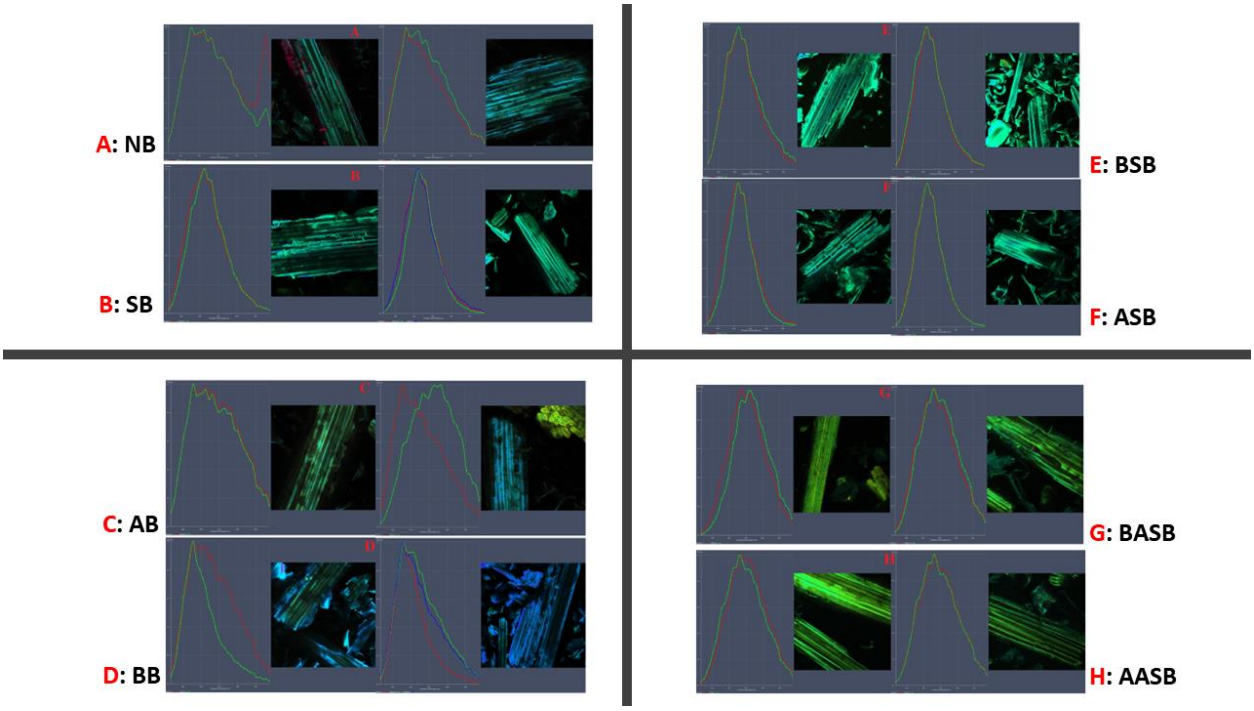

Figure 7-1 - Confocal images of native and pretreated sugar cane bagasse: native bagasse (A: NB); sulfonated bagasse (B: SB)., autoclaved bagasse (C: AB), boiled bagasse (D: BB); boiled sulfonate Bagasse (E: BSB), autoclaved sulfonated bagasse (F: ASB), boiled and alkaline sulfonated bagasse (G: BASB), autoclaved, and alkaline sulfonated bagasse (H: AASB).
Source: By the author

7.1.3 Crystallinity

Cellulose is maintained by intra- and intermolecular hydrogen bonding, which results in the recalcitrant and crystalline structure. Figure 7-2 displays the diffraction profiles for untreated and the different pretreated substrates. Three diffraction peaks around $2\theta = 11.6^{\circ}$,16, and 21.8° are present in native bagasse (NB), boiled, and autoclaved bagasse (BB and AB) (Figure 7-2a, c) diffraction spectra, with slight differences in peak intensities. The peak at $2\theta = 11.6^{\circ}$ decreased in intensity after LHW pretreatments, and the crystallinity enhanced slightly (Figure 7- 2d), indicating structural reorganization biomass after pretreatment. Moreover, the nearly identical NB, BB, and AB spectra (Figure 7-2c) confirmed no significant changes in bagasse structures after boiled and autoclaved treatments and are consistent with the limited changes in the chemical composition of

these samples (Table 8). After sulfonations, all diffractogram profiles (Figure 7-2) delivered a predominance of cellulose I, attested by the detected peaks at $2\theta = 16^{\circ}$, 22.5°, and 35°, corresponding to the planes (1 1 0), (0 0 2), and (0 0 4) (203). The perfect identification of structure I of cellulose can be associated with the efficiency of pretreatments that allow lignin removal and the exposition of available cellulose. The crystallinity indexes (CrI) and the average crystallite sizes (CS) of native and pretreated bagasse were computed from the diffraction scans data (Figure.7-2d). The native sugarcane bagasse has a CrI of 31.07 %. Crystallinity indexes increased after each pretreatment stage and achieved a maximum of 58.79% and 54.96% for AASB and BASB, respectively. Enhancement of crystallinity indexes can be correlated with delignification since more delignified samples showed the highest crystallinity (Table 1). The average crystallite sizes of bagasse were also increased after each pretreatment stage. Pretreatment steps lead to lignin removal and cellulose fiber swelling. The following pretreated biomass drying step can provoke the crystalline chain rearrangements by hornification and recrystallization, increasing crystallite sizes. (204)

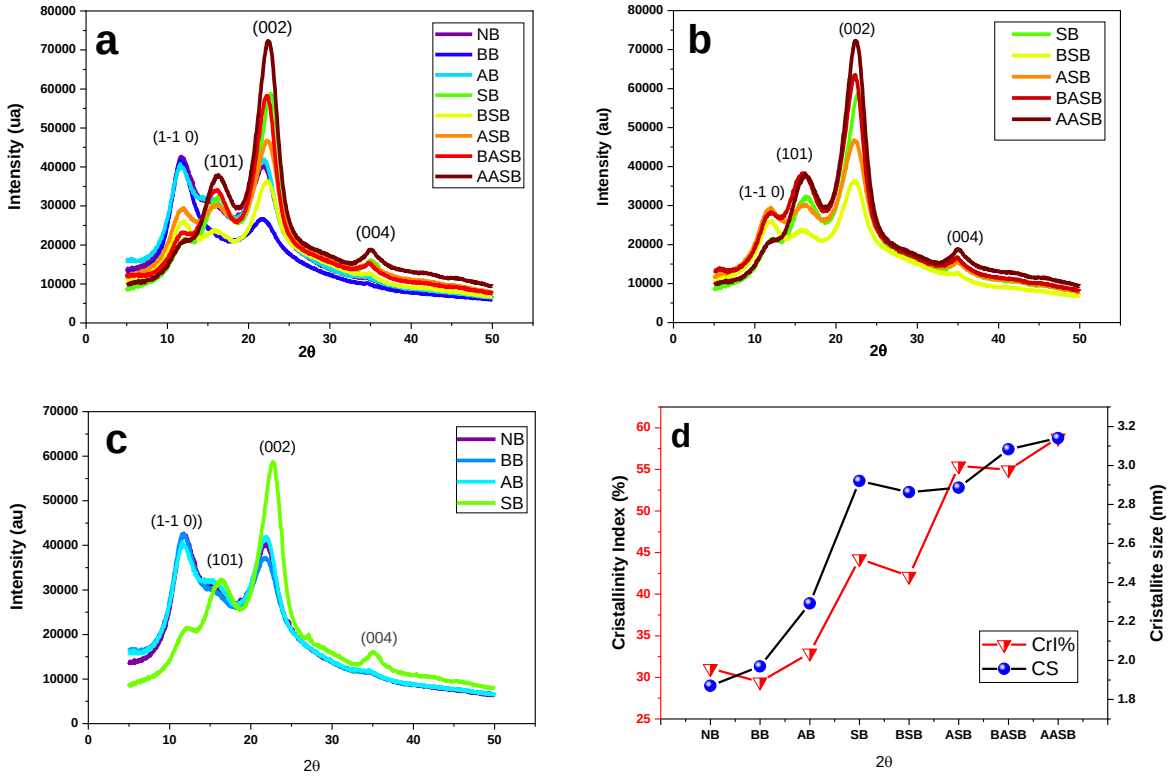

Figure 7-2 - Crystallinity Indexes of native bagasse (NB), sulfonated bagasse (SB), LHW pretreated bagasse (BB and AB), boiled and autoclaved sulfonated bagasse (BSB and ASB), Boiled and alkaline sulfonated bagasse (BASB), Autoclaved and alkaline sulfonated bagasse (AASB).
Source: By the author

7.1.4 Enzymatic hydrolysis analysis

The enzymatic hydrolysis of untreated and pretreated bagasse was performed, and the yields of released monomeric were reported in Figures 7- 3 and 7-4. Overall, enzymatic hydrolysis of the autoclaved bagasse is slightly more efficient than hydrolysis of boiled bagasse (Figure 7-3). The effects of pretreatment times (30,60, and 120 min) and enzyme loadings (5,10, and 25 mg/g) on enzymatic hydrolysis were evaluated considering yields of released glucose after LHW pretreatments, as shown in Figure 7-3. For untreated, boiled, and autoclaved substrates, the saccharification increased with enzyme loadings and achieved, after 72h, a maximum of 48.59 % for autoclaved bagasse and 46.6 ± 0.4 for boiled substrate (Figure 7-3). The enzymatic hydrolysis yield of untreated or native bagasse (NB) reached the maximum of 37.2 ± 1.5 after 72h. Regarding saccharification (with 10 mg/g as enzyme loading), the best pretreatment time was t = 30 min for

the boiled substrate, while the optimal pretreatment time was t = 60 min for the autoclaved substrate. Hence, the maximum enzymatic hydrolysis yield obtained with a boiled and autoclaved substrate after 72 h was less than 50%. We subjected the LHW pretreated bagasse to sulfonation in a neutral and alkaline medium to optimize the saccharification efficiency. Considering the chemical composition analysis and the enzymatic convertibility (Table 1 and Figure 7-3), the LHW pretreatment time chosen for the rest was 60 min, and the enzyme loading was 10mg/g. Thus, the boiled and autoclaved bagasse for 60 min was submitted to neutral and alkaline sulfonation for 120 min. Then, the enzymatic hydrolysis of obtained substrates was performed using enzyme loading of 10 mg/g. The released glucose and xylose yields are illustrated in Figure 7-4. Neutral sulfonation allowed a release of xylose and glucose, which achieved yields of 73.54 % (GY) and 55.94 % (XY) for BSB, 63.88 % (GY), and 50.22 % (XY) for ASB. The significant release of monomeric sugars of sulfonated bagasse (BSB and ASB) could be correlated with lignin modifications. Indeed, neutral sulfonation has been proven to be an effective method to selectively modify the lignin by incorporating the sulfonic acid group onto the lignin. Nucleophilic reagents sulfite (SO_3^{2-}) and bisulfite (HSO_3^-) attract the ether bond of lignin, causing it to break and introduce sulfonic acid. Nucleophilic reagents sulfite (SO_3^{2-}) and bisulfite (HSO_3^-) attract the ether bond of lignin, causing it to break and introduce sulfonic acid. The acid group incorporation by sulphonation can potentially decrease the nonproductive adsorption of enzymes to residual lignin, resulting in improved ease of enzymatic hydrolysis.(208,209) Other studies also proved the neutral sulfonation efficiency to improve cellulose accessibility and decrease the nonproductive binding of cellulases, swelling the substrate(210-211)

Almost all carbohydrates were transformed into fermentable sugars during enzymatic hydrolysis of alkaline sulfonated bagasse. The release glucose yields achieved 98.9 ± 0.8 and 99.6 ± 0.2 for BASB and AASB, respectively (Figure .7-4). In contrast, the xylose released from hemicellulose reached 88.9 % and 90.02 % for BASB and AASB (Figure .7-4). Siqueira *et al.* (212)carried out alkaline sulfite pretreatment (Na_2SO_3/NaOH) at 121ºC for 60 min, lignin solubilization reached 48.8 %, and the residual lignin in the substrate was sulfonated. The residual lignin in the substrate was sulfonated. Their enzymatic yield achieved 82 % at the higher enzyme loading (30 mg/g) than ours (10 mg/g). The outstanding enzymatic convertibility of BASB and AASB is correlated with the two-stage pretreatments applied to the sugar bagasse. As highlighted in the different results,

their collective actions permitted structural disruption of bagasse, sulfonation, and removal of lignin, as well as the swelling of cellulose fibers, improving carbohydrate accessibility. (213-214)

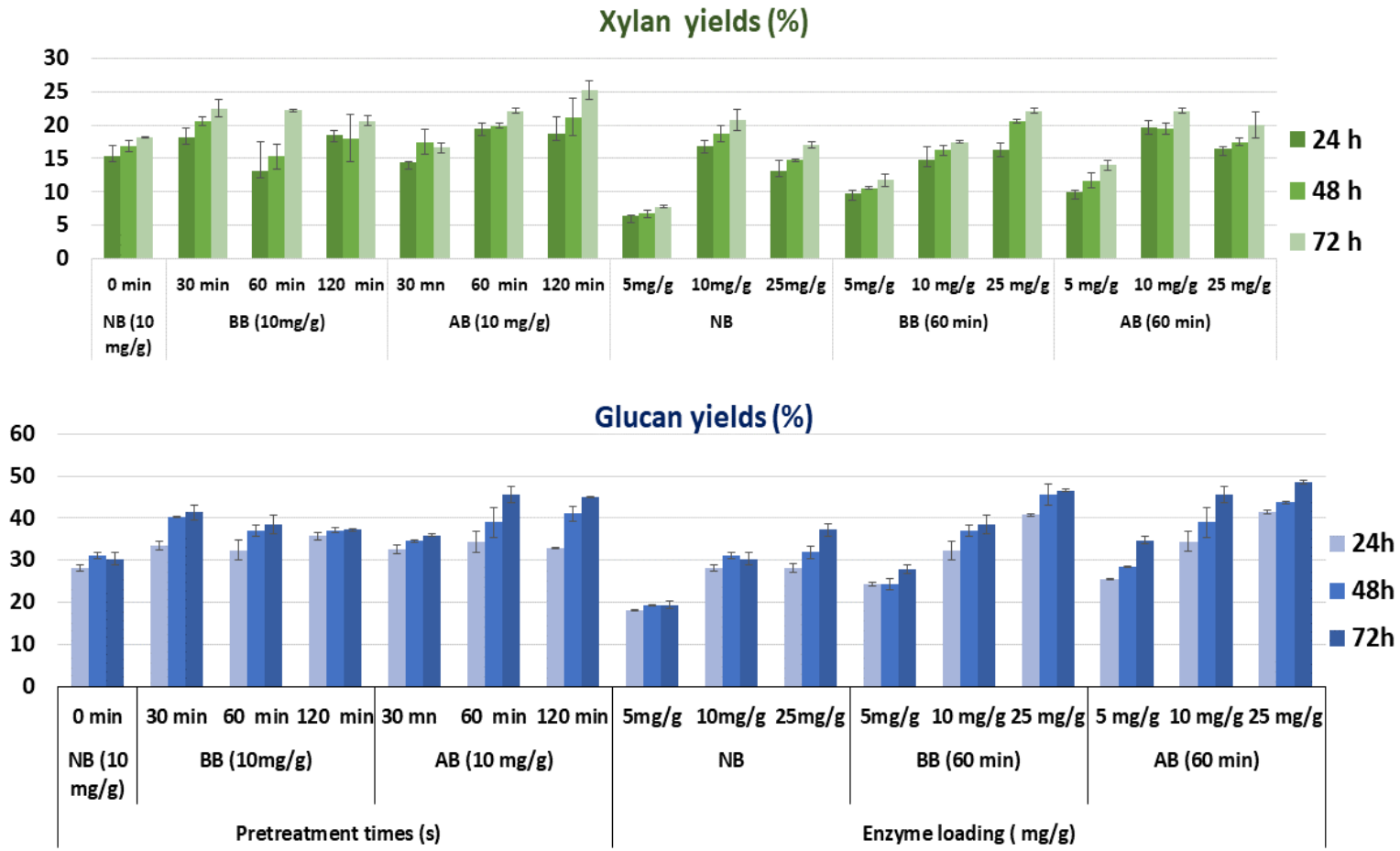

Figure 7-3- Enzymatic hydrolysis yields of native, boiled, and autoclaved cane**:** Effects of pretreatment times (30 min, 60 min, and 120 min) on enzymatic hydrolysis efficacity 10 mg /g as enzyme of biomass ratio, and effects of enzyme loading (5 mg/g,10 mg/g, and 25 mg/g) on enzymatic hydrolysis of native, boiled, and autoclaved cane carried out at 60 min.

Source: By the author

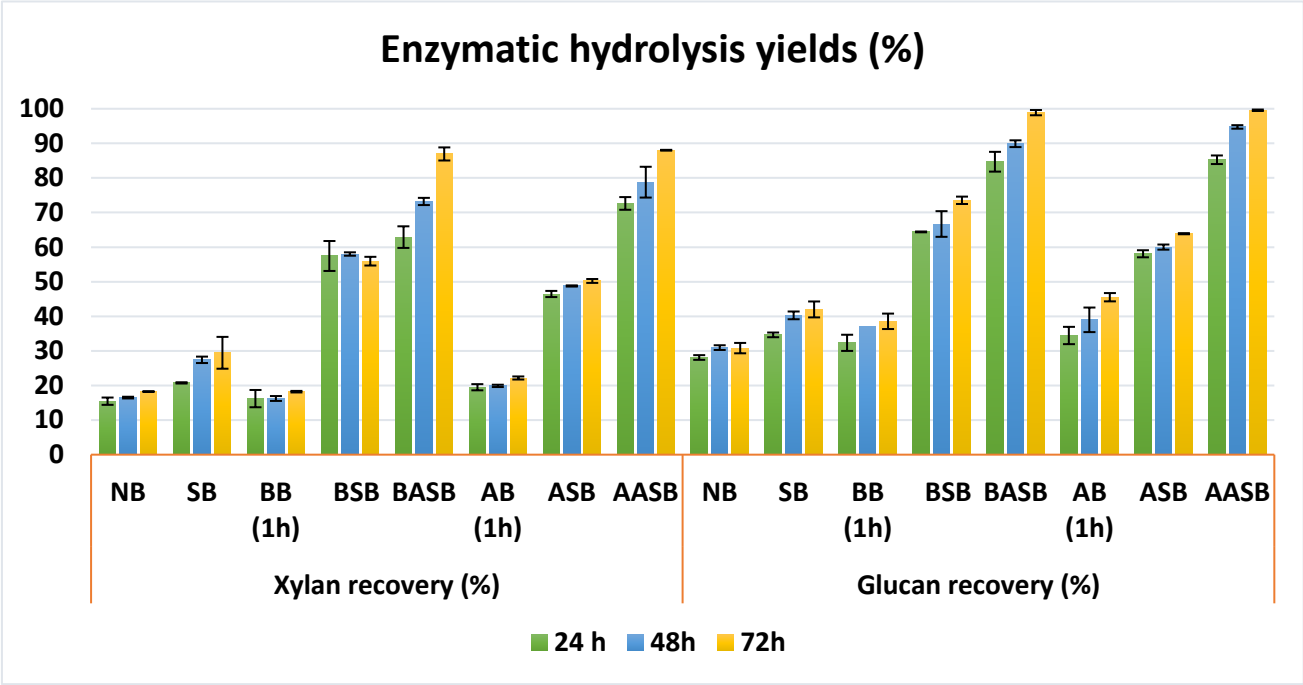

Figure 7-4- Enzymatic hydrolysis yields of native bagasse (NB), sulfonated bagasse (SB), LHW pretreated bagasse ((BB: boiled bagasse, AB: autoclaved bagasse), boiled and autoclaved sulfonated bagasse (BSB and ASB.), boiled and alkaline sulfonated bagasse (BASB), autoclaved and alkaline sulfonated bagasse (AASB).

Source: By the author

7.1.5 ^{1}H Nuclear Magnetic Resonance relaxometry

The amount of water adsorbed by the raw and LHW SCB samples was measured by directly comparing the intensity of the first CPMG echo. To do that, we used a sample with 300 µL of water to calibrate the signal and estimated the volume adsorbed by each sample from the intensity of the NMR signal. Since the samples studied here are unconsolidated materials, i.e., powders, we use the amount of water adsorbed by the weight of dried biomass as a figure of merit. As a quality control, we used the difference in weight of the humid and dry samples to estimate the amount of adsorbed water by each sample.

The main advantage of using NMR to study water adsorption by lignocellulosic samples is its capability to offer how much water is adsorbed and distributed over the complex pore structure of such materials. (215)On lignocellulosic materials, we usually observe three components on the

T_2 distribution related to different interstitial scales of the pore structure, covering several length scales. In particular, for lignocellulosic biomass like the corncob samples used here, we observe three distinct interstitial scales related to different parts of the porous microstructure (216,217). The pores at the microfibril surfaces (microfibrils) are associated with the shortest T_2 observed on the T_2 distribution, usually about 1 ms. The water adsorbed within the lignin-hemicellulose matrix on the surface of the fibers (cell wall) is described by the central component of the distribution, whose T_2 values are tens of milliseconds. The most extended values observed for T_2, about 100 ms, represent water inside tiny luminal pores, between the fibers, or even water confined between the grains of the biomass (lumens). By deconvoluting the T_2 distribution into log-Gaussians assigned to each interstitial scale, we can isolate how much water is adsorbed by each component. Thus, the T_2 distributions for samples that underwent different biochemical processes unveil how the microstructure of the biomass is modified on each length scale of the lignocellulosic microstructure. The amount of water adsorbed by each sample, as well as the by each interstitial scale, is described in Table 2. The T_2 distributions obtained for each sample are shown in Figure 7-5.

Table 2 - Dried mass, adsorbed volume measured, and the adsorbed volume by each interstitial scale for all samples, both raw and LHW pretreated.

Sample	Dried mass (mg)	adsorbed volume (ml)	Adsorbed volume NMR (ml)	Adsorbed volume by mass (g/ml)	Adsorbed volume by mass NMR (g/ml)	Adsorbed water microfibrils (g/ml)	Adsorbed water cell wall (g/ml)	Adsorbed water lumens (g/ml)
NB	21.24(2)	0.22(1)	0.21(1)	4.33(3)	4.17(3)	0.23(1)	2.79(4)	1.25(3)
BB	20.77(2)	0.24(2)	0.25(1)	5.64(4)	5.78(4)	0.28(1)	2.98(5)	2.62(4)
AB	20.04(2)	0.15(1)	0.14(1)	2.47(3)	2.32(3)	0.25(1)	1.83(4)	0.23(1)
SB	16.44(2)	0.31(2)	0.28(1)	3.20(4)	2.84(3)	0.12(1)	1.37(4)	1.50(3)
BSB	20.60(2)	0.28(2)	0.27(1)	5.72(4)	5.50(4)	0.17(1)	2.05(5)	3.20(3)
ASB	15.81(1)	0.28(2)	0.25(1)	5.53(3)	4.99(4)	0.15(1)	2.86(6)	2.42(3)
BASB	21.03(1)	0.34(2)	0.29(1)	6.14(4)	5.38(4)	0.27(1)	3.71(6)	1.70(4)
AASB	17.82(1)	0.34(2)	0.30(1)	6.20(3)	5.49(4)	0.10(1)	3.98(7)	1.51(3)

Source: By the author.

As shown in Table 2, the partial lignin removal induced by sulfonation results in a higher amount of water being adsorbed by the biomass, especially in alkaline sulfonation. We observe that the amount of water adsorbed on the cell wall scale (tens of milliseconds) has a bigger role in the enzymatic hydrolysis since we observe higher adsorption on this scale for the samples with higher glucan and xylan recovery yields (Figure 7-4**)**, namely the samples BSB, ASB, BASB, and AASB. We remark that this feature is not observed in the NB, BB, AB, and SB samples, which have a very different chemical composition and crystallinity from the other four samples.

Finally, while Eq. (14) is a direct relation between T_2 and pore size, the surface relaxivity ρ_2 is an unknown constant that depends directly on several of the properties of the sample, like composition, the affinity between the pore surface, and the liquid used as a molecular probe, among other properties. (61) Thus, we cannot estimate a pore size from our measurements since the pretreatments have different compositions because of the pretreatments. We cannot relate the slight variations in the central T_2 values for each component on the T_2 distributions to changes in pore sizes as the LHW pretreatments (with or without sulfonation) modify the lignin-hemicelluloses matrix. As such, the pretreatments change how water within the biomass interacts with pore surfaces, i.e., changes the surface relaxivity.

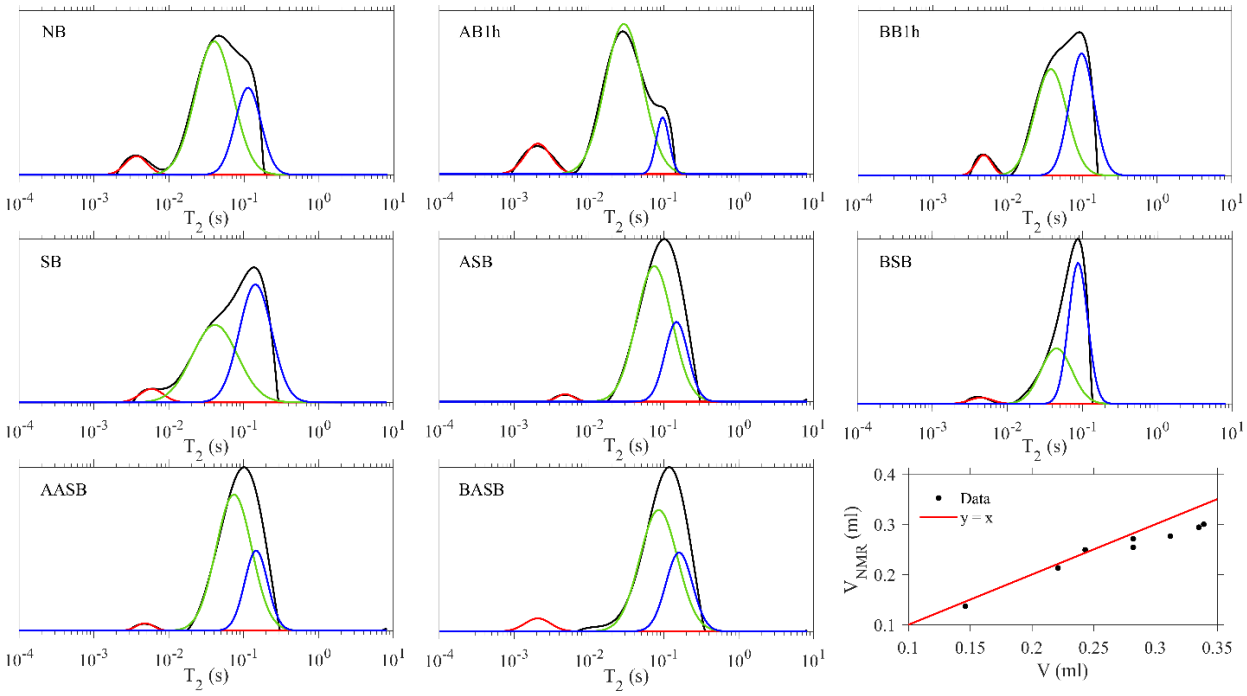

Figure 7-5- T_2 distributions for one of the raw and LHW pretreated samples. The solid black lines represent the distributions, whereas the components associated with each interstitial scale are shown in red (microfibril surfaces), green (cell wall), and blue (lumens). The bottom right panel shows the correlation between the gravimetric and NMR measurements for the adsorbed volumes of water. The solid red line indicates the perfect correlation case, i.e., the $y = x$ line.

Source: By the author

7.1.6 ^{13}C solid-state nuclear magnetic resonance spectroscopy

Solid-state ^{13}C NMR spectroscopy was used to probe changes in the cellulose, hemicellulose, and lignin components of native and pretreated sugarcane bagasse samples (Figure 7-6). The general signal assignment of the native bagasse spectrum shown in Figure 7-7A is based on previous reports. (205–207) The prominent signals in the 60–110 ppm range are mainly ascribed to carbohydrate carbons. (205,206) Signals at 63.5 ppm and 84 ppm are assigned to C6 and C4 carbon in more conformationally disordered carbohydrates chains, which may include cellulose chains in microfibril surface and xylan associated with cellulose in a minor fraction, to aliphatic carbons of lignin. The sole signal at 88 ppm is due to the C4 carbons in the inner part of a cellulose microfibril, sometimes referred to as crystalline cellulose. Aromatic lignin signals are spread out in 112–160 ppm spectral region, while the signal of Aro-OCH_3 carbon appears at 55 ppm. Signals

from carbonyl and methyl carbons of acetyl groups in lignin and hemicellulose are shown at 172 ppm and 20.7 ppm.

As mentioned, the signal at 88 ppm is associated with C4 carbons of the cellulose chains in the inner part of the microfibril, which should be more protected from chemical pretreatment. Thus, to evidence, the pretreatment effects, all spectra shown in Figure 7-6 were normalized by the intensity of this signal. Consistent with the chemical composition analysis (Table 1), the observed similarity among the spectra of native bagasse (NB) and liquid hot water pretreated bagasse (AB and BB) indicates that there was very limited lignin removal and carbohydrate loss during hot water pretreatments (Figure 7-6B). Differences in the relative signal intensities between native and sulfonated bagasse (SB) (Figure 7-6B) are consistent with the notion that sulfonation provoked structural changes in sugarcane bagasse. After sulfonation, several signals associated with lignin and hemicellulose disappeared or decreased their intensity. This behavior is in line with partial removal and structural modifications of lignin and hemicellulose after sulfonation. The spectrum of alkaline sulfonated bagasse samples (AASB, BSAB) confirmed the massive delignification during alkali sulfonation pretreatment (Table 1). Spectra of neutral sulfonated bagasse samples (BSB, ASB) indicate the partial removal of lignin and hemicellulose very similar to sample SB, confirming that this is an effect related to the sulfonation of the samples. Another qualitative feature that can be inferred from Figure 7-6 concerns the microstructure of the cellulose microfibrils. As mentioned, the signal at 88 ppm (indicated by the asterisk in Figure 7-6a) is due to C4 carbons in the inner part of the cellulose microfibril, while the signal at 84 ppm (indicated by the square in Figure 7-6a) is related to C4 carbons in more disorder cellulose chains in the surface of the microfibril as well as to xylan chains associated to cellulose. Slight variation is observed in the intensity ratio between these two signals for neutral sulfonated bagasse samples compared to the native ones. This indicates that sulfonation does not change the structure of the cellulose microfibril appreciably, so the sample crystallinity increase observed in the X-ray diffraction results mostly due to the removal of amorphous components such as lignin and hemicellulose. A small but significant increase in this intensity ratio is observed for the alkaline sulfonated as compared with native bagasse samples. Such change occurs due to a reduction in the intensity of the signal at 84 ppm and can be attributed to the removal of amorphous carbohydrates or aliphatic carbons of lignin.

It is possible to draw some direct correlation between the modifications observed in the ^{13}C NMR and the hydrolysis yield. The ^{13}C NMR data confirm that the higher glucan and xylan

recovery observed for samples AASB and BASB results from the strong delignification of the sulfonation and alkaline pretreatment combination. Neutral and sulfonated bagasse samples (BSB, ASB, SB) presented intermediate glucan and xylan recovery, which is also in line with the moderate degree of delignification of the hemicellulose removal shown by ^{13}C ssNMR. However, despite the ^{13}C ssNMR spectra indicating similar lignin content among these three samples, the sample SB show considerably smaller glucan and xylan recovery yield. This may be related to the different water absorption profiles for the SB samples, as shown in the ^{1}H relaxometry results, and correlates well with the structural reorganization of lignin during the thermal pretreatments, as demonstrated by the confocal microscopy results. Last, samples in which the ^{13}C ssNMR does not indicate a reduction in the lignin and hemicellulose content show smaller, higher glucan and xylan recovery.

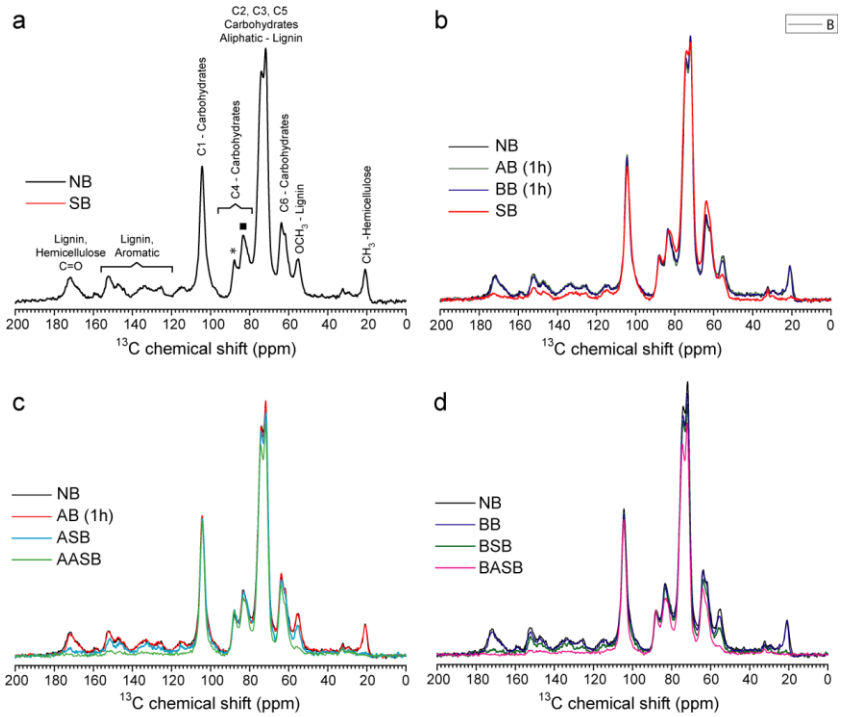

Figure 7-6- Solid-state ^{13}C NMR spectra of untreated and pretreated bagasse. A: Spectro for native bagasse NB B: Comparison between spectra of NB, AB, BB, and SB C: comparison between spectrums of NB, AB (1h), ASB, and AASB. D: comparison between spectrums of NB, BB, BSB, and BASB.

Source: By the author

7.2 Enzyme-assisted production of cellulose nanofibers from bleached and sulfonated sugarcane bagasse

7.2.1 Chemical composition

The enzyme-assisted production of CNF is a sequential process that includes substrate delignification, partial enzymatic hydrolysis, and mechanical defibrillation, as represented in Table3. The initial composition of untreated SCB in cellulose, hemicellulose, and lignin were respectively 42.3, 25, and 20.4 % (Table 3). After the pretreatment steps, an efficient delignification can be noticed, resulting in 75% and 80% of lignin removal for BB, and BSB., respectively. In addition, the cellulose fraction increased compared to the chemical composition of untreated SCB., and only a slight decrease in the hemicellulose fraction was observed for BB (25 to 23.8%). BSB exhibited similar chemical composition after pretreatments, indicating that the sulfonation step did not lead to significant degradation of carbohydrates. The chemical composition of BB and BSB emphasized the pretreatment efficiency with a massive elimination of lignin and the excellent holocellulose (cellulose and hemicellulose) extraction. This retention of hemicellulose and cellulose allowed high-value utilization of raw SCB. In addition, these results predict the formation of cellulose nanofiber (CNF) enriched in hemicellulose as confirmed by chemical composition analysis of obtained cellulose nanofibers (Table 3), which contained 74% cellulose, 20% hemicellulose, and 4% lignin for CNF (0.312) as well as 70% cellulose, 18% hemicellulose and 3 % lignin for SCNF. Cellulose nanofibers with high hemicellulose contents are generally defined as holocellulose CNF (HCNF) and typically have high mechanical properties and molar mass compared to cellulose nanofiber from cellulose only(218–220)

Efficient delignification was achieved by the combined action of sodium hydroxide, which removes lignin through irreversible hydrolysis of the ester bond of lignin-carbohydrate complexes, and H_2O_2, which oxidates the carbonyl and quinoid structures of the lignin side chain. (221) In addition, the reaction between H_2O_2 and the benzoquinone structure of lignin increases the solubility of lignin. Moreover, H_2O_2 can react with the side chain carbonyl and carbon-carbon double bond of lignin to provoke further oxidative degradation, thus enhancing lignin removal. (222) The combined pretreatment using alkaline peroxide (H_2O_2/NaOH) was proven effective for removing the residual lignin while preserving the polysaccharide fractions. (122,223)

Table 3 - Chemical composition of the raw SCB., bleached (BB), bleached-sulfonated bagasse (BSB), CNF (0.312), and SCNF (0.312).

Sample	Content (%)				
	Cellulose	Hemicellulose	Lignin	Ashes	Total
Native SCB *	42.3 ± 0.1	25 ± 1.7	20.4 ± 0.7	1.0 ± 0.1	96 ± 2.7
BB	68.2 ± 0.7	23.8 ± 0.7	5.3 ± 1	2.0 ± 0.4	99.3 ± 2.7
BSB	67.1 ± 0.8	28.6 ± 0.3	4 ± 2	1.0 ± 0.1	100.8 ± 2
CNF (0.312)	74.4 ± 2.7	18.8 ± 1.4	4.0 ± 0.2	1.5 ± 0.1	100 ± 3
SCNF (0.312)	70.5 ± 1.7	18.5 ± 1.6	2.9 ± 1.1	1.4 ± 0.1	93.3± 6

*** Extractives: 7.3 ± 0.1**

Source: By the author.

Sulfonation of the BB substrate did not modify the chemical composition of the substrate considerably (Table 3) but is expected to introduce sulfonic groups that soften the lignin contained in the cell wall and increase its hydrophilicity as well as swelling capacity. (224) BB sulfonation may also provoke partial deconstruction of the three-dimensional cross-linked lignin network, thus influencing nano-fibrillation behavior. (208) Notably, the samples obtained in this work contained a tiny residual lignin fraction, thus decreasing the impacts of pretreatment-induced lignin on CNF production. However, these characteristics are advantageous for lowering energy consumption in separating nanoscale fibrils.

Hemicelluloses and anionic groups allow the fibers to swell extensively, enhancing fibrillation. (225) Indeed, residual hemicellulose in cellulose pulps can increase the CNF yields and prevent cellulose aggregation during fibrillation by inhibiting coalescence. (226) Nevertheless, it was also reported that residual hemicellulose might negatively influence nanocellulose structure, decreasing the tensile strength of nanofibers and interrupting the nanofiber network. (227)

7.2.2 Glucose and CNF yields

BB and BSB samples were hydrolyzed using 0.312 and 0.625 mg enzyme/g substrate (Table 4**)** in a relatively fast enzymatic hydrolysis process (6 h). As expected, higher enzyme dosages resulted in higher glucose yields for both substrates. Due to low enzymatic loads (0.312 mg/g), a small conversion of cellulose to glucose occurred (Table 4). These low conversion yields are desirable for CNF production because higher quantities of partially hydrolyzed cellulose remain available in the solid substrate to be converted to CNF, and only small amounts of the polysaccharide are converted to glucose. Likewise, enzymatic dosages higher than 0.625 mg/g are not suitable for CNF production because they lead to a higher rate of cellulose conversion into glucose, reducing the remaining cellulose fraction in solids to be converted into CNF.

Next, all substrates (including control samples, not subjected to enzymatic hydrolysis) were mechanically defibrillated to isolate CNF. The positive impact of enzymatic hydrolysis on nano fibrillation was noted, as reported in Figure 7-7. CNF yield increased after enzymatic hydrolysis comparing CNF yields of control samples to hydrolyzed samples. Thus, CNF yield increased from 20 to 51% for CNF as well as 19 to 34% for SCNF. Therefore, it is possible to produce up to 2.5-fold more CNF by carrying out an enzymatic hydrolysis step while using the same fibrillation conditions. This increase in the CNF yield is consistent with previous studies that reported improving the enzymatic hydrolysis efficiency in bleached sulfonated thermomechanical pulps. (228,229) Besides, enzymatic low-loading conditions were sufficient to improve the CNF conversion significatively.

BB and BSB control samples had similar CNF yields, which indicated that the sulfonation has not positively impacted the mechanical disintegration in terms of CNF yields, although other previous studies reported that cellulose sulfonation could facilitate mechanical defibrillation. (123,230) However, other parameters, such as the degree of sulfonation, sulfonation methods, etc., could influence the sulfonation effects on nano fibrillation. Our sulfonation step introduces the 0.4 mmol sulfonic groups/g of biomass (Table 5); the charge density is low compared to other works. Sulfated nanofibers were made by Sirviö *et al.* utilizing reactive deep eutectic solvents (sulfamic acid and urea). They showed that sulfated cellulose could easily be disintegrated into sulfated cellulose nanofiber (SCNF) using mild mechanical disintegration with a surface charge density of 2.40 mmol/g and high viscosity at low concentrations. However, they have not determined the yield

of SCNF.(231) CNF with a sulfonate group was previously produced by Pingrey *et al.* (2022) using chlorosulfonic acid (HSO_3Cl) followed by blending. They investigated SCNF yield as a function of the surface charge (30 min blending) observed. They obtained sulfated cellulose that could be disintegrated by high-speed blending (30K rpm, 30 min) to yield 94–97% SCNF with 1.3–2.2 mmol/g charges at ambient temperature. (232)

Considering hydrolyzed samples, overall, the sulfonation enhanced the enzymatic hydrolysis. Thus, cellulose-enriched material available for nano fibrillation decreased. This can explain the high yields of CNF from BB than those from BSB. Sulfonated substrates are more susceptible to enzymatic hydrolysis due to the sulfonic groups, which enhances the swelling of fiber and hinders unproductive adsorption because they are deprotonated in the reaction pH. (233) As shown in Table 1, the sulfonation step added up to 0.4 mmol sulfonic groups/g biomass, which was a possible reason for enhancing enzymatic action.

Table 4 - Yields of glucose and xylose released during enzymatic hydrolysis of BB and BSB

Enzyme loading	0.625 mg/g		0.312mg/g	
Substrate	BSB	BB	BSB	BB
Glucose yield (%)	22.6 ± 0.2	20.1 ± 0.3	15.2 ± 2.34	7.2 ±2.8
Xylose yield (%)	24.05 ± 2.2	33.6 ± 2.1	10.8 ± 0.1	9.78 ± 0.01

Source: By the author

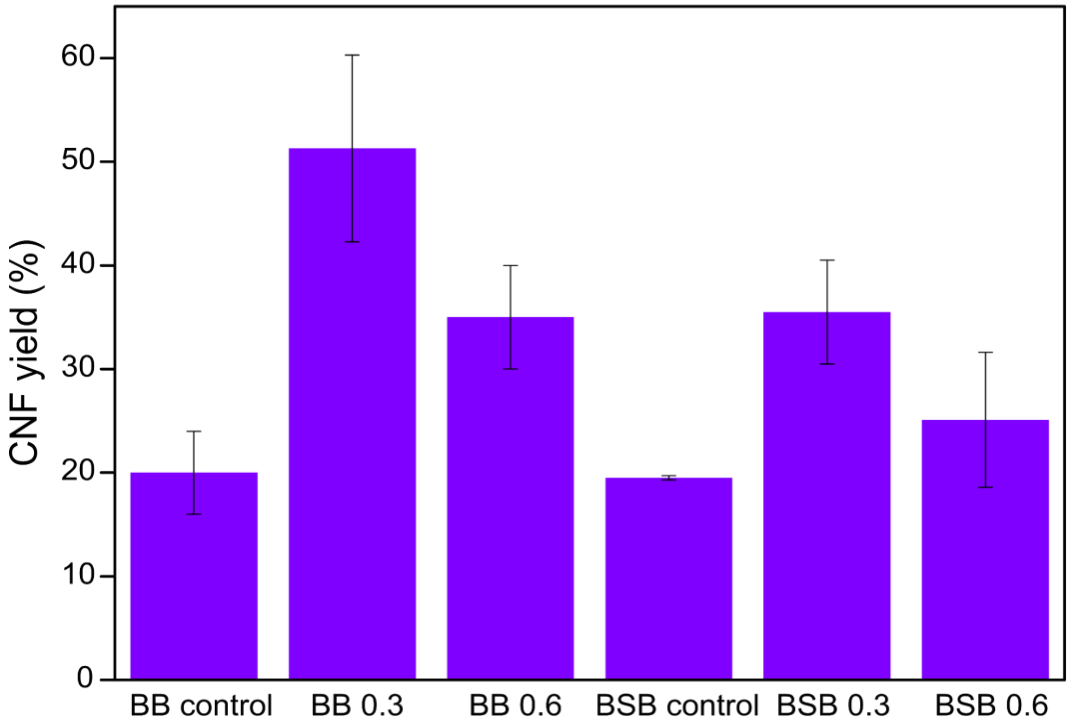

Figure 7-7- CNF and glucose yield after enzymatic hydrolysis and fibrillation. Control samples did not release glucose.

Source: By the author

7.2.3 Morphological analysis of the chemical and enzymatic treated substrates

Morphological analysis of the substrates before and after chemical and enzymatic treatments (Figure 7-8) corroborates with the improved enzymatic action caused by sulfonation. Initially, the natural substrate shows the typical SCB morphology, in which cellulose fibers are covered by parenchymal tissue (Figure 7-8(A-B)). After SCB treatments (Figure 7-8(C-D), respectively), cellulose microfibers from BB and BSB were significantly exposed and separated, which is related mainly to the delignification processes. (99)

After enzymatic hydrolysis, the fibers were more unstructured and detached because of enzymatic action both for BB and BSB samples (Figure 7-8 (E-H)). Figures 7-9F and 7-9 H show cellulose microfibers covered by partially attached nanofibers, revealing an advanced stage of enzymatic action, as reported by Han *et al.* (228) These results confirmed that BSB fibers are more

susceptible to enzymatic hydrolysis than BB fibers, explaining the best yields of glucose and the lowest yields of CNF from BSB.

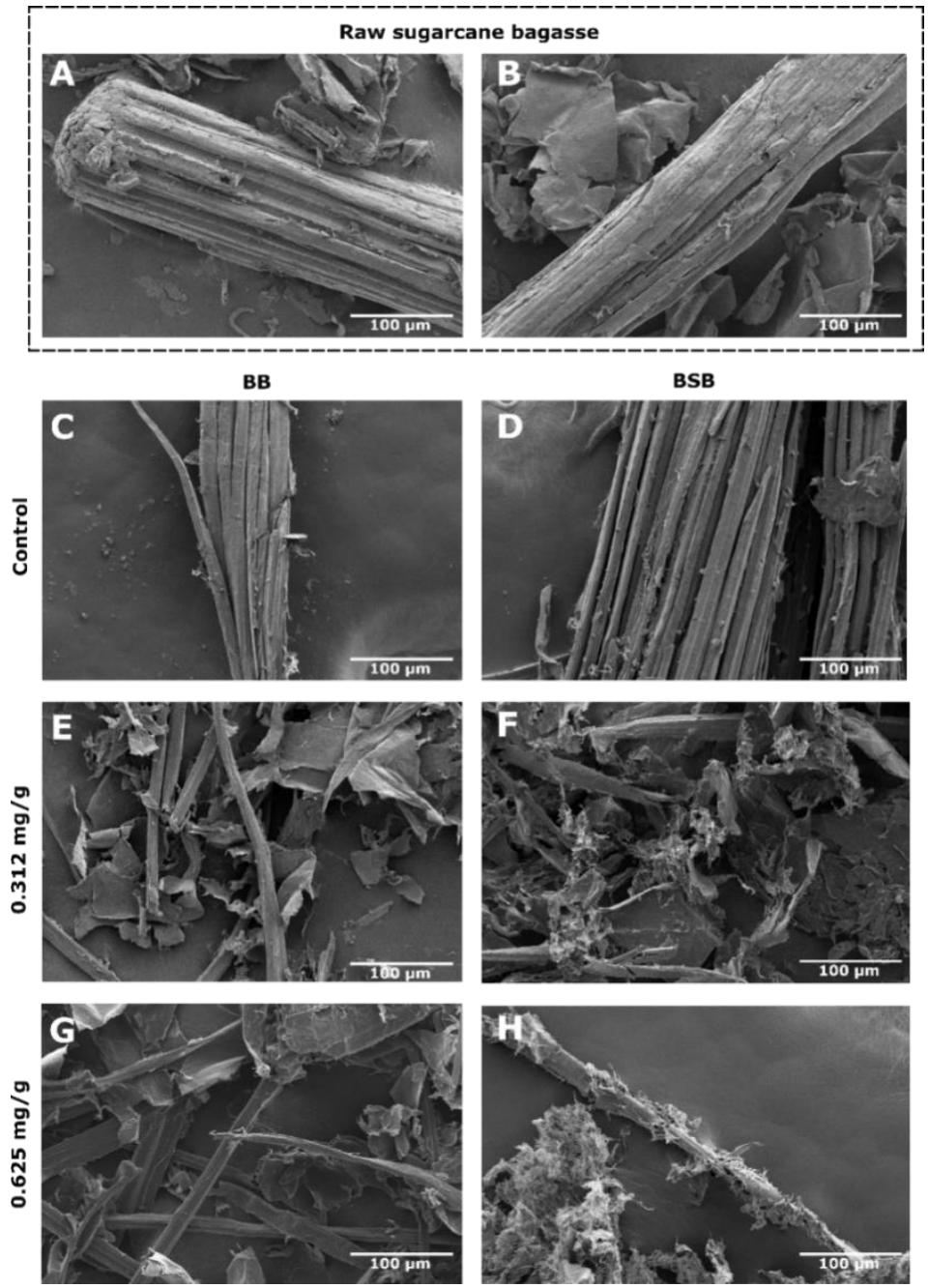

Figure **7-8**- FESEM images of the raw substrate (A-B); after raw substrate delignification: BB (C) and BSB (D); \ after enzymatic treatment using: 0.312 mg enzyme/g enzyme in BB (E) and BSB (F); and 0.625 mg enzyme/g in BB (G) and BSB (H).

Source: By the author

7.2.4 CNF characterization

7.2.4.1 Morphology of CNF and SCNF

In addition to the process yields, nanoparticle properties should be considered to decide on adequate conditions for CNF production aiming at different applications. Morphological analysis carried out by AFM and TEM (Figure 7-9**)** of the CNF isolated from control substrates and after enzymatic hydrolysis using 0.312 mg enzyme/g demonstrates thin and long fibers (in the micrometer scale), which is a typical characteristic of CNF. (Table 5), varying between 5 and 6 nm, with most of the fiber diameters ranging from 1 to 13 nm. These diameter values are similar to those obtained in other processes to obtain CNF from sugarcane bagasse. (234) The longer lengths are a fundamental characteristic of CNF produced by partial enzymatic hydrolysis compared to CNF made from chemical methods (i.e., TEMPO-oxidation), as was previously discussed. (234,235) Longer fibers are easily entangled and suitable for preparing hydrogels and aerogels (236), stabilizing emulsions (237), and manufacturing films. (238)

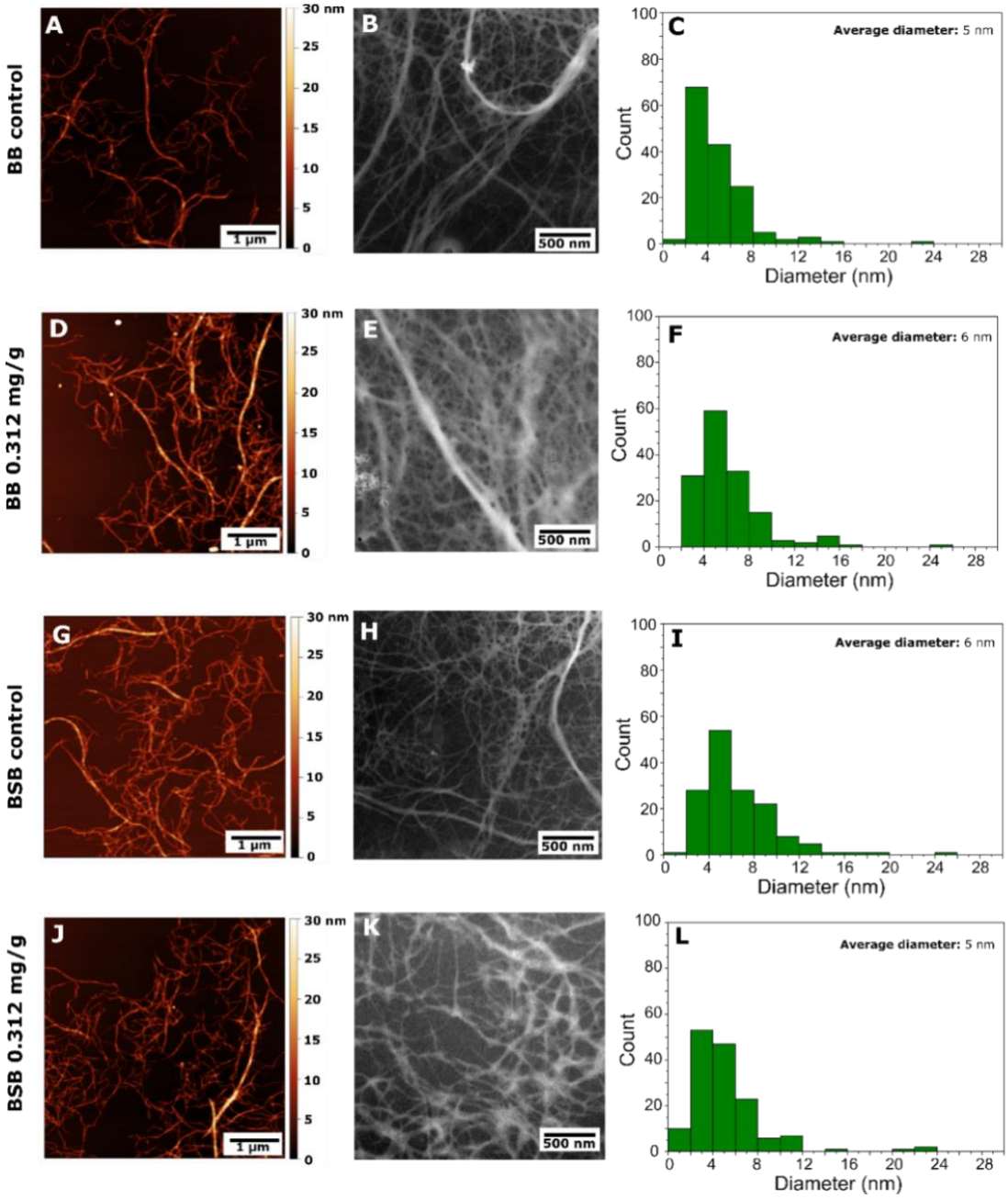

Figure **7-9-** Images of AFM (topography), TEM, and distribution of the sample diameters: CNF control (A-C); CNF (0.312 mg/g (D-F); SCNF control (G-I); and SCNF 0.312 mg/g (J-L). TEM images were acquired by using an energy loss of 25 eV. Diameters were measured by the height of 150 particles in AFM images.

Source: By the author

7.2.4.2 ζ-potential

Overall, cellulose nanofibers from BB and BSB. are colloidally stable because the value of ζ-potential values of obtained CNF turns around the minimum threshold (±30 mV) (Table 5). This stability was due to mechanical treatment. Ultrasonication treatment allows defibrillation of the cellulose fibers transferring ultrasound energy in cellulose chains via the cavitation process. (239). CNF isolated from BSB substrates is slightly more colloidally stable than BB., as indicated by a more negative ζ-potential (Table 5). The sulfonation treatment added 0.3-0.4 mmol of sulfonic groups per gram of CNF. In sulfonated CNF suspensions, the surface sulfonic groups created electrostatic repulsions, enhancing the suspension stability. As previously suggested, the slight difference in colloidal stability between CNF and -SCNF can probably be related to the low degree of sulfation. The presence of sulfonic groups can be decisive for cellulose nanofiber applications, for instance, to enhance the conductivity of membranes for fuel cells without compromising the membrane mechanical properties. (240)

Table 5 - Summary of CNF properties: average diameter, zeta-potential, strong and weak acid groups, and quantity of added sulfonic groups

Sample	Average diameter (nm)	ζ-potential (mV)	Strong acid groups (mmol/g)	Weak acid groups (mmol/g)	Added sulfonic groups (mmol/g)
CNF control	5	-28 ± 2	0.4 ± 0.1	1.1 ± 0.4	-
CNF 0.312	6	-28 ± 2	0.4 ± 0.1	1.5 ± 0.1	-
CNF 0.625	5	-31 ± 2	0.5 ± 0.1	1.6 ± 0.1	-
SCNF control	6	-33 ± 3	0.8 ± 0.1	0.7 ± 0.1	0.4 ± 0.1
SCNF 0.312	5	-35 ± 3	0.8 ± 0.1	1.2 ± 0.3	0.4 ± 0.1
SCNF0.625	5	-28 ± 2	0.8 ± 0.1	1.3 ± 0.1	0.3 ± 0.1

Source: By the author

7.2.4.3 Thermal stability

The thermal decomposition parameters of samples were determined from TGA and DTG curves presented in Figures 7-10A and 7-10B, respectively. Overall, these results indicate that sulfonation and enzymatic hydrolysis affected the thermal stability of cellulose nanofibers.

The initial decomposition temperature (T_{onset}) and temperature of maximum weight loss (T_{max}) (Table 6) exhibit two events of weight loss in CNF samples. Overall, the first thermal degradations occurred between the temperatures of 200 - 380 °C, and the second degradations were observed between 350 °C and 600 °C. The first thermal decomposition stage corresponded to the degradation of holocellulose compounds. As Yang *et al.* reported, the hemicellulose and cellulose thermal decomposition occurred respectively at 220–315 °C and 315–400 °C. The more complex lignin degradation extended to a wide temperature range, from 160 to 900 °C (241); however, the lignin is not so significant in our case. The second degradation stage can be correlated to the decomposition of sulfonated groups.

On the other hand, different thermal degradability behaviors according to CNF samples were noted during each stage. The CNF control thermal degradation starts at lower temperatures (219 °C) than CNF enzymatic-treated samples (244 °C for CNF (0.625 mg/g) (Figure 7-10**).** The SCNF control sample does not present the first degradation peak, but its T_{max} is lower than the SCNF enzymatic treated samples (313 °C for CNF control and 339 °C for SCNF (0.312 and 0.625 mg/g). These results show that the enzymatic hydrolysis step did not decrease the thermal stability of CNF as expected**.** Indeed, enzymes can randomly cleave the glycosidic bonds reducing the molecular size of cellulose chains, leading to smaller cellulose fragments at the molecular level, consequently allowing low thermal degradation temperatures. (242) Equally, enzymatic hydrolysis can remove cellulose fragments, decreasing the molecular weight and T_{onset}. In our case, the loss of cellulose is not significant. Furthermore, it is important to consider the strong presence of hemicellulose in CNF and the enzyme cocktail used to hydrolyze cellulose and hemicellulose. The decrease of hemicellulose after enzymatic hydrolysis can also increase CNF thermal stability, compensating for the effect of cellulose mass reduction.

The sulfate groups on CNF surfaces are supposed to catalyze the thermal decomposition process, leading to less resistance to pyrolysis and decreasing the thermal stability of sulfonated CNF. (243) In our case, the sulfonated CNF is more stable than CNF without a sulfate group. However, it is

demonstrated that the thermal stability of the sulfonated CNF can be influenced by several factors, such as dimensions, crystallinity, degree of polymerization, pretreatment methods, and surface charge density. (244) The high content of sulfate groups on the fiber surface enhances thermal contact areas and can also be responsible for decreased thermal stability. As emphasized previously, the surface charge density in our case is low. These experimentally obtained values are like those previously reported for CNF produced by enzyme-assisted processes from bagasse and softwood.(228,234,242)

These results show that the isolated CNF has good thermal stability, which is important for CNF final applications. For instance, thermal stability is pivotal to producing electronic components and incorporating CNF into nanocomposites that will be extruded or molded, in which thermal stability is essential due to the high variations in temperature. For comparison, TEMPO-oxidized CNF are less thermally stable (decomposition starting at *ca.* 190 °C), demonstrating the superior thermal stability of CNF obtained via partial enzymatic hydrolysis. (234)

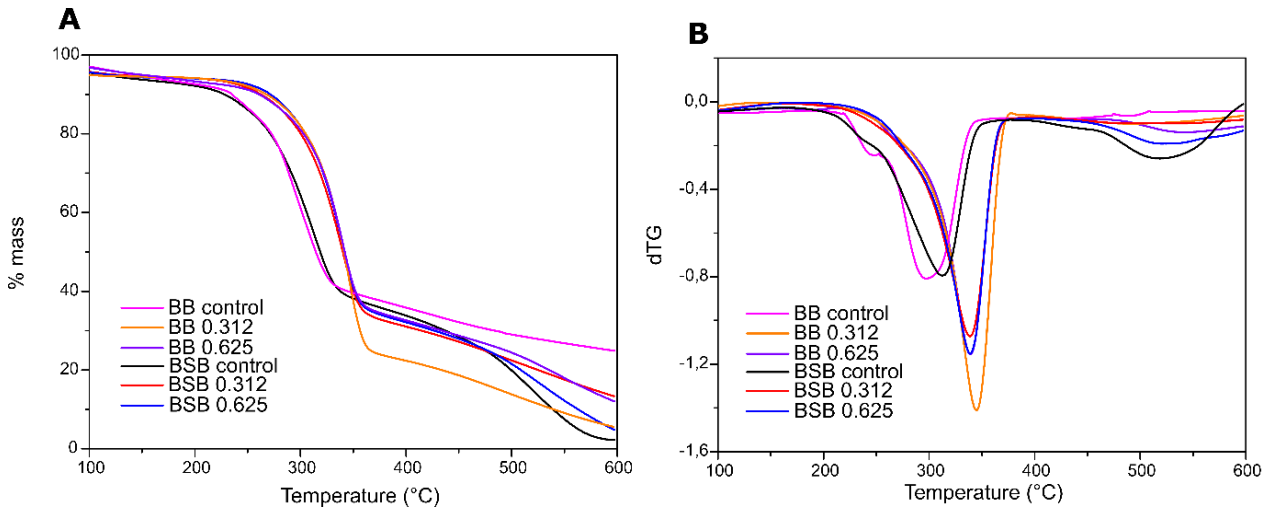

Figure **7-10-** A) TGA curves and B) Derivative thermogravimetric curves of BB and BSB samples before and after enzymatic hydrolysis.

Source: By the author

Table 6 - Initial decomposition temperature (T_{onset}) and temperature of maximum mass loss (T_{max}) of CNFs obtained from TGA

Sample	T_{onset} (°C)	T_{max} (°C)
CNF control	219 (peak 1) 260 (peak 2)	246 (peak 1) 297 (peak 2)
CNF 0.312	246	344
CNF 0.625	244	339
SCNF control	255	313
SCNF 0.312	229	339
SCNF 0.625	237	339

Source: By the author

8 Chapter 8 General Conclusions

The thesis aimed to improve lignocellulosic biomass valorization, optimizing pretreatment bioeconomic strategies and conditions for overcoming lignocellulosic biomass recalcitrance and enhancing its enzymatic conversion into fermentable sugars.

During this thesis, four (4) projects were carried out: Different lignocellulosic biomasses were investigated as a potential feedstock for Bioethanol production through sequential pretreatment stages and enzymatic hydrolysis performances. On the other hand, cellulose nanomaterial or cellulose nanofibers were extracted from blanched SCB as well as blanched and sulfonated SCB through two-step alkaline-sulfonated pretreatment ($NaOH/H_2O_2$-Na_2SO_3) of sugarcane bagasse.

In all these projects, the emphasis was first placed on the characterization of lignocellulosic biomass. LB chemical composition analysis provides information on the relevance of its exploitation for a given application. Besides, the characteristic of the feedstock is the first and foremost parameter that helps in choosing adequate pretreatment methods. Chemical analysis of sugarcane wastes showed that all the varieties are potentially good as raw materials for bioethanol production, with their high cellulose fractions.

All the pretreatments applied in this work allowed to disrupt of efficiently lignocellulosic biomass structure, either by transforming (LHW and neutral sulfonation) or by removing lignin and/or hemicellulose (acidic and alkaline pretreatments). These changes have been evidenced through structural and morphological analysis of untreated and pretreated LB and have influenced their enzymatic digestibility positively. Factors such as crystallinity, lignin behavior, and surface area have been considered. Among these factors, lignin removal was a determinant parameter. The higher the delignification, the higher the enzymatic convertibility of LB. The combination of pre-treatment effects led to high enzymatic digestibility and almost total conversion to fermentable sugar of all LB chosen in this work. Considering the difference in chemical concentrations used for the leaves and culms, these leaves can be as good as culms for bioethanol production under acid–alkali pretreatment. Combined acid–alkali pretreatment accounted for the highest enzymatic hydrolysis efficiency across all four genotypes. The diluted acid pretreatment demonstrated that the enzymatic hydrolysis was more efficient in the energy canes than in the sugarcane varieties. The liquid hot water pretreatment disrupted the bagasse structure, allowing the enzymatic

hydrolysis yield to increase from 37.2 ± 1.5 for NB to 46.6 ± 0.4 for BB and 48.6 ± 0.5 for AB without significant modifications in their chemical compositions. The combination of LHW and sulfonation pretreatments allowed good enzymatic convertibility in neutral medium and outstanding saccharification in alkaline medium with 98.88 ± 0.76 and 99.57 ± 0.21 in released glucose yield for BASB and AASB, respectively, as well as 88.91% and 90.02% in release xylose yield for BASB and AASB.

The alkaline peroxide pretreatment was greatly efficient for cellulose nanofiber production, with a massive delignification and holocellulose (hemicellulose and cellulose) extraction. Moreover, the ecofriendly and safe enzymatic hydrolysis step allowed to improve defibrillation of blanched SCB. For a small enzyme loading (0.312 mg/g of the substrate), colloidally and thermally, cellulose nanofibers were produced. Yields achieved 51% for CNF and 34% for SCNF from 20 % for CNF (control) and 19 % for SCNF (control).

Surface modification of cellulose fibers by sulfonation introduced sulfonic groups to the surface of the cellulose nanofibers. Surface modification of cellulose fibers can favorize the functionalization of CNF and the production of tailored composite materials, widening their range of applications to several fields such as packaging, medical aerospace, electronic industries, automobiles, etc.

As application, we project to produce cellulose nanofiber-based material for energy storage devices. Thus, we are starting by developing sulfonated cellulose-based material as electrodes for supercapacitors and batteries, testing their efficiency as electrodes in terms of power and energy density.

REFERENCE

1 BRITISH PETROLEUM. *Statistical review of world energy globally consistent data on world energy markets*. 70th. 2021. Available from: https://www.bp.com/content/dam/bp/business-sites/en/global/corporate/pdfs/energy-economics/statistical-review/bp-stats-review-2021-full-report.pdf. Accessible at: 30 Oct. 2021.

2 ZOGHLAMI, A. *et al.* Three-dimensional imaging of plant cell wall deconstruction using fluorescence confocal microscopy. *Sustainable Chemistry*, v. 1, n. 2, p. 75-85, 2021, DOI: 10.3390/suschem1020007.

3 VOHRA, K. *et al.* Global mortality from outdoor fine particle pollution generated by fossil fuel combustion: results from GEOS-Chem. *Environmental Research*, v. 195, p. 110754, 2021. DOI: 10.1016/j.envres.2021.110754.

4 SABINE, C. The IPCC fifth assessment report. *Carbon Management*, v. 5, n. 1, p. 17-25, 2014. DOI: 10.4155/cmt.13.80.

5 FRIEDLINGSTEIN, P. *et al.* Global carbon budget 2019. *Earth System Science Data*, v. 11, n. 4, p. 1783-1838, 2019. DOI: 10.5194/essd-11-1783-2019.

6 IEA. *Net Zero by 2050*: a roadmap for the global energy sector. 2021. Available from: https://iea.blob.core.windows.net/assets/deebef5d-0c34-4539-9d0c-10b13d840027/NetZeroby2050-ARoadmapfortheGlobalEnergySector_CORR.pdf. Accessible at 25 March 2022.

7 ZHOU, X *et al.* Eco-friendly consolidated process for co-production of Xylo oligosaccharides and fermentable sugars using self-providing xylonic acid as key pretreatment catalyst. *Biotechnology for Biofuels*, v. 12, n. 1, p. 1-10, 2019. DOI: 10.1186/s13068-019-1614-5

8 AGUILAR-RIVERA, N. *et al.* Effects of public policies on the sustainability of the biofuels value chain. *Sustainable Biofuels*, p. 345-379, 2021. DOI: 10.1016/b978-0-12-820297-5.00004-

9 RIBEIRO, R. S. A. *et al.* Production of nanocellulose by enzymatic hydrolysis: trends and challenges. *Engineering in Life Sciences*, v. 19, n. 4, p. 279-291, 2019. DOI: 10.1002/ELSC.201800158.

10 DE AQUINO, G. S. *et al.* Sugarcane straw management and its impact on production and development of ratoons. *Industrial Crops and Products*, v. 102, p. 58-64, 2017. DOI: 10.1016/j.indcrop.2017.03.018

11 HERRMANN, R. *et al.* Competition between biofuel feedstock and food production: Empirical evidence from sugarcane out grower settings in Malawi. *Biomass Bioenergy*, v. 114, p. 100-111, 2018. DOI: 10.1016/j.biombioe.2017.09.002

12 PREETHI. *et al.* Lignocellulosic biomass as an optimistic feedstock for the production of biofuels as valuable energy source: Techno-economic analysis, Environmental Impact Analysis, Breakthrough and Perspectives. *Environmental Technology & Innovation*, v. 24, p. 102080, 2021. DOI: 10.1016/J.ETI.2021.102080.

13 BROSSE, N. *et al.* Miscanthus: a fast-growing crop for biofuels and chemicals production. *Biofuels, Bioproducts and Biorefining*, v. 6, n. 5, p. 580-598, 2012. DOI: 10.1002/bbb.1353.

14 BIRGEN, C. *et al.* Butanol production from lignocellulosic biomass: Revisiting fermentation performance indicators with exploratory data analysis. *Biotechnology for Biofuels*, v. 12, n. 1, p. 1-15, 2019. DOI: 10.1186/s13068-019-1508-6.

15 KIM, D. G. *et al.* Improved 2,3-butanediol yield and productivity from lignocellulose biomass hydrolysate in metabolically engineered Enterobacter aerogenes. *Bioresource Technology*, v. 309, p. 123386, 2020. DOI: 10.1016/j.biortech.2020.123386

16 YANKOV, D. *et al.* Fermentative lactic acid production from lignocellulosic feedstocks: from source to purified product. *Frontiers in Chemistry*, v. 10, p. 1-34, 2022.DOI: 10.3389/fchem.2022.823005

17 PHILIPPINI, R. *et al.* Agro-industrial byproducts for the generation of biobased products: alternatives for sustainable biorefineries. *Frontiers in Energy Research*, v. 8, p. 1-23, 2020. DOI: 10.3389/fenrg.2020.00152.

18 TRACHE, D. *et al.* Cellulose nanocrystals/graphene hybrids—a promising new class of materials for advanced applications. *Nanomaterials*, v.10, n. 8, p. 1-34, 2020, DOI: 10.3390/NANO10081523.

19 DOMÍNGUEZ, E. *et al. Micro-and nanolignin particles*. 2021. Available from: https://openaccessebooks.com/chemical-engineering/micro-and-nanolignin-particles-development-and-potential-ppplications.pdf. Accessible at: 23 Jan. 2022.

20 ZHAO, Y. *et al.* Hemicellulose-based film: potential green films for food packaging. *Polymers*, v. 12, n. 8, p. 1775, 2020. DOI: 10.3390/polym12081775.

21 HU, J. *et al.* Enzyme mediated nanofibrillation of cellulose by the synergistic actions of an endoglucanase, lytic polysaccharide monooxygenase (LPMO) and xylanase. *Scientific Reports*, v. 8, n.1, p. 3195, 2018. DOI: 10.1038/s41598-018-21016-6.

22 CHANDEL, H. *et al.* Biotechnological advances in biomass pretreatment for bio-renewable production through nanotechnological intervention. *Biomass Conversion and Biorefinery*, v. 1, p.1-23, 2022. DOI: 10.1007/s13399-022-02746-0.

23 AYENI, A. O. *et al.* Compositional analysis of lignocellulosic materials: evaluation of an economically viable method suitable for woody and non-woody biomass. *American Journal of Engineering Research*, v. 4, n. 4, p. 14-19, 2015.

24 NISHIMURA, H. *et al.* Direct evidence for α ether linkage between lignin and carbohydrates in wood cell walls. *Scientific Reports*, v. 8, n. 1, p. 6538, 2018. DOI: 10.1038/s41598-018-24328-9.

25 BRANCO, R. H. R. R. *et al.* Second generation bioethanol production: on the use of pulp and paper industry wastes as feedstock. Fermentation, v. 5, n. 1, p. 4, 2016. DOI : 10.3390/fermentation5010004.

26 TUONG, T. *et al.* Bioethanol production from lignocellulosic biomass. *Renewable and Sustainable Energy Reviews*, v. 31, p. 40-44, 2019. DOI: 10.5772/INTECHOPEN.86437.

27 PARDO, L. M. F. *et al.* Influence of pretreatments on crystallinity and enzymatic hydrolysis in sugar cane residues. *Brazilian Journal of Chemical Engineering*, v. 36, n. 1, p. 131-141, 2019. DOI: 10.1590/0104-6632.20190361s20180093.

28 JÖNSSON, L. J. *et al.* Pretreatment of lignocellulose: formation of inhibitory by-products and strategies for minimizing their effects. *Bioresource Technology*, v. 199, p. 103-112, 2016. DOI: 10.1016/J.BIORTECH.2015.10.009.

29 BRAIDE, W. *et al.* Production of bioethanol from agricultural waste. *Journal of Fundamental and Applied Sciences*, v. 8, n. 2, p. 372, 2016. DOI: 10.4314/jfas. V8i2.14.

30 CONSTANT, S. *et al.* new insights into the structure and composition of technical lignins: a comparative characterization study. *Green Chemistry*, v. 18, n. 9, p. 2651-2665, 2016. DOI: 10.1039/c5gc03043a.

31 KONTOGIANNI, N. *et al.* Effect of alkaline pretreatments on the enzymatic hydrolysis of wheat straw. *Environmental Science and Pollution Research*, v. 26, n. 3, p. 35648-35656, 2019. DOI: 10.1007/s11356-019-06822-.

32 BHALLA, A. *et al.* Performance of three delignifying pretreatments on hardwoods: hydrolysis yields, comprehensive mass balances, and lignin properties. *Biotechnology for Biofuels*, v. 12, n. 1, p. 213, 2019. DOI: 10.1186/s13068-019-1546-0.

33 MALIK, D.S. *et al*. Removal of heavy metals from emerging cellulosic low-cost adsorbents: a review. *Applied Water Science*, v. 7, n. 5, p. 2113-2136, 2017. DOI: 10.1007/S13201-016-0401-8.

34 BETLEJ, I. *et al*. Evaluation of the hydrolysis efficiency of bacterial cellulose gel film after the liquid hot water and steam explosion pretreatments. *Polymers*, v. 14, n. 10, v. 2032, 2022. DOI: 10.3390/polym14102032.

35 SAHAY S. Deconstruction of lignocelluloses: potential biological approaches. In: SAHAY, S. (ed). *Handbook of biofuels*. New York: Academic Press, 2002, p. 207-232. DOI: 10.1016/b978-0-12-822810-4.00010-5.

36 YOUSUF, A. *et al.* Fundamentals of lignocellulosic biomass. In: YOUSUF, A.; PIOZZI, P.; SANNINO, S. (ed). *Lignocellulosic biomass to liquid biofuels*. Berlin: Elsevier, 2019. P. 1-15. DOI: 10.1016/B978-0-12-815936-1.00001-0.

37 NAIR, S. *et al.* Role of size scale of ZnO nanoparticles and microparticles on toxicity toward bacteria and osteoblast cancer cells.Journal of Materials Science: materials in medicine, v. 20, p. 235-241, 2009. DOI: 10.1007/s10856-008-3548-5.

38 MESQUITA FILHO, J. *Strategies to improve the conversion of sugarcane bagasse into second generation ethanol*. 2021. 132 p. Thesis (Doctor) – Instituto de Pesquisa em Bioenergia, Universidade Estadual Paulista, Rio Claro, 2021.

39 SHAHBANDEH M. *Global sugar cane production 2016-2026*. 2020. Available from: www.statista.com/statistics/445636/global-sugar-cane-production-forecast/. Accessible at: 22 June 2022.

40 ARBEX, M. A. *et al.* Air pollution from biomass burning and asthma hospital admissions in a sugar cane plantation area in Brazil. *Journal of Epidemiology & Community Health*, v. 61, n. 5, p. 395-400, 2007. DOI: 10.1136/jech.2005.044743.

41 MARTINEZ-HERNANDEZ, E. *et al.* Sugarcane bagasse valorization strategies for bioethanol and energy production. In: DE OLIVEIRA, A. B (ed). *Sugarcane* - technology, and research. London: Intech Open, 2018, p. 72-83. DOI: 10.5772/intechopen.72237.

42 SUMMERS, J. C. *et al.* Simultaneous control of particulate and NO(x) emissions from diesel engines. *Applied Catalysis B*: environmental, v. 10, n. 1-3, p. 139-156, 1996. DOI : 10.1016/0926-3373(96)00028-8.

43 BRIENZO, M. *et al.* Comparison study on the biomass recalcitrance of different tissue fractions of sugarcane culm. *Bioenergy Research*, v. 7, n. 4, p. 1454-1465, 2014. DOI: 10.1007/s12155-014-9487-8.

44 HODGSON-KRATKY, K. *et al.* Relationship between sugarcane culm and leaf biomass composition and saccharification efficiency. *Biotechnology for Biofuels*, v. 12, n. 1, p. 247, 2019. DOI: 10.1186/s13068-019-1588-3.

45 MASON, P. J. *et al.* Comparison of the root, leaf, and internode transcriptomes in sugarcane (Saccharum spp. hybrids). *Current Research in Biotechnology*, v. 4, p. 167-178, 2022. DOI: 10.1016/j.crbiot.2022.02.005.

46 CHANDEL, A. K. *et al*. Sugarcane bagasse, and leaves: foreseeable biomass of biofuel and bioproducts. *Journal of Chemical Technology and Biotechnology*, v. 87, n. 1, p. 11-20, 2012. DOI: 10.1002/jctb.2742.

47 HOFSETZ, K. *et al*. Brazilian sugarcane bagasse: energy and non-energy consumption. *Biomass Bioenergy*, v. 46, p. 564-573, 2012. DOI: 10.1016/j.biombioe.2012.06.038.

48 SANKARAN, R. *et al.* The expansion of lignocellulose biomass conversion into bioenergy via nanobiotechnology. *Frontiers in Nanotechnology*, v. 3, p. 96, 2021. DOI: 10.3389/fnano.2021.793528.

49 KEW. *Painting 45*: harvesting the sugarcane in Minas Geraes, Brazil. Available from: http://www.kew.org/mng/gallery/045.html. Accessible at: 14 July 2022.

50 O'SULLIVAN, A. C. Cellulose: the structure slowly unravels. *Cellulose*, v. 4, p. 173-207, 1997. DOI: 10.1023/A :1018431705579.

51 FESTUCCI-BUSELLI, R. A. *et al.* Structure, organization, and functions of cellulose synthase complexes in higher plants. *Brazilian Journal of Plant Physiology*, v. 19, n. 1, p.1-13. DOI: 10.1590/s1677-04202007000100001.

52 VIIKARI, L. *et al.* Forest products: biotechnology in pulp and paper processing. *In*: SCHAECHTER, M. (ed). *Encyclopedia of microbiology*. New York: Academic Press, 2009. p. 80-94. DOI: 10.1016/B978-012373944-5.00123-1.

53 WELLARD, H. J. Variation in the lattice spacing of cellulose. *Journal of Polymer Science*, v. 13, n. 71, p. 471-476, 1954. DOI: 10.1002/pol.1954.120137106.

54 MARCHESSAULT, R. H.; SUNDARARAJAN, P. R. Cellulose. *In*: ASPINALL, O. G. (ed). *The polysaccharides*. Toronto: Academic Press, 1983. p. 12-95. DOI: 10.1016/b978-0-12-065602-8.50007-8

55 MAGAGULA L. *et al.* Lignocellulosic biomass waste-derived cellulose nanocrystals and carbon nanomaterials: a review. *International Journal of Molecular Sciences*, v. 23, n. 8, p. 4310, 2022. DOI: 10.3390/ijms23084310

56 BÖRJESSON, M.; WESTMAN, G. Crystalline nanocellulose — preparation, modification, and properties. *In*: POLETTO, M.; ORNAGHI JUNIOR, H. L. (ed.). *Cellulose* - fundamental aspects and current trends. London: Intech Open, 2015. p. 160-191. DOI: 10.5772/61899.

57 SHOKRI, J.; ADIBKI K. Application of cellulose and cellulose derivatives in pharmaceutical industries. *In*: VAN DE VEN, T. G. M. (ed.). *Cellulose* - medical, pharmaceutical, and electronic applications. London: Intech Open, 2013. p. 48-61. DOI: 10.5772/55178.

58 BAGHAEI, B.; SKRIFVARS, M. All-cellulose composites: a review of recent studies on structure, properties, and applications. *Molecules*, v. 25, n. 12, p. 2836, 2020. DOI : 10.3390/molecules25122836.

59 HU, L. *et al.* Hemicellulose-based polymers processing and application. American Journal of Plant Sciences, v. 11, p. 2066-2079, 2020. DOI: 10.4236/ajps.2020.1112146.

60 LUCENIUS, J. *et al.* Understanding hemicellulose-cellulose interactions in cellulose nanofibril-based composites. Journal of Colloid and Interface Science, v. 555, p. 104-114, 2010. DOI: 10.1016/j.jcis.2019.07.053.

61 LU, Y. *et al.* Extraction, and modification of hemicellulose from lignocellulosic biomass: a review. Green Processing and Synthesis. 2021, v. 10, n. 1, p. 779-804, 2021. DOI: 10.1515/gps-2021-0065.

62 NECHITA, P.; IANA-ROMAN M. R. Review on polysaccharides used in coatings for food packaging papers. *Coatings*, v. 10, n. 6, p. 566, 2020. DOI: 10.3390/coatings10060566

63 MARGELLOU, A.; TRIANTAFYLLIDIS, K. S. Catalytic transfer hydrogenolysis reactions for lignin valorization to fuels and chemicals. *Catalysts*, v. 9, n. 1, p. 43, 2020. DOI : 10.3390/catal9010043.

64 WATKINS, D. *et al.* Extraction and characterization of lignin from different biomass resources. *Journal of Materials Research and Technology*, v. 4, n. 1, p. 26-32, 2015. DOI: 10.1016/j.jmrt.2014.10.009.

65 ZHOU Y. *et al.* Lignin-based hollow nanoparticles for controlled drug delivery: grafting preparation using β-Cyclodextrin/enzymatic-hydrolysis lignin. *Nanomaterials*, v. 9, p. 997, 2019. DOI: 10.3390/NANO9070997.

66 RIDHO, M.R. *et al.* Lignin as green filler in polymer composites: development methods, characteristics, and potential applications. *Advances in Materials Science and Engineering*, v. 2022, p 1-33, 2022. DOI: 10.1155/2022/1363481.

67 ERFANI JAZI, M. *et al.* Structure, chemistry and physiochemistry of lignin for material functionalization. *SN Applied Sciences*, v. 1, n. 9, p. 1-19, 2019. DOI: 10.1007/s42452-019-1126-8.

68 VASIC, K. *et al.* Bioethanol production by enzymatic hydrolysis from different. *Molecules*, v. 26, n. 753, p. 1-23, 2021. DOI : 10.3390/molecules26030753.

69 LI, D. G. *et al.* Physico-chemical properties of ethanol-diesel blend fuel and its effect on performance and emissions of diesel engines. *Renewable Energy*, v. 30, n. 6, p. 967-976, 2005. DOI: 10.1016/J.RENENE.2004.07.010.

70 PLEVIN, R. J. *et al.* Greenhouse gas emissions from biofuels' indirect land use change are uncertain but may be much greater than previously estimated. *Environmental Science & Technology*, v. 44, n. 21, p. 8015-8021, 2010. DOI : 10.1021/es101946t.

71 VOLYNETS, B. *et al.* Biomass processing into ethanol: pretreatment, enzymatic hydrolysis, fermentation, rheology, and mixing. *Green Processing and Synthesis*, v. 6, n. 1, p. 1-22, 2017. DOI: 10.1515/GPS-2016-0017/ASSET/GRAPHIC/J_GPS- 20160017_FIG_006.JPG.

72 MEJÍA-BARAJAS, J. A. *et al.* Second-generation bioethanol production through a simultaneous saccharification-fermentation process using kluyveromyces marxianus thermotolerant yeast. *In*: YÜKSEL, E.; GÖK, A.; EYVAZ, M. (ed). *Special topics in renewable energy systems*. London: Intech Open, 2018. p 22-30. DOI: 10.5772/intechopen.78052.

73 HEBBALE, D.; RAMACHANDRA, T. V. Third-generation bioethanol: status, scope, and challenges. *In*: SAHAY, S.(ed). *Handbook of biofuels*. Bhopal: Elsevier, 2022. p. 295-312. DOI: 10.1016/b978-0-12-822810-4.00015-4.

74 ABDULLAH, S. *et al.* Hydrothermal decomposition of various crystalline celluloses as treated by semi-flow hot-compressed water. *Journal of Wood Science*, v. 60, n. 4, p. 278-286, 2014. DOI: 10.1007/s10086-014-1401-7.

75 ZOGHLAMI, A.; PAËS, G. Lignocellulosic biomass: understanding recalcitrance and predicting hydrolysis. lignocellulosic biomass: understanding recalcitrance and predicting hydrolysis. *Frontiers in Chemistry*, v.7, p. 874, 2019. DOI: 10.3389/FCHEM.2019.00874/FULL.

76 GOMES, D. *et al*. Very high gravity bioethanol revisited: main challenges and advances. *Fermentation*, v. 7, p. 38, 2021 DOI : 10.3390/FERMENTATION7010038.

77 SHAH, A.A. *et al*. Biomass pretreatment technologies. *In*: MAITY, S.; GAYEN, K.; TRIDIB, B (ed): *Hydrocarbon biorefinery*: sustainable processing of biomass for hydrocarbon biofuels. Berlin: Elsevier, 2021. p. 203-228. DOI: 10.1016/B978-0-12-823306-1.00014-5.

78 MOKHENA, T. C.; JOHN, M. J. Cellulose nanomaterials: new generation materials for solving global issues. *Cellulose*, v. 27, n. 3, p. 1149-1194, 2019. DOI: 10.1007/S10570-019-02889-W.

79 BARUAH, J. *et al.* Recent trends in the pretreatment of lignocellulosic biomass for value-added products. *Frontiers in Energy Research*, v. 6, n. 18, p. 141, 2018. DOI: 10.3389/FENRG.2018.00141/BIBTEX.

80 SEEHAR, T. H. *et al.* Biocrude production from wheat straw at sub and supercritical hydrothermal liquefaction. *Energies*, v. 13, n. 12, p. 3114, 2020. DOI: 10.3390/en13123114.

81 SHARMA H. K. *et al.* Biological pretreatment of lignocellulosic biomass for biofuels and bioproducts: an overview. *Waste Biomass Valorization*, v. 10, n. 2, p. 235-251, 2019. DOI: 10.1007/s12649-017-0059-y.

82 NAUMAN AFTAB. M. *et al*. Different pretreatment methods of lignocellulosic biomass for use in biofuel production. *In*: ABOMOHRA, A. E. F. (ed). *Biomass for bioenergy* - recent trends and future challenges. London: Intech Open, 2019, p. 1-24. DOI: 10.5772/intechopen.84995.

83 SINDHU, R. *et al.* Biological pretreatment of lignocellulosic biomass - an overview. *Bioresource Technology*, v. 199, p. 76-82, 2016. DOI: 10.1016/j.biortech.2015.08.030.

84 UMMALYMA, S. B. *et al.* biological pretreatment of lignocellulosic biomass-current trends and future perspectives. *In*: BASILE, A.; DALENA, F.(ed). *Second and third generation of feedstocks*: the evolution of biofuels. Berlin: Elsevier; 2019. p. 197-212. DOI: 10.1016/B978-0-12-815162-4.00007-0.

85 KIM, J. S. *et al.* A review on alkaline pretreatment technology for bioconversion of lignocellulosic biomass. *Bioresource Technology*, v. 199, p. 42-48, 2016. DOI : 10.1016/j.biortech.2015.08.085.

86 XU, L. *et al.* Alkali-based pretreatment-facilitated lignin valorization: a review. *Industrial & Engineering Chemistry Research*, v. 59, n. 39, p. 16923-16938, 2020. DOI: 10.1021/acs.iecr.0c01456.

87 XU, H. *et al.* Review of Alkali-based pretreatment to enhance enzymatic saccharification for lignocellulosic biomass conversion. *Industrial & Engineering Chemistry Research*, v. 55, n. 32, p. 8691-8705, 2016. DOI: 10.1021/acs.iecr.6b01907.

88 LIU, C.G. *et al.* Bioethanol: new opportunities for an ancient product. *In*: LI, Y.; GE, X. (ed). *Advances in bioenergy*. Berlin: Elsevier, 2019. v. 4. p. 1-34. DOI: 10.1016/bs.aibe.2018.12.002.

89 TANG, W. *et al.* Natural surfactant-aided dilute sulfuric acid pretreatment of waste wheat straw to enhance enzymatic hydrolysis efficiency. *Bioresource Technology*, v. 324, p. 124651. DOI: 10.1016/j.biortech.2020.124651.

90 CHEN, W. H. *et al.* Disruption of sugarcane bagasse lignocellulosic structure by means of dilute sulfuric acid pretreatment with microwave-assisted heating. *Applied Energy*, v .88, n. 8, p. 2726-2734, 2011. DOI: 10.1016/j.apenergy.2011.02.027.

91 FOSTON, M. *et al.* Changes in the structure of the cellulose fiber wall during dilute acid pretreatment in populus studied by 1H and 2H NMR. *Energy and Fuels*, v. 24, n. 10, p. 5677-5685, 2010. DOI: 10.1021/EF100882T.

92 CHEN, H. *et al.* A review on the pretreatment of lignocellulose for high-value chemicals. *Fuel Processing Technology*, v. 160, p. 196-206, 2017. DOI: 10.1016/j.fuproc.2016.12.007.

93 LIU, W. *et al.* Effects of combined pretreatment of dilute acid pre-extraction and chemical-assisted mechanical refining on enzymatic hydrolysis of lignocellulosic biomass. *RSC Advances*, v. 8, n. 19, p. 10207-10214, 2018. DOI : 10.1039/c7ra12732d.

94 YAO, L. *et al.* Physicochemical changes of cellulose and their influences on Populus trichocarpa digestibility after different pretreatments. *Bioresources*, v. 14, n. 4, p. 9658-9676, 2019. DOI: 10.15376/biores.14.4.9658-9676.

95 PURKAIT, M. K.; HALDAR, D. Conventional pretreatment methods of lignocellulosic biomass. *In*: PURKAIT, M. K. (ed). *Lignocellulosic biomass to value-added products*. Berlin: Elsevier, 2021. p. 31-46. DOI: 10.1016/b978-0-12-823534-8.00009-0.

96 ELALAMI, D.; BARAKAT, A. State of the art of energy production from agricultural residues using thermochemical and biological processes. *In*: TYAG, V.; ABOUDI, K. (ed). *Clean energy and resources recovery*. Berlin: Elsevier, 2021. p. 1–24. DOI :10.1016/c2020-0-00530-x.

97 LI, M. *et al.* The effect of liquid hot water pretreatment on the chemical-structural alteration and the reduced recalcitrance in poplar. *Bioethanol Biofuels*, v. 10, n. 1, p. 237, 2017. DOI: 10.1186/s13068-017-0926-6.

98 REFAAT, A. A. Biofuels from waste materials. *Comprehensive Renewable Energy*, v. 5, p. 217-261, 2012. DOI: 10.1016/B978-0-08-087872-0.00518-7.

99 KANE, A.O. *et al.* Evaluating the potential of culms from sugarcane and energy cane varieties grown in Argentina for second-generation ethanol production. *Waste Biomass Valorization*, v. 13, p. 329–343, 2021. DOI: 10.1007/s12649-021-01528-5.

100 ASHOOR, S. *et al.* Sequential mild acid and alkali pretreatment of rice straw to improve enzymatic saccharification for bioethanol production. *Preparative Biochemistry & Biotechnology*, v. 13, p. 1-8, 2022. DOI: 10.1080/10826068.2022.2073597.

101 BORDIGNON, S. E. *et al.* Combined sugarcane pretreatment for the generation of ethanol and value-added products. *Frontiers in Energy Research*, v. 10, p.123, 2022. DOI: 10.3389/fenrg.2022.834966.

102 SIPPONEN, M. H. *et al.* Isolation of structurally distinct lignin-carbohydrate fractions from maize stem by sequential alkaline extractions and endoglucanase treatment. *Bioresource Technology*, v. 133, p. 522-528, 2013. DOI: 10.1016/j.biortech.2013.01.175.

103 KUMAR, A. *et al.* Characterization of cellulose nanocrystals produced by acid-hydrolysis from sugarcane bagasse as agro-waste. *Journal of Materials Physics and Chemistry*, v. 2, n. 1, p. 1-8. DOI: 10.12691/jmpc-2-1-1.

104 ŚWIĄTEK, K. *et al.* Acid hydrolysis of lignocellulosic biomass: sugars and furfurals formation. *Catalysts*, v. 10, n. 4, p. 437, 2020. DOI : 10.3390/catal10040437.

105 STEINBACH, D. *et al*. Pretreatment technologies of lignocellulosic biomass in water in view of furfural and 5-hydroxymethylfurfural production- a review. *Biomass Conversion and Biorefinery*, v. 7, n. 2, p. 247-274, 2017. DOI: 10.1007/s13399-017-0243-0.

106 MANDELS, M. *et al.* Enzymatic hydrolysis of waste cellulose. *Biotechnology and Bioengineering*, v. 16, n. 11, p. 1471-1493, 1974. DOI: 10.1002/BIT.260161105

107 REZENDE, C. A. *et al*. Chemical and morphological characterization of sugarcane bagasse submitted to a delignification process for enhanced enzymatic digestibility. *Biotechnology for Biofuels*, v. 4, n. 1, p.54, 2011. DOI: 10.1186/1754-6834-4-54.

108 TEERI, T. T. Crystalline cellulose degradation: new insight into the function of cellobiohydrolases. *Trends in Biotechnology*, v. 15, n. 5, p. 160-167, 1997. DOI: 10.1016/S0167-7799(97)01032-9

109 GUPTA, V. K. *et al.* Fungal enzymes for bio-products from sustainable and waste biomass. *Trends in Biochemical Sciences*, v. 41, n. 7, p. 633-645. 2016. DOI: 10.1016/j.tibs.2016.04.006.

110 RANI, S. R. *et al.* Role and significance of lytic polysaccharide monooxygenases (LPMOs) in lignocellulose deconstruction. *Bioresource Technology*, v. 335, p. 125261, 2021. DOI: 10.1016/j.biortech.2021.125261.

111 BURATTI, S.; BENEDETTI, S. Alcoholic fermentation using electronic nose and electronic tongue. *In*: MÉNDEZ, M. L. R. (ed.). *Electronic noses and tongues in food science*. Amsterdam: Elsevier, 2016. p. 291-299. DOI: 10.1016/B978-0-12-800243-8.00028-7.

112 KIM, D. Physico-chemical conversion of lignocellulose: inhibitor effects and detoxification strategies: a mini review. *Molecules*, v. 23, n. 2, p. 309, 2018. DOI: 10.3390/MOLECULES23020309.

113 TSE, T. J. *et al.* Production of bioethanol—a review of factors affecting ethanol yield. *Fermentation*, v. 7, n. 4, p. 268, 2021. DOI: 10.3390/FERMENTATION7040268.

114 SADH, P. K. *et al.* Fermentation: a boon for production of bioactive compounds by processing of food industries wastes (By-Products). *Molecules*, v. 23, n. 10, p. 2560, 2018. DOI : 10.3390/MOLECULES23102560.

115. LIZARDI-JIMÉNEZ, M.A. *et al.* Solid state fermentation (SSF): diversity of applications to valorize waste and biomass. *3 Biotech*, v. 7, n. 1, p. 1-9, 2017. DOI: 10.1007/S13205-017-0692-Y/TABLES/6.

116 KRISHNA, C. Solid-state fermentation systems - an overview. *Critical Reviews in Biotechnology*, v. 25, n. 1-2, p. 1-30, 200. DOI: 10.1080/07388550590925383.

117 BAI, F. W. *et al.* Ethanol fermentation technologies from sugar and starchfeedstocks. *Biotechnology Advances*, v. 26, n. 1, p. 89-105, 2008. DOI: 10.1016/J.BIOTECHADV.2007.09.002.

118 PULIGUNDLA, P. *et al*. Very high gravity (VHG) ethanolic brewing and fermentation: a research update. *Journal of Industrial Microbiology and Biotechnolog*, v. 38, n. 9, p. 1133-1144, 2011. DOI: 10.1007/S10295-011-0999-3.

119 GUCCINI, V. *Nanocellulose*: energy applications and self-assembly. 2019. 103 p. Thesis (Doctor) - Stockholm University, Sweden, 2019.

120 MARKETS AND MARKETS. *Nanocellulose market 2022-2026*. Available from: https://www.marketsandmarkets.com/Market-Reports/nano-cellulose-market-56392090.html. Accessible at: 14 July 2022.

121 HASHIMOTO, T.; KOIZUMI, S. Combined small-angle scattering for characterization of hierarchically structured polymer systems over nano-to-micron meter: part I experiments. *Polymer Science A*: comprehensive reference, v. 2, p. 381-398, 2012. DOI: 10.1016/B978-0-444-53349-4.00297-1

122 NASCIMENTO, S. A.; REZENDE, C. A. Combined approaches to obtain cellulose nanocrystals, nanofibrils and fermentable sugars from elephant grass. *Carbohydrate Polymers*, v. 180, p. 38-45. DOI: 10.1016/j.carbpol.2017.09.099.

123 ÄMMÄLÄ, A. *et al.* Energy consumption, physical properties and reinforcing ability of microfibrillated cellulose with high lignin content made from non-delignified spruce and pine sawdust. *Industrial Crops and Products*, v. 170, p. 113738, 2021. DOI: 10.1016/j.indcrop.2021.113738.

124 XIE, H. *et al.* Recent strategies in preparation of cellulose nanocrystals and cellulose nanofibrils derived from raw cellulose materials. *International Journal of Polymer Science*, v. 2018, p. 25, 2018. DOI: 10.1155/2018/7923068.

125 ISOGAI, A.; ZHOU, Y. Diverse nanocelluloses prepared from TEMPO-oxidized wood cellulose fibers: nanonetworks, nanofibers, and nanocrystals. *Current Opinion in Solid State & Materials Science*, v. 23, n. 2, p. 101-106, 2019. DOI: 10.1016/j.cossms.2019.01.001.

126 LITTUNEN, K. *et al.* Synthesis of cationized nanofibrillated cellulose and its antimicrobial properties. *European Polymer Journal*, v. 75, p. 116-124, 2015. DOI: 10.1016/J.EURPOLYMJ.2015.12.008.

127 TEJADO, A. *et al*. Energy requirements for the disintegration of cellulose fibers into cellulose nanofibers. *Cellulose*, v. 19, n. 3, p. 831-842, 2012. DOI: 10.1007/S10570-012-9694-4.

128 ERROKH, A. *et al.* Morphology of the nanocellulose produced by periodate oxidation and reductive treatment of cellulose fibers. *Cellulose*, v. 25, n. 7, p. 3899-3911, 2018. DOI: 10.1007/S10570-018-1871-7.

129 YING, W. *et al.* In-situ modification of lignin in alkaline-pretreated sugarcane bagasse by sulfomethylation and carboxymethylation to improve the enzymatic hydrolysis efficiency. *Industrial Crops and Products*, v. 182, p. 114863, 2022. DOI: 10.1016/J.INDCROP.2022.114863.

130 MOREAU, C T. *et al.* Lytic polysaccharide monooxygenases (LPMOs) facilitate cellulose nanofibrils production. *Biotechnology for Biofuels*, v. 12, n. 1, p. 156, 2019. DOI: 10.1186/s13068-019-1501-0.

131 WEN, Y. *et al.* Preparation and characterization of lignin-containing cellulose nanofibril from poplar high-yield pulp via TEMPO-mediated oxidation and homogenization. *ACS Sustainable Chemistry & Engineering*, v. 7, n. 6, p. 6131-6139, 2019. DOI: 10.1021/ACSSUSCHEMENG.8B06355.

132 BARRUETABEÑA, N. *et al.* Resurrection of efficient Precambrian endoglucanases for lignocellulosic biomass hydrolysis. *Communications Chemistry*, v. 2, n. 1, 2019. DOI: 10.1038/s42004-019-0176-6.

133 PIERRE, G. *et al.* TEMPO-mediated oxidation of polysaccharides: an ongoing story. *Carbohydrate Polymers*, v. 165, p. 71-85, 2017. DOI: 10.1016/J.CARBPOL.2017.02.028.

134 HU, J. *et al.* Enzyme mediated nanofibrillation of cellulose by the synergistic actions of an endoglucanase, lytic polysaccharide monooxygenase (LPMO) and xylanase. *Science Reports*, p. 4-11, 2017. DOI: 10.1038/s41598-018-21016-6.

135 SQUINCA, P. *et al.* The use of enzymes to isolate cellulose nanomaterials: A systematic map review. *Carbohydrate Polymers Technologies and Applications*, v. 3, p. 100212, 2022. DOI: 10.1016/j.carpta.2022.10021.

136 SLUITER, A. *et al. Determination of structural carbohydrates and lignin in biomass* - NREL/TP. 2008. Available from: http://www.nrel.gov/docs/gen/fy13/42618.pdf. Accessible at: 23 Jan. 2021.

137 HAUTEFEUILLE, M. ; HERNANDEZ-CORDERO, J. UV–VIS spectroscopy. *In*: Presse SPIE (ed.). *Field guide to optoelectronics and photonics*. Washington: Springer-Verlag, 2021. p. 1-251. DOI: 10.1117/3. 2595887.ch84.

138 ROCHA, F.S. *et al.* Experimental methods in chemical engineering: ultraviolet, visible spectroscopy—UV-Vis. *Canadian Journal of Chemical Engineering*, v. 96, n. 12, p. 2512-2517, 2018. DOI: 10.1002/cjce.23344.

139 MAYERHÖFER, T.G. *et al.* The Bouguer-Beer-Lambert law: shining light on the obscure. *ChemPhysChem*, v. 21, p. 2029–2046, 2020. DOI: 10.1002/cphc.202000464.

140 MCCREEDY, T. High-performance liquid chromatography fundamental principles and practice. *Analytica Chimica Acta*, v.347, n. 3, p. 398, 1997. DOI: 10.1016/s0003-2670(97)81192-0.

141 JANDERA, P. High-performance liquid chromatography (analytical chemistry by open learning series). *Journal of Chromatography A*, v. 435, p. 391-392, 1988. DOI: 10.1016/s0021-9673(01)82202-0.

142 MARTIN, B. B. *Column chromatography*. London: Intech, 2013. 140p. DOI: 10.5772/47823.

143 VERONIKA, R. M. *Practical high-performance liquid chromatography*. 5th ed. Switzerland: John Wiley, 2010. 428p.

144 CZAPLICKI, S. Chromatography in bioactivity analysis of compounds. *In*: MARTIN, D. F.; MARTIN, B. B. (ed.). *Column chromatography*. Olsztyn: Intech Open, 2013. p.100-121. DOI: 10.5772/55620.

145 INKSON, B. J. Scanning electron microscopy (SEM) and transmission electron microscopy (TEM) for materials characterization. *In*: HÜBSCHEN, G.; ALPETER, I.; TSCHUNCKY, R.; HERMANN, H. G. (ed). *Materials characterization using nondestructive evaluation (NDE) methods*. Amsterdam: Elsevier, 2016. p. 17- 43. DOI: 10.1016/B978-0-08-100040-3.00002-X.

146 GOLDSTEIN, J. I. *et al.* Scanning electron microscopy and X-ray microanalysis. 4th ed. New York: Springer, 2018. 554p. DOI: 10.1007/978-1-4939-6676-9.

147 ALIOFKHAZRAEI, M.; Ali, N. AFM applications in micro/nanostructured coatings. *Comprehensive Materials Processing*, v. 7, p. 191-241, 2014. DOI: 10.1016/B978-0-08-096532-1.00712-3.

148 FLECK, N. *et al.* Characterization techniques in energy generation and storage. *In*: AHMED, W. BOOTH, M. NOURAFKAN, E. (ed). *Emerging nanotechnologies for renewable energy*. Amsterdam: Elsevier, 2021. p. 259-285. DOI: 10.1016/B978-0-12-821346-9.00003-1.

149 MUŠEVIČ, I. Atomic force microscopy. *Informacije MIDEM*, v. 30, n. 4, p. 223-227, 2000. DOI: 10.1093/Oso/9780198856559.003.0016.

150 VALOTTEAU, C.; SUMBUL, F.; RICO, F. High-speed force spectroscopy: microsecond force measurements using ultrashort cantilevers. *Biophysical Reviews*, v. 11, n. 5, p. 689-699, 2019. DOI: 10.1007/S12551-019-00585-4.

151 FERRI, F. A. *et al.* Magnetic force microscopy: basic principles and applications. *In*: BELLITO, V. (ed). *Atomic force microscopy* - imaging, measuring and manipulating surfaces at the atomic scale. London: Intech Open, 2012, p. 40-53. DOI: 10.5772/34833.

152 WRIGHT, C. J. *et al.* Microscopy: atomic force microscopy. *In*: BATT, C.; PATEL, P.(ed) *Encyclopedia of food microbiology*: second edition. New York: Academic Press; 2014. p. 666-675. DOI: 10.1016/B978-0-12-384730-0.00217-2.

153 ZABEL, R. A.; MORRELL, J. J. Ultrastructural features of wood decay. *In*: ZABEL, R. A.; MORRELL, J. J. (ed.). *Wood microbiology*. Berlin: Elsevier, 2020. p. 245-269. DOI: 10.1016/b978-0-12-819465-2.00009-7.

154 ESCALANTE, C. F. *Fundamentals of transmission electron microscopy, the technique with the best resolution in the world.* 2019. Available from: https://www.researchgate.net/profile/Cristian-Escalante/publication/330999184_Fundamentals_of_transmission_electron_microscopy_the_technique_with_the_best_resolution_in_the_world/links/5c60490ea6fdccb608b758a5/Fundamentals-of-transmission-electron-microscopy-the-technique-with-the-best-resolution-in-the-world.pdf. Accessible at: 23 Jan. 2021.

155 ALI, A. *et al.* X-ray diffraction techniques for mineral characterization: a review for engineers of the fundamentals, applications, and research directions. *Minerals*, v. 12, n. 2, 2022. DOI: 10.3390/min12020205.

156 GUMA, T. *et al.* X-ray diffraction analysis of the microscopies of some corrosion- protective bitumen coatings. *International Journal of Modern Engineering Research (IJMER*), v. 2, n. 6, p. 4387-4395, 2012.

157 FULTZ, B.; HOWE, J. M. *Transmission electron microscopy and diffractometry of materials*. 3rd ed. Heidelberg: Springer, 2008. DOI: 10.1007/978-3-540-73886-2.

158 NASIR, M. *et al.* Nanocellulose: preparation methods and applications. *In*: JAWAID, M.; BOUFI, S.; HPS, A. K.(ed). *Cellulose-reinforced nanofibre composites*. Heidelberg: Elsevier, 2017. p. 261-276. DOI: 10.1016/B978-0-08-100957-4.00011-5

159 HULL, J. B.; JOHN V. B. *Non-destructive testing*. London: Macmillan Education, 1988. 162p. DOI: 10.1007/978-1-349-85982-5.

160 SCHNECKENBURGER, H.; RICHTER, V. Laser scanning versus wide-field—choosing the appropriate microscope in life sciences. *Applied Sciences*, v. 11, n. 2, p 1-17, 2021. DOI : 10.3390/app11020733.

161 CRISTINA, F. *et al*. Confocal laser scanning microscopy as a tool for the investigation of skin drug delivery systems and diagnosis of skin disorders. *In*: LAGALI, N (ed.). *Confocal laser microscopy* - principles and applications in medicine, biology, and the food sciences. London: Intech Open, 2013. DOI: 10.5772/55995.

162 CLAXTON, N. S. *et al.* Laser scanning confocal microscopy (LSCM). *Springer Reference*, v. 1979, n. 21, 2011.

163 BAKHMUTOV, V. I. *Solid-state NMR in materials science*: principles and applications. London: Taylor & Francis, 2016. 280 p. DOI: 10.1201/b11301.

164 NICDAÉID, N. Forensic sciences: systematic drug identification. *In*: WORSFOLD, P. POOLE, C. (ed). *Encyclopedia of analytical science*. 3rd ed. New York: Academic Press; 2019. p. 75-80. DOI: 10.1016/B978-0-12-409547-2.14457-9

165 PURCELL, E. M. *et al.* Resonance absorption by nuclear magnetic moments in a solid [7]. *Physical Review*, v. 69, n. 1-2, p. 37-38, 1946. DOI: 10.1103/PHYSREV.69.37.

166 CROMPTON, T. R. *Thermal methods of polymer analysis*. Shawbury: Smithers Rapra Technology, 2013. 242 p.

167 GAISFORD, S.; KETT, V.; HAINES, P. *Principles of thermal analysis and calorimetry*. 2nd ed. Cambridge: Royal Society of Chemistry, 2002. 238p.

168 TOMODA, B. T. *et al.* Characterization of biopolymer membranes and films: Physicochemical, mechanical, barrier, and biological properties. *In*: MORAES, M.A.; DA SILVA, C.F.; VIEIRA, R. S.(ed.). Biopolymer membranes and films. Berlin: Elsevier; 2020. p. 67-95. DOI: 10.1016/b978-0-12-818134-8.00003-1.

169 CHEN, W. H. *et al.* Progress in biomass torrefaction: principles, applications, and challenges. *Progress in Energy and Combustion Science*, v. 82, p. 100887, 2021. DOI: 10.1016/j.pecs.2020.100887.

170 ABRAHAM, J. *et al.* Thermoanalytical techniques of nanomaterials. *In*: BHAGYARAJ, S. N.; OLUWATOBI, S. O.; KALARIKKA, N.(ed). *Characterization of nanomaterials*: advances

and key technologies. Berlin: Elsevier Science, 2018. p. 213-236. DOI: 10.1016/B978-0-08-101973-3.00008-0.

171 ROCHA, G. J. *et al.* Dilute mixed-acid pretreatment of sugarcane bagasse for ethanol production. *Biomass Bioenergy*, v. 35, n. 1, p. 663-670, 2011. DOI: 10.1016/j.biombioe.2010.10.018.

172 PARK, S. *et al.* Cellulose crystallinity index: Measurement techniques and their impact on interpreting cellulase performance. *Biotechnology for Biofuels*, v. 3, p. 1–10, 2010. DOI: 10.1186/1754-6834-3-10.

173 BERNARDINELLI, O. D. *et al.* Quantitative 13 C multiCP solid - state NMR as a tool for evaluation of cellulose crystallinity index measured directly inside sugarcane biomass. *Biotechnology for Biofuels*, v. 8, n. 1, p. 1-11, 2015. DOI: 10.1186/s13068-015-0292-1.

174 SCHERRER, P. Bestimmung der inneren Struktur und der Größe von Kolloidteilchen mittels Röntgenstrahlen. *Kolloidchemie ein Lehrbuch*, v. 2, n. 26, p. 387-409, 2012. DOI : 10.1007/978-3-662-33915-2_7.

175 MONSHI, A. *et al.* Modified Scherrer equation to estimate more accurately nano-crystallite size using XRD. *World Journal of Nano Science and Engineering*, v. 2, n. 3, p. 154-160, 2012. DOI: 10.4236/WJNSE.2012.23020.

176 COLETTA, V.C. *et al.* Mapping the lignin distribution in pretreated sugarcane bagasse by confocal and fluorescence lifetime imaging microscopy. *Biotechnology for Biofuels*, v. 6, n. 1, p. 1-10. DOI: 10.1186/1754-6834-6-43, 2013.

177 SANTOS, M. *et al.* Industrial crops & products structural and compositional changes in sugarcane bagasse subjected to hydrothermal and organosolv pretreatments and their impacts on enzymatic hydrolysis. *Industrial Crops and Products*, v. 113, p. 64-74, 2018. DOI: 10.1016/j.indcrop.2018.01.014.

178 PROVENCHER, S. W. A constrained regularization method for inverting data represented by linear algebraic or integral equations. *Computer Physics Communications*, v. 27, n. 3, p. 213-227, 1982. DOI: 10.1016/0010-4655(82)90173-4.

179 BORGIA, G. C. *et al.* Uniform-penalty inversion of multiexponential decay data. *Journal of Magnetic Resonance*, v. 132, n. 1, p. 65-77, 1998. DOI: 10.1006/JMRE.1998.138

180 BROWNSTEIN, K. R.; TARR, C. E. Importance of classical diffusion in NMR studies of water in biological cells. *Physical Review A*, v. 19, n. 6, p. 2446-2453, 1979 DOI: 10.1103/PhysRevA.19.2446.

181 CAPITANI, D. *et al.* Nuclear magnetic resonance to characterize and monitor cultural heritage. *Progress in Nuclear Magnetic Resonance Spectroscopy*, v. 64, p. 29-69, 2012. DOI: 10.1016/J.PNMRS.2011.11.001.

182 PROVENCHER, S. W. CONTIN: a general purpose constrained regularization program for inverting noisy linear algebraic and integral equations. *Computer Physics Communications*, v. 27, n. 3, p. 229-242, 1982. DOI: 10.1016/0010-4655(82)90174-6.

183 DI RIENZO, J. A. *et al.* A multiple-comparisons method based on the distribution of the root node distance of a binary tree. *Journal of Agricultural, Biological, and Environmental Statistics*, v. 7, n. 2, p. 129-142, 2002. DOI: 10.1198/10857110260141193.

184 DI RIENZO, J. A. *et al. InfoStat (versión 2010)*. Universidad Nacional de Córdoba, Argentina. Available from: http://www.sciepub.com/reference/139943. Accessible at: 14 Jan. 2021.

185 LI, M. *et al.* The effect of liquid hot water pretreatment on the chemical-structural alteration and the reduced recalcitrance in poplar. *Biotechnology for Biofuels*, v. 10, n. 1, p. 1-13, 2017. DOI: 10.1186/S13068-017-0926-6/SCHEMES/1.

186 RESTIAWATY, E.; DEWI, A. Comparison of pretreatment methods on vetiver leaves for efficient processes of simultaneous saccharification and fermentation by neurospora sp. *Journal of Physics*: conference series, v. 877, n. 1, p.1-8, 2017. DOI: 10.1088/1742-6596/877/1/012048.

187 BU, L. *et al.* Comparative study of sulfite pretreatments for robust enzymatic saccharification of corn cob residue. *Biotechnology for Biofuels*, v. 5, n. 1, p 1-8, 2012. DOI: 10.1186/1754-6834-5-87/FIGURES/5.

188 REZENDE, C. A. *et al.* Chemical and morphological characterization of sugarcane bagasse submitted to a delignification process for enhanced enzymatic digestibility. *Biotechnology for Biofuels*, v. 4, n. 1, p. 54, 2011. DOI: 10.1186/1754-6834-4-54.

189 WANG, C. *et al.* Impact of alkaline pretreatment condition on enzymatic hydrolysis of sugarcane bagasse and pretreatment cost. *Applied Biochemistry and Biotechnology*, v. 193, p. 2087–2097, 2021. DOI: 10.1007/s12010-021-03530-y.

190 WU, J. *et al.* Alkaline sulfonation and thermomechanical pulping pretreatment of softwood chips and pellets to enhance enzymatic hydrolysis. *Bioresource Technology*, v. 315, p. 123789, 2020. DOI : 10.1016/j.biortech.2020.123789

191 ZHOU, H. *et al.* SPORL pretreatment spent liquors enhance the enzymatic hydrolysis of cellulose and ethanol production from glucose. *Energy and Fuels*, v. 32, n. 7, p, 7636-7642, 2018. DOI: 10.1021/acs.energyfuels.8b00864.

192 LASER, M. *et al.* A comparison of liquid hot water and steam pretreatments of sugar cane bagasse for bioconversion to ethanol. *Bioresource Technology*, v.81, n.1, p. 33-44, 2002. DOI: 10.1016/S0960-8524(01)00103-1.

193 ESCAMEZ, S. *et al.* Fluorescence lifetime imaging as an in situ and label-free readout for the chemical composition of lignin. *ACS Sustainable Chemistry & Engineering*, v. 9, n. 51, p. 17381-17392, 2021. DOI: 10.1021/acssuschemeng.1c06780.

194 WIGHTMAN, R. *et al.* Correlative FLIM-confocal-Raman mapping applied to plant lignin composition and autofluorescence. *Micron*, v. 126, p.102733, 2019. DOI: 10.1016/j.micron.2019.102733.

195 AUXENFANS, T. *et al.* Seeing biomass recalcitrance through fluorescence. *Scientific Reports*, n. 71, p.1-8, 2017. DOI: 10.1038/s41598-017-08740-1.

196 GARCÍA-PLAZAOLA, J. I. *et al.* Autofluorescence: biological functions and technical applications. *Plant Science*, v. 236, p. 136-145, 2015. DOI: 10.1016/j.plantsci.2015.03.010.

197 SANT'ANNA, C. *et al.* Sugarcane cell wall structure and lignin distribution investigated by confocal and electron microscopy. *Microscopy Research & Technique*, v. 76, n. 8, p. 829-834, 2013. DOI: 10.1002/jemt.22235.

198 WU, J. *et al.* Alkaline sulfonation and thermomechanical pulping pretreatment of softwood chips and pellets to enhance enzymatic hydrolysis. *Bioresource Technology*, v. 315, p. 123789, 2020. DOI : 10.1016/J.BIORTECH.2020.123789.

199 CHU, Q. *et al.* Prétraitement en deux étapes avec sulfonation alcaline et traitement à la vapeur de la biomasse ligneuse d'eucalyptus pour améliorer sa digestibilité enzymatique pour la production de bioéthanol. *Energy Conversion and Management*, v. 175, p. 236–245, 2018. DOI: 10.1016/j.enconman.2018.08.100.

200 ESPÍRITO SANTO, M. C. *et al.* When the order matters: impacts of lignin removal and xylan conformation on the physical structure and enzymatic hydrolysis of sugarcane bagasse. *Industrial Crops and Products*, v. 180, p. 114708, 2022. DOI: 10.1016/j.indcrop.2022.114708.

201 COLETTA, V. C. *et al.* Mapping the lignin distribution in pretreated sugarcane bagasse by confocal and fluorescence lifetime imaging microscopy. *Biotechnology for Biofuels*, v.6, n. 1, p. 43, 2013. DOI: 10.1186/1754-6834-6-43.

202 SELIG M. J. *et al.* Deposition of lignin droplets produced during dilute acid pretreatment of maize stems retards enzymatic hydrolysis of cellulose. *Biotechnology Progress*, v. 23, n. 6, p. 1333-1339, 2007. DOI : 10.1021/bp0702018.

203 BALEA, A. *et al.* Influence of pretreatment and mechanical nanofibrillation energy on properties of nanofibers from Aspen cellulose. *Cellulose*, v. 28, n. 14, p. 9187-9206, 2021. DOI: 10.1007/S10570-021-04109-W.

204 LING, Z. *et al.* Unraveling variations of crystalline cellulose induced by ionic liquid and their effects on enzymatic hydrolysis. *Scientific Reports*, v. 7, n. 1, p. 1-11, 2017. DOI : 10.1038/s41598-017-09885-9.

205 ISHIDA, N. *et al.* Special feature: biotechnology for sustainable and aging societies structural analysis of lignocellulose biomass using nuclear magnetic resonance. *2 R&D Review of Toyota CRDL*, v. 48, n. 1, p 1-9, 2017.

206 AKHTAR, J.; IDRIS, A. Oil palm empty fruit bunches a promising substrate for succinic acid production via simultaneous saccharification and fermentation. *Renewable Energy*, v. 114, p. 917-923, 2017. DOI: 10.1016/j.renene.2017.07.113.

207 HOLTMAN, K.M. *et al.* Chemical structure and heterogeneity differences of two lignins from loblolly pine as investigated by advanced solid-state NMR spectroscopy. *Journal of Agricultural and Food Chemistry*, v. 58, n. 18, p. 9882-9892, 2010. DOI: 10.1021/jf101258x.

208 CHANDRA, R.P. *et al.* The influence of lignin on steam pretreatment and mechanical pulping of poplar to achieve high sugar recovery and ease of enzymatic hydrolysis. *Bioresource Technology*, v. 199, p. 135-141, 2016. DOI: 10.1016/J.BIORTECH.2015.09.019.

209 KUMAR, L. *et al.* The lignin present in steam pretreated softwood binds enzymes and limits cellulose accessibility. *Bioresource Technology*, v. 103, n .1, p. 201-208, 2012. DOI: 10.1016/j.biortech.2011.09.091.

210 BU, L. *et al.* Comparative study of sulfite pretreatments for robust enzymatic saccharification of corn cob residue. *Biotechnology for Biofuels*, v. 5, n.1, p. 1-8, 2012. DOI: 10.1186/1754-6834-5-87/FIGURES/5.

211 ZHU, J. Y. *et al.* Sulfite pretreatment (SPORL) for robust enzymatic saccharification of spruce and red pine. *Biotechnology for Biofuels*, v. 100, n. 8, p. 2411-2418, 2009. DOI: 10.1016/J.BIORTECH.2008.10.057.

212 SIQUEIRA, G. *et al.* Limitation of cellulose accessibility and unproductive binding of cellulases by pretreated sugarcane bagasse lignin. *Biotechnology for Biofuels*, v. 10, n. 1, p. 176, 2017. DOI: 10.1186/s13068-017-0860-7.

213 ZHANG, X. *et al.* Cellulose modification by recyclable swelling solvents. *Biotechnology for Biofuels*, v. 11, n. 1, p. 1-12, 2018. DOI: 10.1186/S13068-018-1191-Z/TABLES/4

214 SETIATI, R. *et al.* Laboratory optimization study of sulfonation reaction toward lignin isolated from bagasse. *In*: BASSO, T. P. BASSO, T. O. BASSO,L. C. (ed.). *Biotechnological applications of biomass*. London: IntechOpen, 2020. p. 1-16. DOI: 10.5772/INTECHOPEN.93662.

215 FELBY, C. *et al.* Cellulose-water interactions during enzymatic hydrolysis as studied by time domain NMR. *Cellulose*, v. 15, n. 5, p. 703-710, 2008. DOI: 10.1007/S10570-008-9222-8.

216 MENG, X.; RAGAUSKAS, A. J. Recent advances in understanding the role of cellulose accessibility in enzymatic hydrolysis of lignocellulosic substrates. *Current Opinion in Biotechnology*, n. 27, p. 150-158, 2014. DOI: 10.1016/J.COPBIO.2014.01.014.

217 TSUCHIDA, J. E. *et al.* Nuclear magnetic resonance investigation of water accessibility in cellulose of pretreated sugarcane bagasse. *Biotechnology for Biofuels*, v. 7, n. 1, p. 1-13. DOI : 10.1186/s13068-014-0127-5.

218 RAO, J. *et al.* Rapid processing of holocellulose-based nanopaper toward an electrode material. *ACS Sustainable Chemistry & Engineering*, v. 9, n. 8, p. 3337-3346, 2021. DOI: 10.1021/acssuschemeng.0c09408.

219 DING, Q. *et al.* Efficient preparation of holocellulose nanofibers and their reinforcement potential. *Cellulose*, v. 29, n. 15, p. 8229-8242, 2022. DOI : 10.1007/s10570-022-04765-6

220 GALLAND, S. *et al.* Holocellulose nanofibers of high molar mass and small diameter for high-strength nanopaper. *Biomacromolecules*, v. 16, n. 8, p. 2427-2435, 2015. DOI : 10.1021/acs.biomac.5b00678.

221 WU, Y. *et al.* Effect of H2O2 bleaching treatment on the properties of finished transparent wood. *Polymers*, v. 11, n. 5, p. 776, 2019. DOI : 10.3390/polym11050776.

222 MITTAL, A. *et al*. Alkaline peroxide delignification of corn stover. *ACS Sustainable Chemistry & Engineering*, v. 5, n. 7, p. 6310-6321, 2017. DOI: 10.1021/acssuschemeng.7b01424.

223 HAFEMANN, E. *et al.* Enhancing chlorine-free purification routes of rice husk biomass waste to obtain cellulose nanocrystals. *Waste Biomass Valorization*, v. 11, n. 12, p. 6595-6611, 2020. DOI: 10.1007/S12649-020-00937-2/FIGURES/12.

224 ÄMMÄLÄ, A. *et al.* Key role of mild sulfonation of pine sawdust in the production of lignin containing microfibrillated cellulose by ultrafine wet grinding. *Industrial Crops and Products*, v. 140, p. 111664, 2019. DOI: 10.1016/j.indcrop.2019.111664.

225 HANHIKOSKI, S. *et al.* Fibrillation and characterization of lignin-containing neutral sulphite (NS) pulps rich in hemicelluloses and anionic charge. *Cellulose*, v. 27, n. 12, p. 7203-7214, 2020. DOI: 10.1007/S10570-020-03237-Z.

226 NORRRAHIM, M. N. *et al.* Performance evaluation of cellulose nanofiber with residual hemicellulose as a nanofiller in the polypropylene-based nanocomposite. *Polymers*, v. 13, n. 7, 2021. DOI: 10.3390/POLYM13071064.

227 NORRRAHIM, M. N. F. *et al.*. Emerging development of nanocellulose as an antimicrobial material: an overview. *Materials Advances*, v. 2, n. 11, p. 3538-3551, 2021. DOI: 10.1039/d1ma00116g.

228 HAN, X. *et al.* Potential to produce sugars and lignin-containing cellulose nanofibrils from enzymatically hydrolyzed chemi-thermomechanical pulps. *ACS Sustainable Chemistry & Engineering*, v. 8, p. 14955-14963, 2020. DOI: 10.1021/acssuschemeng.0c05183.

229 CEBREIROS, F. *et al.* Enhancing cellulose nanofibrillation of eucalyptus Kraft pulp by combining enzymatic and mechanical pretreatments. *Cellulose*, v. 28, n. 1, p.189-206, 2021. DOI: 10.1007/s10570-020-03531-w.

230 VISANKO, M. *et al.* Mechanical fabrication of high-strength and re-dispersible wood nanofibers from unbleached groundwood pulp. *Cellulose*, v. 24, n. 10, p. 4173-4187, 2017. DOI: 10.1007/S10570-017-1406-7/FIGURES/8.

231 SIRVIÖ, J. A. *et al*. Direct sulfation of cellulose fibers using a reactive deep eutectic solvent to produce highly charged cellulose nanofibers. *Cellulose*, v. 26, n. 4, p. 2303-2316, 2019. DOI: 10.1007/s10570-019-02257-8/Figures/5.

232 PINGREY, B.; HSIEH, Y. L. O. Sulfated cellulose nanofibrils from chlorosulfonic acid treatment and their wet spinning into high-strength fibers. *Biomacromolecules*, v. 23, n. 3, p. 1269-1277, 2022.

233 BU, L. *et al.* Comparative study of sulfite pretreatments for robust enzymatic saccharification of corn cob residue. *Biotechnology for Biofuels*, v. 5, n. 1, p. 1-8, 2012. DOI: 10.1186/1754-6834-5-87/FIGURES/5.

234 ROSSI, B. *et al.* Cellulose nanofibers production using a set of recombinant enzymes. *Carbohydrate Polymers*, v. 256, p. 117510, 2021. DOI: 10.1016/J.CARBPOL.2020.117510.

235 LIU X. *et al.* Tuning of size and properties of cellulose nanofibers isolated from sugarcane bagasse by endoglucanase-assisted mechanical grinding. *Industrial Crops and Products*, v.146, p. 112201, 2020. DOI: 10.1016/j.indcrop.2020.112201.

236 DE FRANCE, K.J. Review of hydrogels and aerogels containing nanocellulose. *Chemistry of Materials*, v. 29, n. 11, p. 4609-4631, 2017 DOI: 10.1021/acs.chemmater.7b00531.

237 KEDZIOR, S.A. *et al.* Cranston ED. Nanocellulose in Emulsions and Heterogeneous Water-Based Polymer Systems: a review. *Advanced Materials*, v. 33, n. 28, p. 2002404, 2021. DOI: 10.1002/ADMA.202002404.

238 CAMARGOS, C. H. M.; REZENDE, C.A. Structure-property relationships of cellulose nanocrystals and nanofibrils: implications for the design and performance of nanocomposites and all-nanocellulose systems. *ACS Applied Nano Materials*, v. 4, n. 10, p. 10505-10518, 2021. DOI: 10.1021/acsanm.1c02008.

239 CHEN, W. *et al.*. Individualization of cellulose nanofibers from wood using high intensity ultrasonication combined with chemical pretreatments. *Carbohydrate Polymers*, v. 83, n. 4, p. 1804-1811, 2011. DOI : 10.1016/J.CARBPOL.2010.10.040

240 BAYER, T. *et al.* Spray deposition of sulfonated cellulose nanofibers as electrolyte membranes in fuel cells. *Cellulose*, v. 28, n. 3, p. 1355-1367, 2021. DOI: 10.1007/S10570-020-03593-W/FIGURES/4.

241 YANG, H. *et al.* Characteristics of hemicellulose, cellulose, and lignin pyrolysis. *Fuel*, v. 86, n. 12-13, p. 1781-1788, 2007. DOI: 10.1016/J.FUEL.2006.12.0

242 BERTO, G. L. *et al.* Single-step fiber pretreatment with mon component endoglucanase: defibrillation energy and cellulose nanofibril quality. *ACS Sustainable Chemistry & Engineering*, v. 9, n. 5, p. 2260-2270, 2021. DOI: 10.1021/acssuschemeng.0c08162.

243 ROMAN, M.; WINTER, W.T. Effect of sulfate groups from sulfuric acid hydrolysis on the thermal degradation behavior of bacterial cellulose. *Biomacromolecules*, v. 5, n. 5, p. 1671-1677, 2004. DOI : 10.1021/bm034519+.

244 LAM, D. N. *et al.* Thermally stable cellulose nanospheres prepared from office wastepaper by complete removal of hydrolyzed sulfate groups. *Carbohydrate Polymers*, v. 297, p 120009, 2022. DOI: 10.1016/j.carbpol.2022.120009.